GEMS & GEMOLOGY

SUMMER 2012
VOLUME XLVIII

THE QUARTERLY JOURNAL OF THE GEMOLOGICAL INSTITUTE OF AMERICA

Gemesis CVD synthetic diamond
New sapphires from Sri Lanka
Cultured pearls from Micronesia

THE 4Cs APP THAT ALSO PUTS YOU ON THE MAP.

List your retail location on GIA's free 4Cs app for consumers. In addition to learning more about diamonds and the 4Cs through videos and fun interactive tools, consumers will soon be able to use the app to locate registered retailers who carry GIA-graded diamonds or have GIA-trained staff. The feature will be available on both the iPad and iPhone apps. Register for the Retailer Locator today at **www.retailer.gia.edu.**

The Retailer Locator feature is scheduled to be released in the fall of 2012.

You can also visit **www.retailer.gia.edu** to download a free retailer iPad version of the 4Cs app for use at point of sale.

Apps currently available for Apple devices. Android version for smartphone and tablet coming this summer.

GIA®

GEMS & GEMOLOGY
Summer 2012
VOLUME 48, No. 2


pg. 81


pg. 103


pg. 150

Editorial Staff

Editor-in-Chief
Jan Iverson
jan.iverson@gia.edu

Editor and Technical Specialist
Brendan M. Laurs
blaurs@gia.edu

Managing Editor
Justin Hunter
justin.hunter@gia.edu

Associate Editor
Stuart D. Overlin
soverlin@gia.edu

Editorial Assistant
Brooke Goedert

Editors, Lab Notes
Thomas M. Moses
Shane F. McClure

Editors, Book Reviews
Susan B. Johnson
Jana E. Miyahira-Smith

Contributing Editors
James E. Shigley
Andy Lucas

Editor-in-Chief Emeritus
Alice S. Keller

Customer Service
Norine Honea
(760) 603-4000, ext. 7306
nhonea@gia.edu

Production Staff

Creative Director
Faizah Bhatti

Image Specialist
Kevin Schumacher

Senior Illustrator
Peter Johnston

Photographer and Photo Editor
Robert Weldon

Multimedia Specialists
Joseph Kaus
Juan Zanahuria

Production Supervisor
Richard Canedo

Video Producer
Pedro Padua

Editorial Review Board

Ahmadjan Abduriyim
Tokyo, Japan

Shigeru Akamatsu
Tokyo, Japan

Edward W. Boehm
Chattanooga, Tennessee

James E. Butler
Washington, DC

Alan T. Collins
London, UK

John L. Emmett
Brush Prairie, Washington

Emmanuel Fritsch
Nantes, France

Jaroslav Hyršl
Prague, Czech Republic

A. J. A. (Bram) Janse
Perth, Australia

E. Alan Jobbins
Caterham, UK

Mary L. Johnson
San Diego, California

Anthony R. Kampf
Los Angeles, California

Robert E. Kane
Helena, Montana

Lore Kiefert
Lucerne, Switzerland

Michael S. Krzemnicki
Basel, Switzerland

Thomas M. Moses
New York, New York

Mark Newton
Coventry, UK

George R. Rossman
Pasadena, California

Kenneth Scarratt
Bangkok, Thailand

James E. Shigley
Carlsbad, California

Christopher P. Smith
New York, New York

Wuyi Wang
New York, New York

Christopher M. Welbourn
Reading, UK

GEMS & GEMOLOGY

gia.edu/gandg

Subscriptions
Copies of the current issue may be purchased for $29.95 plus shipping. Subscriptions are $79.99 for one year (4 issues) in the U.S. and $99.99 elsewhere. Canadian subscribers should add GST. Discounts are available for group subscriptions, GIA alumni, and current GIA students. For institutional rates, contact the Managing Editor. Subscriptions include *G&G*'s monthly gemological e-newsletter, the *G&G eBrief*.

To purchase subscriptions and single issues (print or PDF), visit store.gia.edu or contact Customer Service.

PDF versions of individual articles and sections from Spring 1981 forward can be purchased at gia.metapress.com for $12 each. Visit gia.edu/gandg for free online access to the 1934–2011 subject and author indexes and all 1934–1980 issues.

Database Coverage
Gems & Gemology's five-year impact factor (for 2005–2009) is 1.737, according to the 2010 Thomson Reuters Journal Citation Reports (issued June 2011). *Gems & Gemology* is abstracted in Thomson Reuters products (Current Contents: Physical, Chemical & Earth Sciences and Science Citation Index—Expanded, including the Web of Knowledge) and other databases. For a complete list of sources abstracting *G&G*, go to gia.edu/gandg.

Manuscript Submissions
Gems & Gemology welcomes the submission of articles on all aspects of the field. Please see the Guidelines for Authors at gia.edu/gandg or contact the Editor. Letters on articles published in *Gems & Gemology* are also welcome.

Copyright and Reprint Permission
Abstracting is permitted with credit to the source. Libraries are permitted to photocopy beyond the limits of U.S. copyright law for private use of patrons. Instructors are permitted to photocopy isolated articles for noncommercial classroom use without fee. Copying of the photographs by any means other than traditional photocopying techniques (Xerox, etc.) is prohibited without the express permission of the photographer (where listed) or author of the article in which the photo appears (where no photographer is listed). For other copying, reprint, or republication permission, please contact the Managing Editor.

Gems & Gemology is published quarterly by the Gemological Institute of America, a nonprofit educational organization for the gem and jewelry industry.

Postmaster: Return undeliverable copies of *Gems & Gemology* to GIA, The Robert Mouawad Campus, 5345 Armada Drive, Carlsbad, CA 92008.

Our Canadian goods and service registration number is 126142892RT.

Any opinions expressed in signed articles are understood to be opinions of the authors and not of the publisher.

About the Cover

CVD synthetic diamonds produced by Gemesis Corp. have attained color and clarity grades that are comparable to top-quality natural diamonds. They can be confidently identified with a combination of photoluminescence spectroscopy and UV fluorescence imaging techniques. The 0.24–0.90 ct Gemesis samples on the cover are depicted with a DiamondView image of a 0.57 ct CVD synthetic diamond. Photos by Robert Weldon (Gemesis samples) and GIA's laboratory (DiamondView image).

Printing is by Allen Press, Lawrence, Kansas.
GIA World Headquarters The Robert Mouawad Campus 5345 Armada Drive Carlsbad, CA 92008 USA

© 2012 Gemological Institute of America All rights reserved.

ISSN 0016-626X

FSC
www.fsc.org
MIX
Paper from responsible sources
FSC® C006300

TRANSPARENCY AND SYNTHETIC DIAMONDS

In recent months, the trade press has covered developments involving near-colorless synthetic diamonds—highly sophisticated, high-purity synthetics that cannot be detected using magnification and other traditional means. These stories resonate powerfully with members of the industry, causing some to wonder: Can laboratories still distinguish between natural and synthetic diamonds?

After the development of synthetic diamonds in the mid-1950s, the next major breakthrough happened in 1970, when General Electric announced the first gem-quality synthetic diamond (examined in the Summer 1971 *G&G*, pp. 302–314). Over the next two decades, these products were manufactured in presses using the HPHT (high-pressure, high-temperature) growth method. The stones were mostly small, and the manufacturers—namely GE, Sumitomo, and De Beers—did so for industrial applications and research purposes. But as the quality and size of these goods improved to jewelry standards, a new paradigm emerged.

So did another method of diamond synthesis: chemical vapor deposition (CVD). In this process, carbon atoms from a gas such as methane (CH_4) are deposited onto a small seed platform. The latest generation of CVD products are even more difficult to detect than HPHT synthetics. But even the most sophisticated synthetics can be detected with the advanced analytical tools and expertise found in a handful of gemological laboratories worldwide.

As gem-quality synthetic diamond continues to mature, interesting wrinkles have developed. Faster growth rates and lower production costs. A host of new manufacturers with varying degrees of transparency about the nature of their products. Post-growth treatments intended to enhance color. The possibility of synthetic melee smaller than the cost-effective threshold for grading natural diamonds. Detection measures led to increasingly sophisticated, often secretive countermeasures, a cycle that has escalated into something of an arms race.

For more than 40 years, *Gems & Gemology* has been on the front lines of identifying synthetic diamonds. This issue continues that tradition with three informative articles on the subject. The first is a study by Dr. Wuyi Wang and coauthors on the latest near-colorless CVD synthetics from Florida-based Gemesis Corp. Accompanying it are an overview of the CVD growth process and a report on the world's first "diamond sphere": a synthetic nano-polycrystalline diamond fashioned with pulsed lasers. You'll also find timely features on a recent sapphire rush in Sri Lanka and the emerging Micronesian cultured pearl industry, plus a wide-ranging assortment of Lab Notes and Gem News International updates.

Ultimately, the identification of synthetic diamonds stands at the core of the gem and jewelry industry...

Ultimately, the identification of synthetic diamonds stands at the core of the gem and jewelry industry, and at the core of GIA's mission of ensuring the public trust in gems and jewelry: While some consumers are drawn to the undeniable beauty and affordability of today's mass-produced synthetics, many others insist on diamonds created by nature. But all buyers, regardless of their position on synthetic diamonds, have the right to know exactly what they're purchasing.

Cheers,

Jan Iverson | Editor-in-Chief | jan.iverson@gia.edu

CVD Synthetic Diamonds from Gemesis Corp.

Wuyi Wang, Ulrika F. S. D'Haenens-Johansson, Paul Johnson, Kyaw Soe Moe, Erica Emerson, Mark E. Newton, and Thomas M. Moses

Gemological and spectroscopic properties of CVD synthetic diamonds from Gemesis Corp. were examined. Their color (colorless, near-colorless, and faint, ranging from F to L) and clarity (typically VVS) grades were comparable to those of top natural diamonds, and their average weight was nearly 0.5 ct. Absorption spectra in the mid- and near-infrared regions were free from defect-related features, except for very weak absorption attributed to isolated nitrogen, but all samples were classified as type IIa. Varying intensities of $[Si\text{-}V]^-$ and isolated nitrogen were detected with UV-Vis-NIR absorption spectroscopy. Electron paramagnetic resonance was used to quantify the neutral single substitutional nitrogen content. Photoluminescence spectra were dominated by N-V centers, $[Si\text{-}V]^-$, H3, and many unassigned weak emissions. The combination of optical centers strongly suggests that post-growth treatments were applied to improve color and transparency. PL spectroscopy at low temperature and UV fluorescence imaging are critical in separating these synthetic products from their natural counterparts.

Along with the conventional high-pressure, high-temperature (HPHT) growth technique, single-crystal synthetic diamond can be produced using chemical vapor deposition (CVD). Technological advances and a greater understanding of the crystal growth processes have led to significant improvements in quality over the last decade. Today, CVD-grown faceted synthetic diamonds are present in the jewelry market in a variety of colors and sizes (e.g., Wang et al., 2003, 2005; Martineau et al., 2004). Furthermore, post-growth treatments to improve the color and transparency of these materials have been investigated.

In November 2010 Gemesis Corp., a well-known manufacturer of gem-quality HPHT synthetic diamonds, announced plans to market colorless and near-colorless CVD synthetics (Graff, 2010). Since March 2012, the company has sold mounted and loose CVD synthetic diamonds (e.g., figure 1).

Because of the high cost and difficulty to manufacture colorless HPHT synthetics, growth methods have traditionally focused on fancy colors. However, now it is colorless and near-colorless CVD synthetics, such as those developed by Gemesis, that pose the greatest commercial challenge to natural diamonds (treated and untreated) of comparable quality. This study follows an initial report by Wang and Moses (2011) and presents gemological characteristics and spectroscopic features of new CVD synthetics from Gemesis. Key identification features that help separate these products from natural diamonds are also discussed.

CVD Growth. While HPHT growth takes place under temperature and pressure conditions in which diamond is the stable phase of carbon, the CVD technique enables growth under conditions where diamond is metastable with respect to graphite. This means that although diamond is kinetically stable, it is thermodynamically unstable. The technique is based on a gas-phase chemical reaction involving a hydrocarbon gas (such as methane) in an excess of hydrogen gas occurring above a substrate. For single-crystal synthetic diamond growth the substrate is also a synthetic diamond, usually in the form of a {100}-oriented polished plate. Multiple substrates can be placed simultaneously in the CVD reaction chamber.

See end of article for About the Authors and Acknowledgments.
Gems & Gemology, Vol. 48, No. 2, pp. 80–97,
http://dx.doi.org/10.5741/GEMS.48.2.80.
© 2012 Gemological Institute of America

Figure 1. These faceted CVD synthetic diamond samples (0.24–0.90 ct) obtained from Gemesis Corp. were examined in this study. Color grades are mainly in the range of colorless to near-colorless, and clarity is dominantly in VVS or better categories. These features are comparable to top-quality natural counterparts. Composite photo by Jian Xin (Jae) Liao.

The gas-phase precursor molecules can be activated in a variety of ways, typically by microwaves. Once the complex chain of reactions has been initiated, carbon atoms are added to the substrate (see Overview article on pp. 124–127 of this issue). The growth parameters are optimized to ensure the formation of a tetrahedrally bonded (sp^3) carbon lattice, of which diamond is composed, rather than sp^2-bonded graphitic material, and that the latter material is selectively etched. The reactions occur at pressures of 10–200 torr, and the substrate is held at temperatures ranging from 700 to 1,000°C during the active growth period.

One of the main advantages of the CVD method is the ability to dope the synthesized diamond by the controlled addition of gases containing the intended impurity atom (e.g., nitrogen, silicon, or boron). Nevertheless, unintentional impurity doping can also occur due to their presence in the gas sources or the reactor components. Goodwin and Butler (1997) and Butler et al. (2009) provided a thorough review of the important features of the synthesis environment and critical aspects of the growth process.

HPHT Processing for the Removal of Brown Color. Interest in the cause of brown color in both natural and CVD-grown type IIa diamond has heightened ever since it was reported that HPHT treatment could decolorize these goods and greatly improve their commercial value (Moses et al., 1999; Fisher and Spits, 2000; Wang et al., 2003; Martineau et al., 2004). The color arises from a gradual, featureless rise in the absorption spectrum from ~1200 nm to the diamond absorption edge at ~225 nm. No specific threshold for the rise has been identified, and it has been suggested that the absorption originates from extended defects rather than impurity-related point defects (Hounsome et al., 2006). Most brown CVD synthetics also show broad bands at 365 and 520 nm, and absorption from the latter band may further contribute to the color intensity (Martineau et al., 2004).

The brown color in natural diamond is often concentrated along slip bands (though not all plastically deformed diamonds are brown), which suggests that dislocations or defects produced by movement of the dislocations are responsible for the color (Collins et al.,

2000). However, analysis of the dislocation densities (~10^9/cm^2) and their expected absorption strengths indicates that they alone cannot account for the observed color intensities (Fall et al., 2002; Willems et al., 2006; Mäki et al., 2007; Fisher et al., 2009). Other studies have proposed that the brown color is produced by absorption from vacancy clusters or {111}-oriented vacancy discs also found in heavily distorted regions of the diamond lattice (Avalos and Dannefaer, 2003; Hounsome et al., 2006; Bangert et al., 2009). The presence of clusters in brown natural diamond has been confirmed by positron annihilation experiments, which demonstrated that the smaller clusters are optically active. These clusters have been shown to anneal out and/or aggregate to form larger, optically inactive clusters at the HPHT annealing temperatures (up to ~2500°C) required to remove brown color from natural diamond (Avalos and Dannefaer, 2003; Fisher et al., 2009).

In Brief

- Gemesis Corp. has sold mounted and loose CVD synthetic diamonds since March 2012.
- The latest generation products examined for this report ranged up to 0.90 ct, and most were near-colorless and had clarity grades between IF and VVS; all but one were round brilliants.
- Spectroscopic evidence indicates a likelihood that these CVD synthetics have undergone post-growth HPHT processing to enhance their color and possibly their clarity.
- This material is conclusively identified by PL spectroscopy and DiamondView fluorescence images.

X-ray topography of brown single-crystal as-grown CVD synthetic diamond has not shown significant plastic deformation (Martineau et al., 2004). Dislocations in CVD material appear to have nucleated at the interface with the substrate, thus forming approximately perpendicular to the growth surface (Martineau et al., 2004, 2009). The dislocation densities in as-grown CVD synthetic diamond are relatively low (~10^4–10^6/cm^2) and thus are not considered the main cause of brown color. Positron annihilation studies have shown that brown as-grown CVD synthetics may contain vacancy clusters of various sizes, ranging from monovacancies to nanometer-size voids (Mäki et al., 2007). The smaller clusters anneal out in a temperature range (1400–1600°C) similar to that at which the brown color is removed in CVD synthetic diamond (Charles et al., 2004; Martineau et al., 2004; Mäki et al., 2007). Yet it has not been conclusively demonstrated that these clusters are responsible for coloration, especially as several other point defects in CVD synthetic diamond are created and destroyed at these temperatures. The difference in the temperature stability of color-causing defects between natural and CVD synthetic brown diamond is not yet understood, and theoretical and experimental studies are ongoing.

Gem-quality CVD specimens with post-growth treatments have occasionally been submitted to gem laboratories for grading (Chadwick, 2008a,b). The purpose of the treatment is not limited to changing the color from brown to colorless, as intense pink CVD synthetic diamonds from Apollo (Wang et al., 2010) have also shown evidence of treatment with multiple steps.

MATERIALS AND METHODS

For this investigation, we purchased 16 faceted CVD synthetic diamonds from Gemesis (table 1; see also figure 1). These ranged from 0.24 to 0.90 ct, with an average weight of 0.46 ct. The majority (94%) were cut as round brilliants, with depths of 2.41 to 3.69 mm, averaging 2.93 mm. These CVD synthetics are representative of the current production being sold on the Gemesis website.

Experienced members of GIA's diamond grading staff determined color and clarity grades using GIA's grading system. Internal features were examined with a standard gemological binocular microscope and a research-grade Nikon microscope, using a variety of lighting techniques, including darkfield and fiber-optic illumination and polarization. Reactions to UV radiation were tested in a darkened room with a conventional 4 watt combination long-wave (365 nm) and short-wave (254 nm) UV lamp. We also examined the samples for fluorescence, phosphorescence, and crystal growth characteristics using the Diamond Trading Company (DTC) DiamondView instrument (Welbourn et al., 1996). Phosphorescence images were collected with a 0.1 second delay and 5 seconds of exposure time.

Phosphorescence spectra were collected on all samples at room temperature with an Ocean Optics HR4000 spectrometer. After illuminating the samples for 30 seconds with an Avantes AvaLight-DH-S deuterium-halogen light source (emission wave-

TABLE 1. CVD synthetic diamonds from Gemesis Corp. examined in this study.

Sample	Weight (ct)	Color	Cut	Clarity	UV fluorescence		N_S^0 (ppb)	$[NVH]^-$ (ppb)
					Long-wave	Short-wave		
GS02	0.30	G	Round	VVS_1	Inert	Very weak green	na[a]	na
GS03	0.41	F	Round	VVS_2	Inert	Very weak green	na	na
GS04	0.26	G	Round	VVS_1	Very weak green	Weak green	na	na
GS05	0.31	G	Round	IF	Inert	Very weak green	na	na
GS06	0.24	G	Round	VS_1	Inert	Very weak green	na	na
GS07	0.24	F	Round	VVS_2	Inert	Very weak green	72 ± 10	<5
GS08	0.39	F	Round	VVS_2	Inert	Very weak green	170 ± 25	<10
GS09	0.48	G	Round	VS_1	Inert	Weak green	180 ± 20	<10
GS10	0.41	G	Round	VVS_1	Very weak green	Weak green	180 ± 20	<10
GS11	0.47	G	Round	VVS_2	Very weak green	Weak green	150 ± 20	<5
GS12	0.47	I	Round	VS_1	Very weak green	Weak green	220 ± 30	<10
GS13	0.47	G	Round	VVS_1	Inert	Very weak green	170 ± 25	<10
GS14	0.39	G	Round	VS_2	Inert	Weak green	150 ± 20	<5
GS15	0.70	I	Round	VVS_2	Weak green	Moderate green	280 ± 40	<10
GS16	0.83	J	Round	VVS_2	Inert	Weak green	340 ± 30	<10
GS17	0.90	L	Rectangle	VVS_2	Very weak green	Weak green	450 ± 50	<15

[a] *Abbreviation: na = not analyzed.*

length of 215–2500 nm), we began data collection. A 1 second spectral integration time was used, and data collection continued for 60–100 seconds.

Infrared absorption spectroscopy of all samples was performed in the mid-IR (6000–400 cm^{-1}, at 1 cm^{-1} resolution) and near-IR (up to 11,000 cm^{-1}, at 4 cm^{-1} resolution) ranges at room temperature with a Thermo Nicolet Nexus 6700 Fourier-transform infrared (FTIR) spectrometer equipped with KBr and quartz beam splitters. Samples were first cleaned in an ultrasonic bath of acetone and dried with compressed air. A DRIFT (diffuse reflectance infrared Fourier transform) unit focused the incident beam on the sample, and up to 256 spectral scans were averaged for increased signal-to-noise ratios. Additionally, the sample chamber was purged with nitrogen gas. The mid- and near-IR spectra were normalized relative to the two- and three-phonon diamond absorptions, enabling quantitative analysis of impurity-related peak intensities.

Continuous-wave electron paramagnetic resonance (EPR) was used to investigate paramagnetic point defects (see box A) in 11 of the samples. Spectra were acquired at room temperature using a commercial X-band (~9.7 GHz) Bruker EMX-E spectrometer equipped with a super-high-Q (SHQ) spherical resonant cavity and a Bruker ER 041 XG-H microwave bridge. The samples were held in dual-axis goniometers that enabled accurate positioning within the EPR cavity. Further details regarding signal optimization and the simulation and fitting of EPR spectra of paramagnetic defects is described by Edmonds et al. (2008). Defect concentrations in the study samples were calculated by comparing their EPR-integrated intensities to those of a type Ib HPHT synthetic diamond (single growth sector) reference sample with a known concentration of neutral single-substitutional nitrogen (N_S^0). The N_S^0 concentration of this sample was originally determined using EPR and infrared absorption spectroscopy.

Absorption spectra in the ultraviolet through visible to near-infrared range (UV-Vis-NIR, 250–1000 nm) were recorded on all samples with a custom-built instrument using an Avantes AvaSpec-2048 spectrometer and two broadband light sources (AvaLight-HAL and AvaLight-DH-S). This high-resolution apparatus enabled the detection of very weak and sharp absorptions at liquid-nitrogen temperature (77 K). The sampling interval in this four-channel device was 0.04–0.07 nm, depending on the specific wavelength ranges, with a 10 µm entrance slit width. Using 200 scans per spectrum, we achieved spectral resolution better than 0.2 nm, as well as a very good signal-to-noise ratio. Samples were immersed in a specially designed bath containing multiple layers of liquid

BOX A: ELECTRON PARAMAGNETIC RESONANCE OF POINT DEFECTS IN DIAMOND

EPR spectroscopy is an extremely sensitive quantitative tool for chemical and structural identification of paramagnetic point defects in diamond and other nonmetallic materials. A paramagnetic defect in diamond, such as the single substitutional nitrogen center (N_S^0 or C-center), contains one or more unpaired electrons. An electron has an intrinsic magnetic moment, which can be visualized as a small bar magnet or compass needle. This magnetic moment arises from the quantum mechanical property called *spin* (*S*). Thus, EPR is also known as electron spin resonance (ESR). An electron has an intrinsic spin $S = ½$. In systems containing more than one electron, the resultant total spin can be zero (i.e., two electrons in a chemical bond) or non-zero. In diamond, covalent bonds are formed between neighboring carbon atoms. Each carbon atom has four electrons available for bonding and "points" four hybrid atomic orbitals at neighboring atoms. These orbitals on neighboring atoms interact, producing bonding and anti-bonding molecular orbitals between neighbors. Each bonding molecular orbital accommodates two anti-parallel paired electrons (a consequence of the Pauli Exclusion Principle) with an overall spin $S = 0$ (figure A-1, left). The covalent bonds produced by the carbon atoms sharing electrons are very strong. The anti-bonding orbital is much higher in energy and is empty. Thus pure diamond is not EPR-active.

Nitrogen contains one more electron than carbon, and when it substitutes for a carbon atom in the diamond lattice (N_S^0), it can bond with neighboring carbons, but one electron is left over, resulting in an overall spin of $S = ½$. This lone electron is accommodated in an anti-bonding orbital formed between the nitrogen and one of its carbon neighbors. This unpaired electron has two spin states split by a magnetic field, the lower energy one corresponding to the magnetic moment of the electron parallel to the applied field, and the upper one anti-parallel (figure A-1, right). The interaction between the applied magnetic field and the electron spin (magnetic moment) is known as the (anomalous) *Zeeman effect*. Magnetic dipole transitions between the two spin states can be driven with microwave radiation that matches the energy separation. Usually the magnetic field is swept (i.e., increased or decreased in a swift manner across a chosen magnetic field range) to produce an EPR spectrum; when the energy of the fixed frequency microwave radiation matches the separation of the levels, an EPR signal is observed.

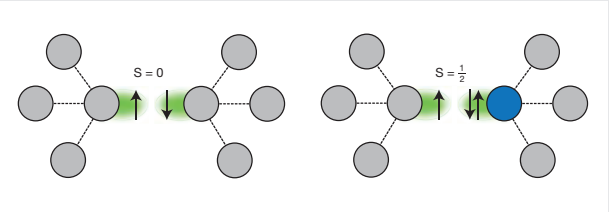

Figure A-1. Pure diamond is not EPR-active because each bonding molecular orbital accommodates two anti-parallel paired electrons with an overall spin S = *0 (left). When a nitrogen atom substitutes for a carbon atom in the diamond lattice (N_S^0) the additional electron is accommodated in an anti-bonding orbital formed between the nitrogen and one of its carbon neighbors. This unpaired electron has a spin* S = *½, so N_S^0 is EPR-active (right).*

Fortunately, an unpaired electron is highly sensitive to its environment, and it is these interactions that produce more complex spectra with a wealth of information about the nature and constituents of the defects under investigation. For example, an unpaired electron can interact with neighboring nuclei that possess nuclear spin. This produces a local magnetic field, which will have the effect of either increasing or decreasing the effective magnetic field experienced by the unpaired electron, depending on the relative orientation of the two spins. Consequently, additional "satellite" resonance lines due to nuclei with nuclear spin will appear about the center of the spectrum.

EPR has a very high sensitivity, and N_S^0 defect concentrations of ~1 ppb can be routinely measured in minutes. Usually the spectra contain overlapping contributions from several defects, but these can be deconvolved, facilitating detailed quantitative analysis even when multiple defect species are present in the same sample.

nitrogen (patent pending), ensuring consistent temperature and a stable environment free of nitrogen gas bubbles.

A commercial Renishaw InVia Raman confocal microspectrometer, equipped with the liquid nitrogen bath setup used for UV-Vis-NIR spectroscopy, was used for low-temperature photoluminescence (PL) spectral analysis of all samples. Various defect centers were excited using five excitation wavelengths produced by four laser systems. An Ar-ion laser was operated at excitation wavelengths of 488.0 nm (for the 490–850 nm range) and 514.5 nm (for the 517–850 nm range). PL spectra were collected in the 640–850 nm range using an He-Ne laser (632.8 nm), and in the 835–1000 nm range using a diode laser (830.0 nm). In addition, an He-Cd metal-vapor laser (324.8 nm) was used for the 370–800 nm range. Up to three scans were accumulated for each spectrum to improve the signal-to-noise ratio.

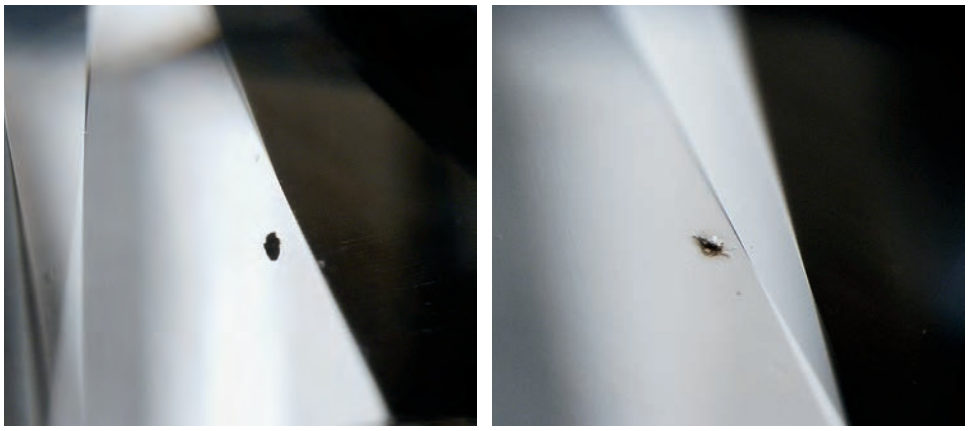

Figure 2. Internal features in the CVD synthetic diamonds consisted of small (generally <50 µm) irregular black inclusions (left, image width 1.0 mm), likely composed of non-diamond carbon. Radial fractures surrounded some of the larger inclusions (right, image width 1.3 mm), a result of strong, highly localized strain. Photomicrographs by W. Wang.

RESULTS

Color and Shape. Three of the 16 samples were graded as colorless (F color) and 12 as near-colorless (G–J; see table 1). Only one was faintly colored (L), with the color falling within the yellow hue range. The three largest diamonds had the poorest color grades. The largest sample (0.90 ct) was the only one polished into a rectangular shape; the other 15 samples were round brilliants.

Clarity. The samples showed very high clarity (again, see table 1). Twelve of them had clarity grades between IF and VVS. This marked the first time GIA has given an IF grade to a CVD synthetic diamond (sample GS05, 0.31 ct). Only four samples fell in the VS category. Clarity grades in those samples were lowered by small black inclusions with irregular shapes (probably non-diamond carbon; figure 2). Most of these inclusions were smaller than 50 µm. Small petal-shaped radial fractures were occasionally observed around some of the larger inclusions. It is noteworthy that none of the samples contained noticeable fractures.

Birefringence. Dislocation-related graining is a common feature in many CVD synthetics. Nevertheless, graining was not observed in these Gemesis samples. Microscopic imaging with crossed polarizers did reveal relatively weak anomalous double refraction patterns compared with those of CVD samples in previous studies (Wang et al., 2003, 2005, 2010). These irregular, linear, or occasionally "tatami" patterns were characterized by low-order interference colors, including gray and blue (figure 3, left and center). Extremely high-order interference colors with characteristic symmetrical patterns were only observed around small black inclusions, a good indication of increased strain in highly localized regions (figure 3, right).

Fluorescence and Phosphorescence. A remarkable property of the Gemesis synthetics was their response to UV radiation (table 1). Unlike the orange-red fluo-

Figure 3. Relatively weak anomalous double refraction was seen when viewing these synthetic diamonds with crossed polarizers, showing low-order gray and blue interference colors with irregular, linear, or occasionally "tatami" type patterns (left and center, image widths 3.3 and 3.1 mm, respectively). Petal-shaped regions of birefringence with characteristic symmetrical patterns were sometimes observed around small black inclusions (right, image width 0.9 mm). Photomicrographs by W. Wang.

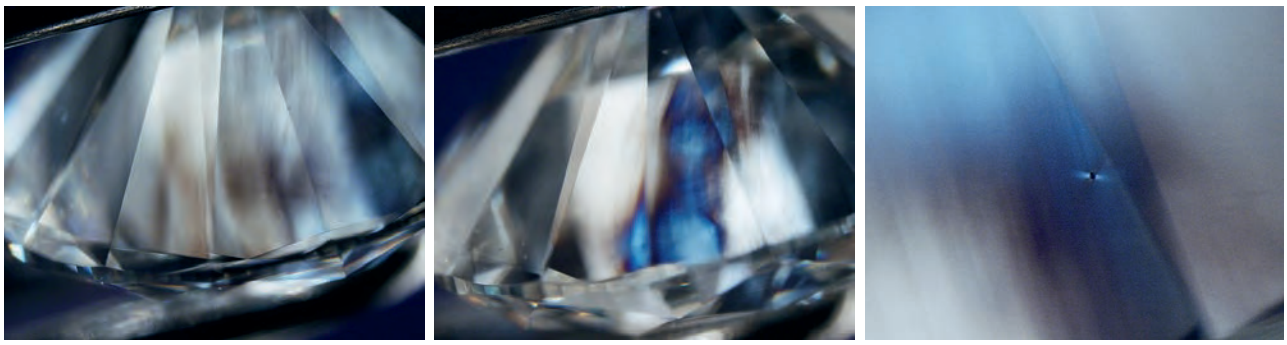

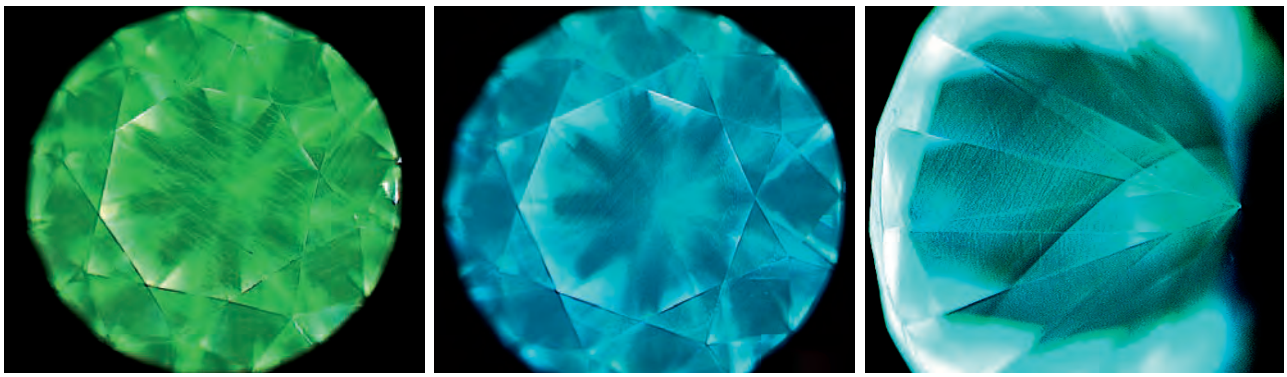

Figure 4. In the DiamondView, three of the synthetic diamond samples were dominated by green fluorescence (e.g., left, 0.30 ct). Four showed strong blue fluorescence (center, 0.47 ct), and the other samples showed transitional features. Even in those dominated by blue fluorescence, the green striations were still clearly observable. In 12 of the 16 samples, the DiamondView revealed a sharp, well-defined fluorescence boundary with a ~45° angle to the table face (right, 0.41 ct). One side of the boundary showed normal green-blue fluorescence, while the other had much weaker fluorescence. Images by W. Wang.

rescence commonly associated with CVD material, the samples in this study displayed green fluorescence (mostly of weak to very weak intensity) to short-wave UV. Additionally, six samples fluoresced weak to very weak green when exposed to long-wave UV radiation, while the remainder were inert.

The high-intensity ultra-short UV wavelength of the DTC DiamondView (~225 nm radiation) revealed growth striations in all the samples, with green fluorescence of varying intensity. An alternating pattern of very narrow green striations was occasionally distributed throughout the whole specimen (figure 4, left). Three of the synthetics were dominated by green fluorescence and four showed strong blue fluorescence, while other samples showed transitional features. Even in those dominated by blue fluorescence, the green striations were still clearly visible (figure 4, center). In 12 of the 16 samples, the DiamondView fluorescence image also revealed a sharp, well-defined boundary separating areas showing dominant green fluorescence or where the fluorescence was significantly weaker or nearly undetectable (figure 4, right). Similar banding structures were reported in Apollo CVD synthetics (e.g., Wang et al., 2010), but with a different orientation of the bands relative to the table facet. The bands in the Apollo samples were mostly aligned parallel to the table, while those in Gemesis samples intersected the table at ~45°. The four samples in this study that did not show the banding structure were among the smallest pieces (0.24–0.31 ct).

The Gemesis CVD synthetics displayed evenly distributed blue phosphorescence of varying inten-

Figure 5. Blue phosphorescence with varying intensity, observed in the DiamondView, was distributed evenly throughout each of the synthetic diamonds, as shown here for samples weighing 0.26, 0.39, and 0.24 ct. Images by W. Wang.

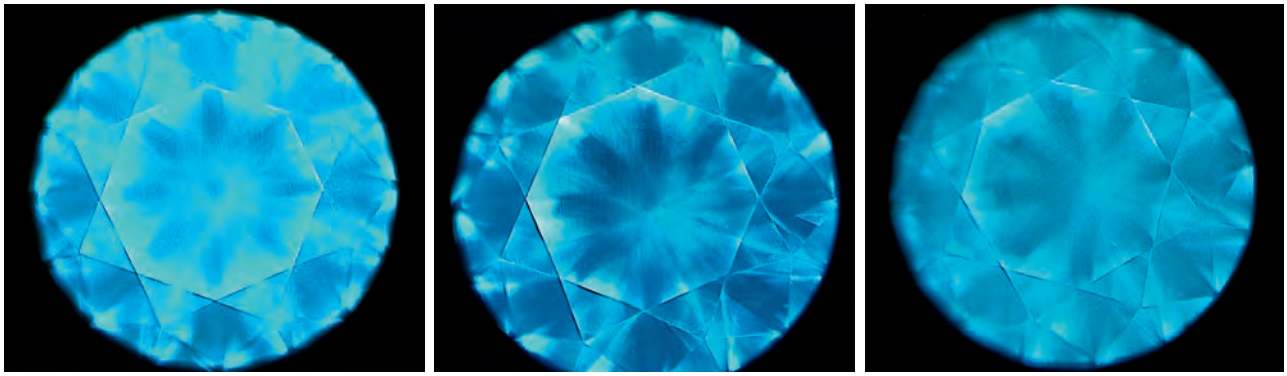

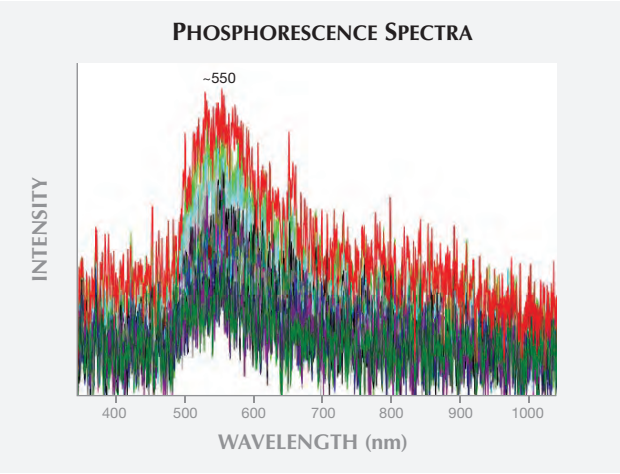

Figure 6. The five synthetic diamonds that showed strong phosphorescence in the DiamondView had a broad but clear band centered at ~550 nm in their phosphorescence spectra.

sity (figure 5). Only weak phosphorescence was observed in the samples dominated by green fluorescence. The phosphorescence was markedly stronger in those that displayed intense blue fluorescence. Phosphorescence spectra were dominated by a broad band centered at ~550 nm, which was best defined in the samples that showed strong emissions in the DiamondView (figure 6).

Infrared Absorption Spectroscopy. The Gemesis samples displayed relatively featureless absorption spectra in the infrared region, unlike those reported in CVD synthetics from other sources (Wang et al., 2003, 2005, 2010; Martineau et al., 2004). Defect-related absorptions were only observed in the 1500–1100 cm^{-1} region. These features (e.g., figure 7) included a relatively sharp peak at 1332 cm^{-1} and another peak at 1344 cm^{-1}, both attributed to different charge states of the single substitutional nitrogen defect. The 1332 cm^{-1} absorption is due to the positive charge state, N_S^+ (Lawson et al., 1998), while the 1344 cm^{-1} line is associated with the neutral charge state, N_S^0 (Collins et al., 1987).

While the 1332 cm^{-1} peak was recorded in each sample, the 1344 cm^{-1} peak was not detected in two of them (GS02 and GS07). The intensity of the 1344 cm^{-1} absorption varied from sample to sample, but generally fell below 0.01 cm^{-1}, corresponding to an N_S^0 concentration of <1 ppm carbon atoms. Interestingly, we did not detect the 3123 cm^{-1} local vibration mode attributed to the neutral charge state of the nitrogen vacancy-hydrogen-complex $[N\text{-}V\text{-}H]^0$, as reported previously in CVD synthetic diamond (Fuchs et al., 1995a,b; Wang et al., 2003; Martineau et al., 2004; Khan et al., 2009, 2010; Liggins, 2010). Furthermore, the absorption line at 3107 cm^{-1}, which can sometimes be introduced into a brown CVD synthetic after HPHT treatment, was not observed (Charles et al., 2004; Martineau et al., 2004). Spectroscopy in the near-infrared region did not reveal any other absorption peaks previously reported in CVD synthetics, such as lines at 8753, 7354, 6856, 6524, and 5564 cm^{-1} (Wang et al., 2003; Martineau et al., 2004).

Electron Paramagnetic Resonance Spectroscopy. EPR spectroscopy is useful for identifying the presence of CVD-specific paramagnetic defects (e.g., Glover et al., 2003, 2004; Edmonds et al., 2008; D'Haenens-Johansson et al., 2010, 2011). This technique can be used to quantify the concentrations of N_S^0 (Smith et al., 1959; Cox et al., 1994) and the negatively charged state of the nitrogen-vacancy-hydrogen defect ($[N\text{-}V\text{-}H]^-$; Glover et al., 2003); results for the 11 Gemesis samples tested are reported in table 1. The EPR spectrum for GS11, shown in figure 8, is representative of the samples. The N_S^0 concentrations ranged from as low as 72 ± 10 ppb (GS07, F color) to as high as 450 ± 50 ppb (GS17, L color). The average concentration was 215 ppb, with a standard deviation of 105 ppb. Although there was not a wide distribution of color grades for the samples tested (F–L, with 45% having a G color), comparison between the grades and the N_S^0 concentrations suggest that as the concentration increased the grade fell lower on the color scale. This is understandable, since isolated nitrogen is known

Figure 7. Absorption spectra of the Gemesis synthetic diamonds in the middle and near-infrared regions are very "clean." Only weak absorptions at 1344 and 1332 cm^{-1} (due to isolated nitrogen) were detected in some samples. Spectra are shifted vertically for clarity.

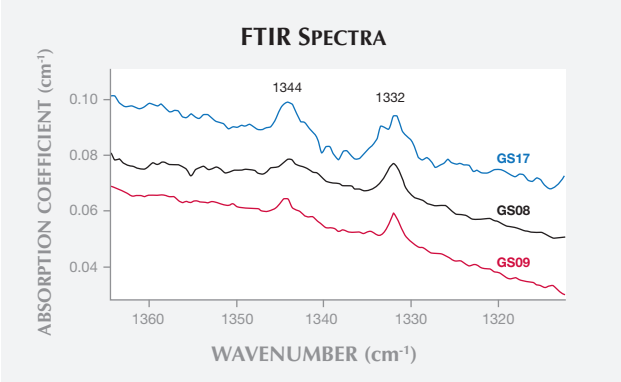

to impart yellow color in diamond. The $[N\text{-}V\text{-}H]^-$ center was not detected by EPR, with upper concentration limits ranging from 5 to 15 ppb (table 1).

UV-Vis-NIR Absorption Spectroscopy. Since the faceting of the samples made it impossible to accurately determine the pathlength of the beam, the absorbance of the samples could not be converted into absorption coefficients, as was done with the FTIR absorption data, limiting quantitative data analysis. Nevertheless, several absorption features were identified, indicating the presence of certain impurity defects.

A gradual, shallow increase was observed in the absorption spectra from approximately 300 nm down to the diamond absorption edge at ~225 nm (figure 9A). Defect-related absorptions were detected in the infrared and deep-UV regions, with the visible region (400–700 nm) appearing featureless. Notably absent were the absorption lines at 586 nm (different from the 596/597 nm doublet sometimes observed in PL) and 625 nm, which have been reported in some brown CVD synthetics (Wang et al., 2003; Martineau et al., 2004).

A broad absorption band centered at ~270 nm and sharp peaks at 271.5 and 268.0 nm were detected in all of the samples (again, see figure 9A). These absorptions are attributed to the isolated nitrogen impurity in diamond (Dyer et al., 1965). The intensity of these absorption peaks varied significantly, though they were more pronounced in samples with higher N_S^0 concentrations. It is noteworthy that the ~270 nm band was detectable even in samples with very low nitrogen concentrations, such as GS07 (72 ± 10 ppb). This synthetic diamond had a relatively low carat weight (0.24 ct), so its path length was not expected to be longer than that of the others, which might have skewed the results. These observations demonstrated the effectiveness of UV-Vis-NIR absorption spectroscopy in detecting traces of isolated nitrogen, even in samples weighing ~0.5 ct. Readily detectable N_S concentrations are rare in natural diamonds.

An absorption doublet at 736.6 and 736.9 nm (figure 9B) was detected in 14 of the samples (absent from GS11 and GS17). This feature, which was active in both absorption and luminescence, has been attributed to the negative charge state of the silicon split-vacancy center, $[Si\text{-}V]^-$ (Vavilov et al., 1980; Clark et al., 1995; Goss et al., 1996). The $[Si\text{-}V]^-$ center is frequently observed in the absorption and PL spectra of CVD synthetics (Wang et al., 2003, 2005, 2007; Martineau et al., 2004). The strongest $[Si\text{-}V]^-$ absorbance was recorded in

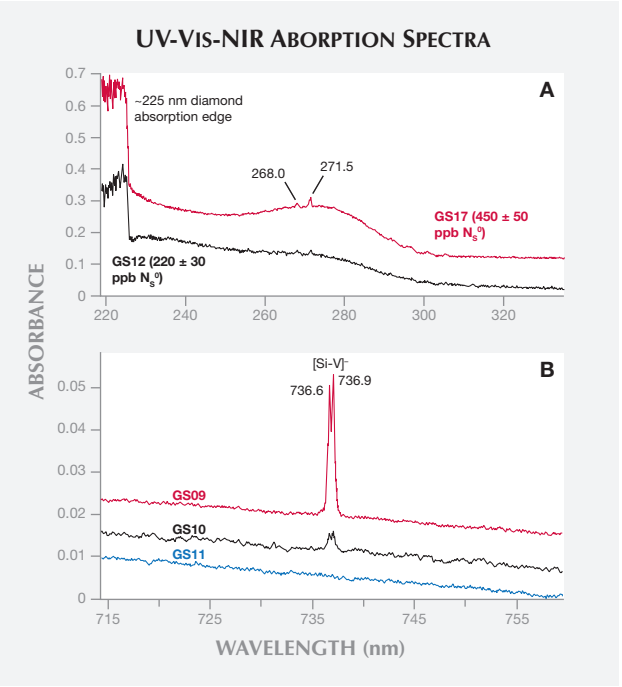

Figure 9. UV-Vis-NIR absorption spectroscopy of the Gemesis synthetic diamonds at liquid-nitrogen temperature revealed a broad absorption band centered ~270 nm from isolated nitrogen in every sample (A). Sharp doublet absorptions at 736.6/736.9 nm from the $[Si\text{-}V]^-$ center were present in most samples (B). Spectra are shifted vertically for clarity.

Figure 8. The EPR spectrum of sample GS11 (labeled "experimental") shown here is representative of all the analyzed Gemesis samples and was taken with the magnetic field along [111]. The relative intensities and positions of the spectral lines agreed with those of the simulated spectrum for N_S^0, identifying the paramagnetic species and allowing the determination of N_S^0 concentrations (see table 1). No other paramagnetic defects were detected.

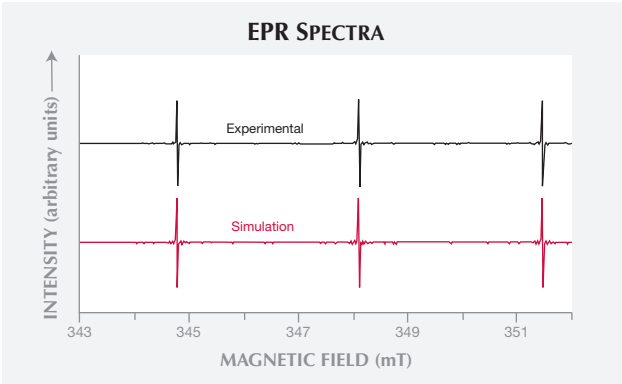

samples GS03, GS08, GS09, and GS14. Even so, there was no clear correlation between diamond color grades and concentrations of Si-related defects.

Photoluminescence. With an appropriate excitation wavelength, the detection limit for optical emission peaks from luminescence defects may be significantly lower than that for their absorption peaks, revealing the presence of otherwise unexpected defects. The excitation efficiencies of the zero phonon lines (ZPLs) depend on the excitation wavelength chosen. Therefore, five different excitations were used to collect PL spectra, spanning the ultraviolet through infrared regions, so certain emission centers were detected under multiple excitation conditions. The major PL features are summarized below on the basis of individual laser excitation in each defect's most sensitive region.

The PL spectra acquired using 514.5 nm (green) laser excitation are shown in figure 10A. The ZPL emissions for $[Si\text{-}V]^-$ (736.6/736.9 nm doublet) and nitrogen-vacancy centers in neutral ($[N\text{-}V]^0$ at 574.9 nm) and negative ($[N\text{-}V]^-$ at 637.0 nm) states dominated the spectra. A broad asymmetric band at 766 nm was also observed. This band is part of the vibronic structure of $[Si\text{-}V]^-$, and thus the feature's intensity correlated with that of the $[Si\text{-}V]^-$ ZPL (Clark and Dickerson, 1991). In 13 of the samples (81%), the 637.0 nm ZPL was more intense than the 574.9 nm peak, with a ratio ranging from 1.09 to 2.97. For the three remaining samples (GS10, GS12, and GS14), this ratio fell in the 0.44–0.99 range. A doublet emission at 596.5 and 597.0 nm, previously documented as a common feature of colorless, near-colorless, and brown as-grown CVD synthetics (Wang et al., 2003, 2007; Martineau et al., 2004), was not observed in these Gemesis samples. Numerous emission peaks were also observed in the 520–580 nm region, including peaks at 525.4, 535.1, 540.4, 546.1, and 572.9 nm (figure 10B). The defects responsible for these emission lines have not been identified.

Figure 10. In photoluminescence spectra of the Gemesis synthetic diamonds collected with 514.5 nm laser excitation at liquid-nitrogen temperature, emissions from N-V and $[Si\text{-}V]^-$ centers were observed in each sample (A). Numerous sharp peaks were recorded in the 520–580 nm region, including major ones at 525.4, 535.1, 540.4, 546.1, and 572.9 nm (B). The assignment of these emissions remains unclear.

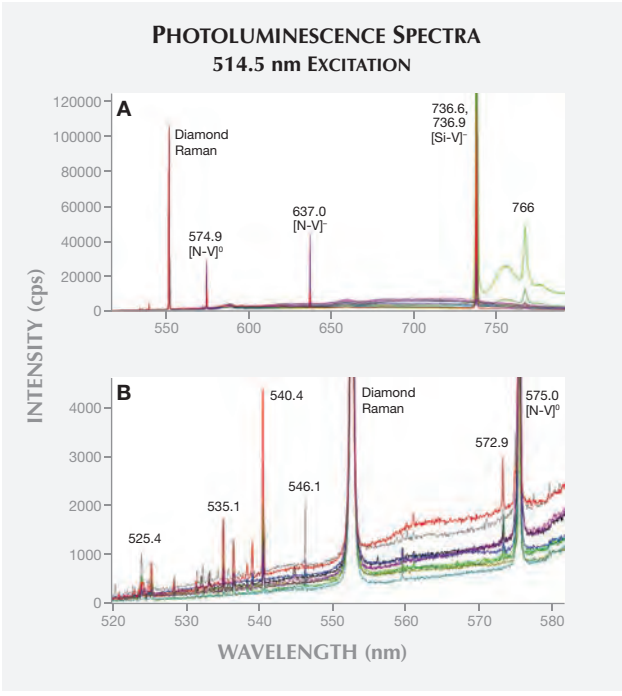

ZPL widths are sensitive to lattice dislocations in diamond, widening with increased local strain. Fisher et al. (2006) reported the effective use of the full width at half maximum (FWHM) of the neutral vacancy defect (GR1) in probing the strain in natural and HPHT-processed natural diamonds. GR1 is not detected in CVD synthetic diamond unless irradiated, so this feature could not be used to characterize the strain of the samples in this study. However, Fisher et al. (2006) also noted that the FWHM for the N-V peaks corresponded with those measured for GR1 (in milli-electron volts). For the Gemesis samples in our investigation, the FWHM of the 574.9 nm peak showed a limited variation of 0.20–0.30 nm, with an average of 0.24 nm. In contrast, the FWHM of the 637.0 nm emission line varied from 0.16 to 0.33 nm, with an average of 0.21 nm. In these samples, a positive correlation existed between widths of these two peaks, and their plots overlapped the narrowest FWHM data for natural type IIa diamonds (figure 11). In contrast, the same peaks in both pink and colorless CVD synthetics by Apollo (Wang et al., 2007, 2010, and unpublished data) are much broader than those of the Gemesis CVD samples we studied, and overlap the broad FWHM data of natural type IIa diamonds.

The PL spectra taken with 324.8 nm laser excitation are shown in figure 12. This laser wavelength excited a very weak luminescence line at 415 nm in nine of the samples (56%). This line has been attributed to the N3 defect in diamond, which consists of three nitrogen atoms in a {111} plane, bonded to a single vacancy (Davies, 1974; Davies et al., 1978; Mar-

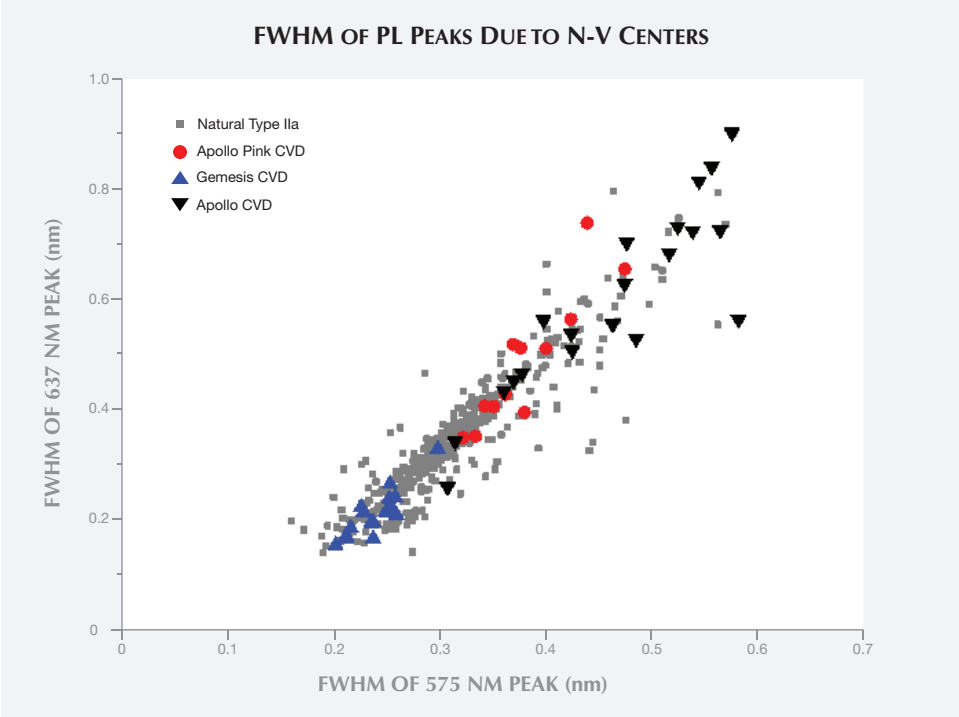

Figure 11. The width of the PL peaks due to N-V centers in the Gemesis synthetic diamonds overlapped the narrowest values in natural type IIa diamonds. These peaks in the Gemesis CVD synthetics were clearly narrower than those documented in Apollo samples.

tineau et al., 2004). An additional series of lines in the 451–459 nm range was detected in all of the samples; these were previously reported in HPHT-processed CVD synthetics by Martineau et al. (2004). These lines have not been reported in natural diamond.

PL spectra collected using blue laser (488.0 nm) excitation revealed a relatively strong emission at 503.2 nm, attributed to the H3 defect (figure 13). Many unidentified sharp peaks were recorded in the 495–535 nm region. Several of them, including a 524.5 nm peak, were excited by both the 488.0 nm and 514.5 nm lasers. These are probably part of all sharp emissions that continuously spread from 580 nm to the high-energy side; the 520–580 nm region was recorded in 514.5 nm laser excitation PL spectra (figure 10B).

The only features detected using 633.0 nm laser excitation were the 736.6/736.9 nm doublet from the

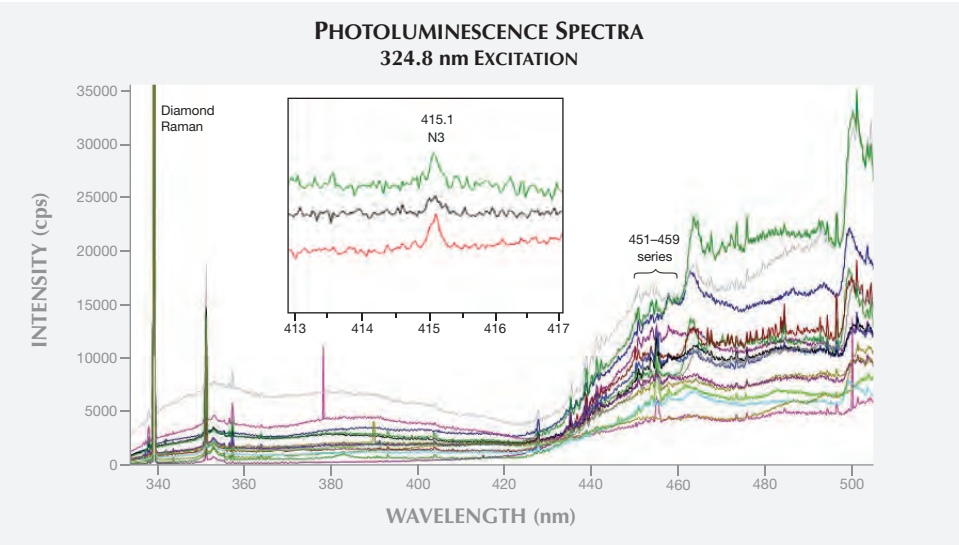

Figure 12. A weak emission at 415.1 nm from the N3 optical center was detected in many of the Gemesis synthetic diamonds using 324.8 nm laser excitation.

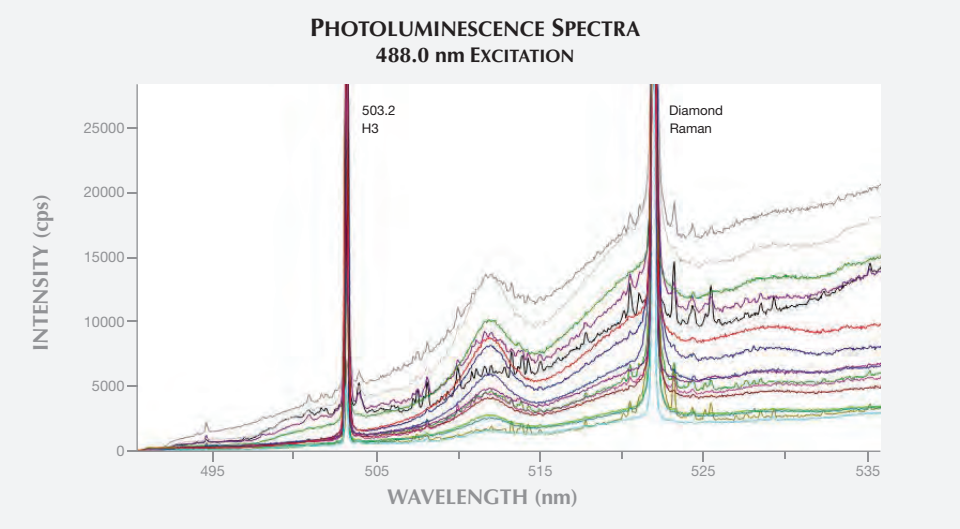

Figure 13. The dominant feature in PL spectra of the Gemesis CVD samples with 488.0 nm laser excitation is the strong H3 emission, responsible for the green fluorescence to short-wave UV radiation observed in all 16 samples.

[Si-V]$^-$ center and the corresponding vibronic structure (figure 14).

PL ZPLs at 850.0 and 875.5 nm were detected in all of the samples when excited with an 830.0 nm laser. Furthermore, a 946.0 nm emission was observed in five of them (figure 15). This ZPL has been attributed to the neutral charge state of the silicon split-vacancy defect, [Si-V]^0 (D'Haenens-Johansson et al., 2010; 2011). In addition, sample GS14 displayed emissions at 882.7 and 884.4 nm. Both the peak positions and their relative intensities agree with those assigned to nickel-related centers.

Although only semiquantitative analysis of the PL and absorption data was possible, the presence of certain optical centers could be determined. It was noted that the samples with relatively high concentrations of Si-related defects, characterized by strong [Si-V]$^-$ absorption, also showed emission lines at 946 nm ([Si-V]^0) and 766 nm. The intensity of the 850.0 and 875.5 nm emissions also showed a positive correlation with the 946 nm line.

DISCUSSION

Progress in Quality of Synthetic CVD Gem Diamonds. CVD synthetic diamonds produced for the jewelry market have shown significant improvement in the past decade. The early products from Apollo

Figure 14. Emissions recorded in the Gemesis synthetic diamonds with 633.0 nm laser excitation consisted of a 736.6/736.9 nm doublet from the [Si-V]$^-$ defect and a broad peak at 766 nm. This confirmed the positive correlation in peak intensities between the [Si-V]$^-$ emission and the 766 nm peak, also observed with 514.5 nm laser excitation.

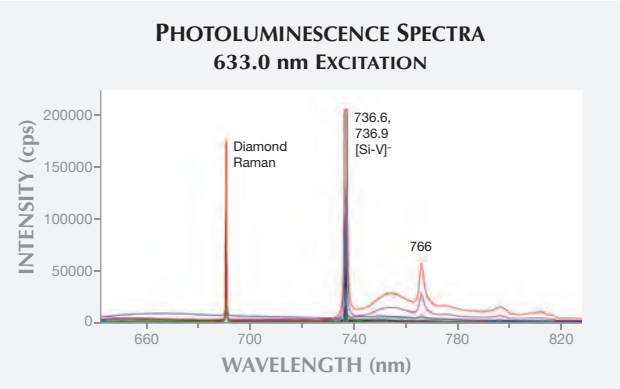

Figure 15. With 830.0 nm laser excitation, PL emissions at 850.0 and 875.5 nm were recorded in each of the Gemesis synthetic diamonds. Also observed in five samples was the [Si-V]^0 emission at 946.0 nm. Sample GS14 also displayed 882.7 and 884.4 nm emissions from well-known Ni-related defects. The spectrum for GS14 is shifted vertically for clarity.

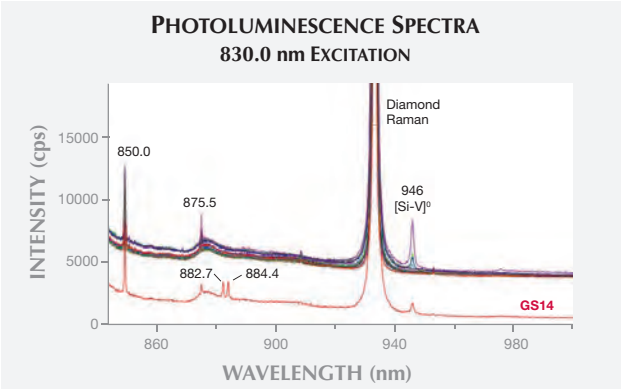

(Doering and Linares, 1999; Linares and Doering, 1999; Wang et al., 2003) consisted of relatively thin plates and the faceted gems were small, with distinct and sometimes intense brown coloration. Inclusions were common, resulting in medium or low clarity grades such as SI and I. Although the color and clarity of Apollo's products improved over time, their size (0.15–0.30 ct) was still limited by the achievable table-to-culet depths and by cut grading considerations (Wang et al., 2007). The Gemesis CVD samples in this study had high color and clarity grades, with most being colorless or near-colorless and VVS or better. Sample GS05 (0.31 ct) is the first documented faceted CVD synthetic diamond with IF clarity. Moreover, the average carat weight of the samples we examined, 0.46 ct, falls within the range of the most popular diamond weights in the market. We can expect even better gem-quality CVD products as synthesis methods continue to improve. In fact, CVD could become the preferred method for growing colorless gem diamonds commercially. The HPHT growth of colorless or near-colorless gem diamonds continues to face the challenges of effectively preventing isolated nitrogen from entering the diamond lattice, and keeping metallic catalysts/solvents from being incorporated as inclusions. Both of these factors require a reduction in the synthetic diamond growth rate under HPHT conditions.

Spectroscopic Features and Possible Post-Growth Treatment. Previously documented as-grown CVD synthetic diamonds were colorless, near-colorless, or (most often) some shade of brown (Martineau et al., 2004; Wang et al., 2007). Specific absorptions in the mid-IR and near-IR regions and doublet emissions at 596.5 and 597.0 nm are important for separating as-grown CVD synthetics from natural diamonds. These centers are formed during synthesis but may, under the right conditions, be destroyed by post-growth treatments. Such enhancements may be revealed by the introduction of defects not observed in as-grown CVD material.

The Gemesis products in this study had a distinctly different combination of lattice defects from as-grown CVD synthetics. Their absorption spectra in the mid- and near-IR regions were surprisingly featureless, and the 3123 cm^{-1} band was notably absent from every sample. Only weak absorptions at 1344 and 1332 cm^{-1} due to isolated nitrogen were observed in some samples' FTIR spectra.

Similarly, the UV-Vis-NIR absorption spectra differed from those of conventional CVD synthetics. There was a gradual, generally featureless increase in absorption from ~700 nm down to the diamond edge at ~225 nm (from lower to higher energies). Absorption features that are characteristic of as-grown CVD samples, such as the 596 and 625 nm (Martineau et al., 2004), were not detected.

H3 Center. PL spectroscopy using 488.0 nm laser excitation revealed the presence of the H3 defect (503.2 nm) in all of the Gemesis samples. (The H3 concentration was below the detection limit for UV-Vis-NIR absorption.) When excited, the H3 defect emits green light centered at ~520 nm; this defect is responsible for the green fluorescence excited by the short-wave UV lamp and the DiamondView (figure 4). The low-temperature synthesis conditions of the CVD method are not favorable for the production of multi-nitrogen defects such as H3 ($[N\text{-}V\text{-}N]^0$). Instead, nitrogen impurities in as-grown CVD synthetic diamond usually exist in isolated forms such as N_S, N-V, and N-V-H. The H3 center is therefore not observed in as-grown CVD synthetic diamond, though it may be introduced by post-growth treatments (Collins, 1978, 1980; Charles et al., 2004; Martineau et al., 2004; Meng et al., 2008).

Creating H3 defects usually involves irradiation and annealing at relatively high temperatures approaching (or including) HPHT conditions. Pre-annealing irradiation introduces vacancies, while annealing mobilizes the necessary nitrogen and vacancy components to form complex nitrogen-aggregated defects, including H3. Modest concentrations of H3 can be formed even without the irradiation step, as long as there is a source of vacancies in the pretreated material (Charles et al., 2004; Martineau et al., 2004; Meng et al., 2008). Annealing temperatures as low as 1500°C have been reported to introduce the H3 defect in CVD synthetic diamond (Meng et al., 2008). H3 in natural diamond is associated with distinct plastic deformation and dislocation features, which release vacancies when annealed either in nature or by laboratory treatment. It is noteworthy, however, that some brown CVD synthetics have low dislocation densities and do not show significant plastic deformation (Martineau et al., 2004; Mäki et al., 2007). Positron annihilation experiments have shown that vacancy clusters can be formed in as-grown CVD synthetic diamond, and that their distribution and size changes after annealing above 1400°C (Mäki et al., 2007).

At typical HPHT-annealing temperatures, N-V and N-V-H defects will break up, N_S may be mobile, and some of the vacancy clusters will dissociate

(Collins, 1980; Charles et al., 2004; Mäki et al., 2007). Thus the formation of H3 in treated CVD synthetic diamond is possible, as the constituents are available and mobile. Significant concentrations of H3 may remain after the treatment so long as the temperature is not sufficiently high to break up the H3 centers.

Analysis of the relative intensities of the H3 (503.2 nm) and N-V centers ($[N\text{-}V]^0$ at 575 nm and $[N\text{-}V]^-$ at 637 nm) may provide information regarding the Gemesis samples' annealing temperature range. A study by Charles et al. (2004) HPHT-annealed different segments of a single CVD synthetic diamond at temperatures of 1900°C (1 hour, 6.5 GPa), 2200°C (1 hour, 7.0 GPa), and 2200°C (10 hours, 7.0 GPa). In PL spectra taken with 488 nm laser excitation, the H3 defect was present after annealing at 1900°C, but less intense than the N-V peaks. Conversely, PL spectra for the CVD sectors annealed at 2200°C displayed a dominant H3 peak. These results agree with those of the HPHT and LPHT (low-pressure, high-temperature) annealing investigation of CVD synthetic diamond by Meng et al. (2008). They found that the N-V peaks were stronger than the H3 peak after LPHT annealing at 1970°C, yet HPHT annealing at 2030°C reversed this relationship. Furthermore, LPHT annealing at 1500°C introduced H3 defects, but their concentration became appreciable only at temperatures above 1700°C. From these published results, it can be inferred that the significant H3 concentrations detected in our Gemesis samples (figure 13) indicated annealing temperatures of at least 1500°C, and probably above 1700°C. The fact that the H3 peaks were less intense than the N-V features suggests that the maximum annealing temperature was ~2000°C.

N3 Center. Another multi-nitrogen defect in diamond, the N3 center (N_3-V) with characteristic emission at 415 nm, has not been observed in as-grown CVD synthetic diamond. Similar to H3, however, this defect can be produced by HPHT-processing a CVD sample, becoming particularly strong after prolonged annealing at 2200°C (Charles et al., 2004; Martineau et al., 2004). This center was weakly detected in 56% of the Gemesis samples.

3123 cm^{-1} Feature. The local vibrational mode at 3123 cm^{-1} is frequently observed in nitrogen-doped CVD synthetics (Wang et al., 2003; Martineau et al., 2004; Khan et al., 2009, 2010). Notably, this absorption was not detected in the Gemesis samples' FTIR spectra. Isotopic substitution experiments using deuterium indicated that the center responsible for the 3123 cm^{-1} line is hydrogen-related (Fuchs et al., 1995a,b; Chevallier et al., 2002). The line has been specifically attributed to $[N\text{-}V\text{-}H]^0$ (Khan et al., 2009, 2010).

The temperature stability of the 3123 cm^{-1} absorption line was investigated by Cruddace (2007) and Cruddace et al. (2007), who annealed CVD-grown diamond samples at temperatures ranging from 900 to 1600ºC, at 100°C increments. The 3123 cm^{-1} line did not start to anneal out until 1200°C, and even then the rate of decay was slow, with ~90% of the initial intensity/concentration remaining after the treatment. Within the uncertainty limits, however, there was no conclusive evidence that the absorption line annealed out until 1500°C. Meng et al. (2008) performed LPHT annealing experiments (1400–2200°C, 150–300 Torr) on single-crystal, as-grown CVD synthetic diamonds in a hydrogen environment using microwave plasma techniques for durations ranging from less than a minute to a few hours. Heating at 1600°C for 10 minutes reduced the intensity of the 3123 cm^{-1} peak (reported as 3124 cm^{-1}), but it was still clearly present. This indicates that even higher temperatures or longer annealing times are needed to entirely anneal out N-V-H centers. The absence of both the 3123 cm^{-1} line in the FTIR spectra and the $[N\text{-}V\text{-}H]^-$ defect in the EPR data (with a detection limit from 5 to 15 ppb) further supports that the Gemesis samples were annealed at temperatures above 1600°C.

3107 cm^{-1} Feature. An IR absorption line at 3107 cm^{-1} is often seen in type I natural diamonds, but only occasionally in type IIa material (Runciman and Carter, 1971; Chrenko et al., 1967; Woods and Collins, 1983; Iakoubovskii and Adriaenssens, 2002). The center responsible for this line can also be introduced into type Ib HPHT-grown synthetics by HPHT annealing at temperatures above 2100°C (Kiflawi et al., 1996). Although not detected in as-grown CVD synthetics, this line has been reported to anneal-in after HPHT treatment at >1700°C (Charles et al., 2004; Martineau et al., 2004; Liggins, 2010; Liggins et al., 2010). While the structure of the defect has not been identified, ^{12}C:^{13}C isotopic substitution experiments have shown that the line originates from a C–H stretch vibration (Woods and Collins, 1983; Kiflawi et al., 1996).

The 3107 cm^{-1} line was not detected in the 16 Gemesis CVD samples. The annealing temperature may not have been high enough to create the center responsible for the feature. Assuming that the reported relationship between the 3107 cm^{-1} line intensity and

nitrogen concentration in HPHT-treated CVD synthetics (Liggins, 2010; Liggins et al., 2010) holds for these lower-nitrogen samples, the resulting concentration of 3107 cm^{-1} centers would be too low to detect.

Synopsis of Evidence for HPHT Treatment. The presence and intensities of H3 and N3, and the absence of $[N\text{-}V\text{-}H]^0$ (3123 cm^{-1}) and $[N\text{-}V\text{-}H]^-$ in the Gemesis samples, strongly suggest annealing temperatures ranging from 1700°C to 2000°C. Although the color saturation of brown diamond decreases after annealing at ~1700°C, it is more likely that temperatures in excess of 1900°C were used to optimize the color change and reduce the necessary annealing time (Meng et al., 2008). However, annealing at these temperatures will lead to graphitization and the destruction of the specimen unless a stabilizing pressure is applied (Davies and Evans, 1972). LPHT annealing (pressure <300 Torr) in the 1400–2200°C range is also possible, though the practice is not widespread (Meng et al., 2008; Liang et al., 2009). Also, the sample must be very carefully prepared prior to LPHT annealing to prevent cracking and graphitization. Thus, it is likely that HPHT treatment was used to improve the color and possibly even the transparency of the Gemesis samples.

The low concentrations of N3, H3, and N-V defects in the Gemesis samples, which were not detected in absorption spectra, suggest that the dominant form of nitrogen impurity is single substitutional nitrogen. Martineau et al. (2004) reported that type IIa (no observable absorption at 1344 cm^{-1}) CVD synthetic diamonds could be grown even when doped with nitrogen. The 1344 cm^{-1} absorption in the majority of the Gemesis samples, and the relatively high N_S^0 concentrations (72 ± 10 to 450 ± 50 ppb), indicate that nitrogen was intentionally introduced during growth. Although nitrogen-doped CVD synthetic diamond is often unappealingly brown (Martineau et al., 2004), the method benefits from significantly higher diamond growth rates (e.g., Tallaire et al., 2005). Hence, it may be commercially viable to produce high-quality colorless or near-colorless CVD products by HPHT treatment of nitrogen-doped brown material.

As-grown faceted CVD synthetics comparable in quality to the Gemesis samples have been produced in the United Kingdom by Element Six Ltd., a De Beers technology company, but these were synthesized purely for research and education purposes (Martineau et al., 2004). They were produced using exhaustive measures to exclude impurities from the growth environment. The technical difficulty, extended growth times, and high cost associated with the synthesis of comparable high-purity as-grown CVD material suggests that manufacturers targeting the colorless diamond sector will instead focus their efforts on developing treatments to improve efficiently produced poor-quality brown material.

Si-Related Defects. Relatively strong doublet emissions at 736.6/736.9 nm (often referred to simply as "737 nm") were recorded in the PL spectra of all the Gemesis CVD samples tested (figure 10A), and this feature was also detected in the UV-Vis-NIR absorption spectra of all but two of the synthetic diamonds in this study (figure 9B).

The detection of silicon impurities in diamond is usually verified by the 737 nm line in either PL or absorption spectra (Clark et al., 1995). Natural type Ia and type IIa diamonds rarely show this feature, which was first reported in natural specimens by Breeding and Wang (2008). Since then it has been observed in several natural stones, but far less than 1% of those studied by GIA (unpublished data). Conversely, silicon is often unintentionally introduced into CVD synthetic diamond by the etching of Si-containing components in the reactor, such as silica windows (Robins et al., 1989; Barjon et al., 2005). Although the feature is not specific to CVD, it has often been part of gemological identification criteria (Wang et al., 2003, 2007; Martineau et al., 2004). Si-V centers have high temperature stability, withstanding annealing up to 2200°C (Clark and Dickerson, 1991). Therefore, it is not surprising that the Gemesis CVD samples contain this defect. A line at 946 nm, observed in Si-containing diamond in both absorption and emission, has been attributed to $[Si\text{-}V]^0$ (Evans et al., 2006; D'Haenens-Johansson et al., 2010, 2011). The 946 nm peak was not observed in the absorption spectra of the Gemesis samples. Since the 737 nm peak intensity revealed by absorption spectroscopy was weak (e.g., figure 9B) it would not be surprising if the 946 nm peak was below the detection limit. PL spectroscopy (830.0 nm excitation), which has a higher sensitivity than absorption spectroscopy, detected the 946 nm peak in five samples (GS03, GS08, GS10, GS13, and GS14).

Identification Features. Separating these new CVD synthetic diamonds from their natural counterparts is becoming increasingly difficult using conventional gemological procedures, and may not even be possible without advanced spectroscopic techniques. The color and clarity grades, as well as weak interference colors and birefringence patterns, are comparable to those

seen in natural diamonds. The H3 defect is common in natural type IIa diamonds, and the associated green fluorescence is frequently observed. Small black irregular inclusions such as those seen in CVD synthetic diamond are occasionally observed in natural stones. However, the petal-shaped, highly localized stress patterns around such inclusions are good indicators of CVD synthesis.

Previous studies relied heavily on infrared absorption spectroscopy for the identification of CVD synthetic diamonds, citing features such as the absorption line at 3123 cm^{-1}. With further developments in growth techniques and post-growth treatment, however, infrared absorption spectroscopy of the samples in this study did not show identification features that easily separated them from natural or HPHT-grown synthetic type IIa diamonds. Instead, our samples displayed mid- and near-IR spectra that were remarkably similar to those of natural type IIa diamond. Traces of isolated nitrogen in a type IIa sample have generally served as an alert to CVD growth, but N_S^0 was hardly detectable in these specimens—and HPHT-treated natural type IIa diamonds can also contain isolated nitrogen.

The most useful identification features were revealed by PL spectroscopy and DiamondView fluorescence images. Strong emissions of $[Si\text{-}V]^-$ at 736.6 and 736.9 nm were observed in all of the samples, and this defect was also detected in the UV-Vis-NIR spectra of most samples. Its presence remains a very strong (but not conclusive) indication of CVD synthesis. Very few natural type IIa diamonds show these emissions (Breeding and Wang, 2008). Emission at 946 nm from the $[Si\text{-}V]^0$ optical center was detected in one-third of the samples. Because this feature has not been reported in natural diamond, it can be used to indicate CVD synthesis. In the DiamondView, fine growth striations are a unique feature of CVD synthetic diamond. While the point defects (including $[Si\text{-}V]^-$) can be removed or modified by post-growth treatment, the growth striations remain unchanged. For example, H-related absorption in the infrared region was destroyed and the H3 center was introduced in the samples we studied, but the striations were still clearly observable. The distribution of H3 centers actually followed the striations, as shown by the DiamondView images in figure 4. Another interesting feature was the series of sharp emission peaks in the 495–580 nm region revealed by 488.0 and 514.5 nm laser excitations, such as those at 525.4, 535.1, 540.4, 546.1, and 572.9 nm (figures 10B and 13). While their assignment is unclear, their occurrence as a group could offer a reliable indication of CVD growth.

In short, CVD synthetic diamonds from Gemesis are entirely identifiable. Proper analysis using PL spectroscopy and fluorescence imaging techniques is critical to ensuring that these materials are clearly distinguished from their type IIa counterparts, such as natural, natural but HPHT treated, and HPHT-grown synthetic diamonds.

CONCLUDING REMARKS

The new CVD synthetic diamonds from Gemesis showed clear improvements over those reported previously from other sources. These gems average nearly half a carat, the most popular diamond weight in the marketplace, and their color and clarity are comparable to top-quality natural diamonds. These synthetic materials can be identified with a combination of photoluminescence and UV fluorescence imaging techniques. There is no question that the size and quality of CVD synthetic diamonds will continue improving. Post-growth treatment improves color and possibly clarity. It appears that the striated growth pattern of CVD synthetic diamonds cannot be altered by any treatment, so it remains the most important if not the only visual identification feature.

ABOUT THE AUTHORS

Dr. Wang (wwang@gia.edu) is the director of research and development, Dr. D'Haenens-Johansson is a research scientist, Mr. Johnson is the supervisor of diamond advanced testing, Mr. Moe is a research associate, and Mr. Moses is senior vice president at GIA's New York laboratory. Ms. Emerson was a research technician at GIA and is currently working on her master's degree. Dr. Newton is a professor in experimental physics at the University of Warwick, UK.

ACKNOWLEDGMENTS

The authors thank Ivana Kayes, Siau Fung Yeung, and Dr. Christopher M. Breeding of GIA's New York and Carlsbad laboratories for their many suggestions and assistance with this study. Dr. Christopher Welbourn at the University of Warwick is thanked for his help with EPR analysis. We are grateful to Stephen Lux of Gemesis Corp. for providing the samples for this study.

REFERENCES

Avalos V., Dannefaer S. (2003) Vacancy-type defects in brown diamonds investigated by positron annihilation. *Physica B*, Vol. 340–342, pp. 76–79, http://dx.doi.org/10.1016/j.physb.2003.09.006.

Bangert U., Barnes R., Gass M.H., Bleloch A.L., Godfrey I.S. (2009) Vacancy clusters, dislocations and brown colouration in diamond. *Journal of Physics: Condensed Matter*, Vol. 21, No. 36, article 364208, http://dx.doi.org/10.1088/0953-8984/21/36/364208.

Barjon J., Rzepka E., Jomard F., Laroche J.-M., Ballutaud D., Kociniewski T., Chevallier J. (2005) Silicon incorporation in CVD diamond layers. *Physica Status Solidi* (a), Vol. 202, No. 11, pp. 2177–2181, http://dx.doi.org/10.1002/pssa.200561920.

Breeding C.M., Wang W. (2008) Occurrence of the Si-V defect in natural colorless gem diamonds. *Diamond and Related Materials*, Vol. 17, No. 7–10, pp. 1335–1344, http://dx.doi.org/10.1016/j.diamond.2008.01.075.

Butler J.E., Mankelevich Y.A., Cheesman A., Ma J., Ashfold M.N.R. (2009) Understanding the chemical vapor deposition of diamond: Recent progress. *Journal of Physics: Condensed Matter*, Vol. 21, article 364201, http://dx.doi.org/ 10.1088/0953-8984/21/36/364201.

Chadwick K. (2008a) Lab Notes: First CVD synthetic diamond submitted for Dossier grading. *G&G*, Vol. 44, No. 1, pp. 67–69.

Chadwick K. (2008b) Lab Notes: HPHT-treated CVD synthetic diamond submitted for Dossier grading. *G&G*, Vol. 44, No. 4, pp. 365–367.

Charles S.J., Butler J.E., Feygelson B.N., Newton M.E., Carroll D.L., Steeds J.W., Darwish H., Yan C.-S., Mao H.K., Hemley R.J. (2004) Characterization of nitrogen doped chemical vapor deposited single crystal diamond before and after high pressure, high temperature annealing. *Physica Status Solidi (a)*, Vol. 201, No. 11, pp. 2473–2485, http://dx.doi.org/10.1002/pssa.200405175.

Chevallier J., Jomard F., Teukam Z., Koizumi S., Kanda H., Sato Y., Deneuville A., Bernard M. (2002) Hydrogen in n-type diamond. *Diamond and Related Materials*, Vol. 11, pp. 1566–1571, http://dx.doi.org/10.1016/S0925-9635(02)00063-8.

Chrenko R.M., McDonald R.S., Barrow K.A. (1967) Infra-red spectra of diamond coat. *Nature*, Vol. 213, pp. 474–476, http://dx.doi.org/10.1038/213474a0.

Clark C.D, Dickerson C.B. (1991) The 1.681 eV center in polycrystalline diamond. *Surface and Coatings Technology*, Vol. 47, No. 1–3, pp. 336–343, http://dx.doi.org/10.1016/0257-8972(91)90299-C.

Clark C.D., Kanda H., Kiflawi I., Sittas G. (1995) Silicon defects in diamond. *Physical Review B*, Vol. 51, No. 23, pp. 16681–16688, http://dx.doi.org/10.1103/PhysRevB.51.16681.

Collins A.T. (1978) Migration of nitrogen in electron-irradiated type Ib diamond. *Journal of Physics C: Solid State Physics*, Vol. 11, No. 10, pp. L417–L422, http://dx.doi.org/10.1088/0022-3719/11/10/002.

——— (1980) Vacancy enhanced aggregation of nitrogen in diamond. *Journal of Physics C: Solid State Physics*, Vol. 13, No. 14, pp. 2641–2650, http://dx.doi.org/10.1088/0022-3719/13/14/006.

Collins A.T., Stanley M., Woods G.S. (1987) Nitrogen isotope effects in synthetic diamonds. *Journal of Physics D: Applied Physics*, Vol. 20, No. 7, pp. 969–974, http://dx.doi.org/10.1088/0022-3727/20/7/022.

Collins A.T., Kanda H., Kitawaki H. (2000) Colour changes produced in natural brown diamonds by high-pressure, high-temperature treatment. *Diamond and Related Materials*, Vol. 9, No. 2, pp. 113–122, http://dx.doi.org/10.1016/S0925-9635(00)00249-1.

Cox A., Newton M.E., Baker J.M. (1994) ^{13}C, ^{14}N and ^{15}N ENDOR measurements on the single substitutional nitrogen centre (P1) in diamond. *Journal of Physics: Condensed Matter*, Vol. 6, No. 2, pp. 551–563, http://dx.doi.org/10.1088/0953-8984/6/2/025.

Cruddace R.C. (2007) Magnetic Resonance and Optical Studies of Point Defects in Single Crystal CVD Diamond. Ph.D. Thesis, University of Warwick, UK.

Cruddace R.C., Newton M.E., Smith H.E., Davies G., Martineau P.M., Twitchen D.J. (2007) Identification of the 3123 cm^{-1} absorption line in SC-CVD diamond as the NVH^- defect. *Proceedings of the 58th De Beers Diamond Conference*, Coventry, UK, July 11–13, Poster No. 15.

Davies G. (1974) Vibronic spectra in diamond. *Journal of Physics C: Solid State Physics*, Vol. 7, No. 20, pp. 3797–3809, http://dx.doi.org/10.1088/0022-3719/7/20/019.

Davies G., Evans T. (1972) Graphitization of diamond at zero pressure and at high pressure. *Proceedings of the Royal Society of London A*, Vol. 328, No. 1574, pp. 413–427, http://dx.doi.org/10.1098/rspa.1972.0086.

Davies G., Welbourn C.M., Loubser J.H.N. (1978) Optical and electron paramagnetic effects in yellow type Ia diamonds. *Diamond Research*, pp. 23–30.

D'Haenens-Johansson U.F.S., Edmonds A.M., Newton M.E., Goss J.P., Briddon P.R., Baker J.M., Martineau P.M., Khan R.U.A., Twitchen D.J., Williams S.D. (2010) EPR of a defect in CVD diamond involving both silicon and hydrogen that shows preferential alignment. *Physical Review B*, Vol. 82, No. 15, article 155205, http://dx.doi.org/10.1103/PhysRevB.82.155205.

D'Haenens-Johansson U.F.S., Edmonds A.M., Green B.L., Newton M.E., Davies G., Martineau P.M., Khan R.U.A., Twitchen D.J. (2011) Optical properties of the neutral silicon split-vacancy center in diamond. *Physical Review B*, Vol. 84, No. 24, article 245208, http://dx.doi.org/10.1103/PhysRevB.84.245208.

Doering P.J., Linares R.C. (1999) Large area single crystal CVD diamond: Properties and applications. *Proceedings of Applied Diamond Conference/Frontier Carbon Technology Joint Conference 1999*, Tsukuba, Japan, Aug. 31–Sept. 3, pp. 32–35.

Dyer H.B., Raal F.A., Du Preez L., Loubser J.H.N. (1965) Optical absorption features associated with paramagnetic nitrogen in diamond. *Philosophical Magazine*, Vol. 11, No. 112, pp. 763–774, http://dx.doi.org/10.1080/14786436508230081.

Edmonds A.M., Newton M.E., Martineau P.M., Twitchen D.J., Williams S.D. (2008) Electron paramagnetic resonance studies of silicon-related defects in diamond. *Physical Review*, Vol. 77, No. 24, article 245205, http://dx.doi.org/10.1103/PhysRevB.77.245205.

Evans D.J.F., Kelly C.J., Leno P., Martineau P.M., Taylor A.J. (2006) Silicon doped single crystal CVD diamond grown using silane. *Proceedings of the 57th De Beers Diamond Conference*, Cambridge, UK, July 10–12, pp. 38–40.

Fall C.J., Blumenau A.T., Jones R., Briddon P.R., Frauenheim T., Gutierrez-Sosa A., Bangert U., Mora A.E., Steeds J.W., Butler J.E. (2002) Dislocations in diamond: Electron energy-loss spectroscopy. *Physical Review B*, Vol. 65, No. 20, article 205206, http://dx.doi.org/10.1103/PhysRevB.65.205206.

Fisher D., Spits R.A. (2000) Spectroscopic evidence of GE POL HPHT-treated natural type IIa diamonds. *G&G*, Vol. 36, No. 1, pp. 42–49, http://dx.doi.org/10.5741/GEMS.36.1.42.

Fisher D., Evans D.J.F., Glover C., Kelly C.J., Sheehy M.J., Summerton G.C. (2006) The vacancy as a probe of the strain in type IIa diamonds. *Diamond and Related Materials*, Vol. 15, No. 10, pp. 1636–1642, http://dx.doi.org/10.1016/j.diamond.2006.01.020.

Fisher D., Sibley S.J., Kelly C.J. (2009) Brown colour in natural diamond and interaction between the brown related and other colour-inducing defects. *Journal of Physics: Condensed Matter*, Vol. 21, No. 36, article 364213, http://dx.doi.org/10.1088/0953-8984/21/36/364213.

Fuchs F., Wild C., Schwarz K., Koidl P. (1995a) Hydrogen-related IR absorption in chemical vapour deposited diamond. *Diamond and Related Materials*, Vol. 4, No. 5–6, pp. 652–656, http://dx.doi.org/10.1016/0925-9635(94)05247-6.

Fuchs F., Wild C., Schwarz K., Muller-Sebert W., Koidl P. (1995b) Hydrogen induced vibrational and electronic transitions in chemical vapor deposited diamond, identified by isotopic sub-

stitution. *Applied Physics Letters*, Vol. 66, No. 2, pp. 177–179, http://dx.doi.org/10.1063/1.113126.
Glover C., Newton M.E., Martineau P., Twitchen D.J., Baker J.M. (2003) Hydrogen incorporation in diamond: The nitrogen-vacancy-hydrogen complex. *Physical Review Letters*, Vol. 90, No. 18, article 185507, http://dx.doi.org/10.1103/PhysRevLett.90.185507.
Glover C., Newton M.E., Martineau P.M., Quinn S., Twitchen D.J. (2004) Hydrogen incorporation in diamond: The vacancy-hydrogen complex. *Physical Review Letters*, Vol. 92, No. 13, article 135502, tp://dx.doi.org/10.1103/PhysRevLett.92.135502.
Goodwin D.G., Butler J.E. (1997) Theory of diamond chemical vapor deposition. In M.A. Prelas, G. Popovici, and L.K. Biglow, Eds., *Handbook of Industrial Diamonds and Diamond Films*, Marcel Dekker Inc., New York, pp. 527–581.
Goss J.P., Jones R., Breuer S.J., Briddon P.R., Oberg S. (1996) The twelve-line 1.682 eV luminescence center in diamond and the vacancy-silicon complex. *Physical Review Letters*, Vol. 77, No. 14, pp. 3041–3044, http://dx.doi.org/10.1103/PhysRevLett.77.3041.
Graff M. (2010) Gemesis to sell lab-grown whites to consumers. *National Jeweler*, http://www.nationaljeweler.com/nj/diamonds/a/~20714-Gemesis-to-sell-labgrown-whites [date accessed: May 14, 2012].
Hounsome L.S., Jones R., Martineau P.M., Fisher D., Shaw M.J., Briddon P.R., Öberg S. (2006) Origin of brown coloration in diamond. *Physical Review B*, Vol. 73, No. 12, article 125203, http://dx.doi.org/10.1103/PhysRevB.73.125203.
Iakoubovskii K., Adriaenssens G.J. (2002) Optical characterization of natural Argyle diamonds. *Diamond and Related Materials*, Vol. 11, No. 1, pp. 125–131, http://dx.doi.org/10.1016/S0925-9635(01)00533-7.
Khan R.U.A., Martineau P.M., Cann B.L., Newton M.E., Twitchen D.J. (2009) Charge transfer effects, thermo and photochromism in single crystal CVD synthetic diamond. *Journal of Physics: Condensed Matter*, Vol. 21, No. 36, article 364214, http://dx.doi.org/10.1088/0953-8984/21/36/364214.
Khan R.U.A., Martineau P.M., Cann B.L., Newton M.E., Dhillon H.K., Twitchen D.J. (2010) Color alterations in CVD synthetic diamond with heat and UV exposure: Implications for color grading and identification. *G&G*, Vol. 18, No. 2, pp. 18–26, http://dx.doi.org/10.5741/GEMS.18.2.18.
Kiflawi I., Mainwood A., Kanda H., Fisher D. (1996) Nitrogen interstitials in diamond. *Physical Review B*, Vol. 54, No. 23, pp. 16719–16726, http://dx.doi.org/10.1103/PhysRevB.54.16719.
Lawson S.C., Fisher D., Hunt D.C., Newton M.E. (1998) On the existence of positively charged single-substitutional nitrogen in diamond. *Journal of Physics: Condensed Matter*, Vol. 10, No. 27, pp. 6171–6180, http://dx.doi.org/10.1088/0953-8984/10/27/016.
Liang Q, Yan C.-S., Meng Y., Lai J., Krasnicki S., Mao H.-K., Hemley R.J. (2009) Recent advances in high-growth rate single-crystal CVD diamond. *Diamond and Related Materials*, Vol. 18, pp. 698–703, http://dx.doi.org/10.1016/j.diamond.2008.12.002.
Liggins S. (2010) Identification of Point Defects in Treated Single Crystal Diamond. Ph.D. thesis, University of Warwick, UK.
Liggins S., Cruddace R.J., Cann B.L., Newton M.E., Khan R.U.A., Martineau P.M., Twitchen D.J., Goss J.P., Briddon P.R. (2010) Studies of hydrogen related defects in diamond. *61st De Beers Diamond Conference*, University of Warwick, Coventry, UK, July 11–13, Poster No. 23.
Linares R.C., Doering P.J. (1999) Properties of large single crystal diamond. *Diamond and Related Materials*, Vol. 8, No. 2–5, pp. 909–915, http://dx.doi.org/10.1016/S0925-9635(98)00382-3.
Mäki J.-M., Tuomisto F., Kelly C., Fisher D., Martineau P. (2007) Effects of thermal treatment on optically active vacancy defects in CVD diamonds. *Physica B*, Vol. 401–402, pp. 613–616, http://dx.doi.org/10.1016/j.physb.2007.09.034.
Martineau P.M., Lawson S.C., Taylor A.J., Quinn S.J., Evans D.J.F., Crowder M.J. (2004) Identification of synthetic diamond grown using chemical vapor deposition (CVD). *G&G*, Vol. 40, No. 1, pp. 2–25, http://dx.doi.org/10.5741/GEMS.40.1.2.
Martineau P.M., Gaukroger M., Khan R., Evans D. (2009) Effect of steps on dislocations in CVD diamond grown on {001} substrates. *Physica Status Solidi C*, Vol. 6, No. 8, pp. 1953–1957, http://dx.doi.org/10.1002/pssc.200881465.
Meng Y.F., Yan C.S., Lai J., Krasnicki S., Shu H., Yu T., Ling Q., Mao H.K., Hemley R.J. (2008) Enhanced optical properties of chemical vapor deposited single crystal diamond by low-pressure/high-temperature annealing. *Proceedings of the National Academy of Sciences*, Vol. 105, No. 46, pp. 17620–17625, http://dx.doi.org/10.1073/pnas.0808230105.
Moses T.M., Shigley J.E., McClure S.F., Koivula J.I., Van Daele M. (1999) Observations on GE-processes diamonds: A photographic record. *G&G*, Vol. 35, No. 3, pp. 14–22, http://dx.doi.org/10.5741/GEMS.35.3.14.
Robins L.H., Cook L.P., Farabaugh E.N., Feldman A. (1989) Cathodoluminescence of defects in diamond films and particles grown by hot-filament chemical-vapor deposition. *Physical Review B*, Vol. 39, No. 18, pp. 13367–13377, http:// dx.doi.org//10.1103/PhysRevB.39.13367.
Runciman W.A., Carter T. (1971) High resolution infra-red spectra of diamond. *Solid State Communications*, Vol. 9, No. 5, pp. 315–317, http://dx.doi.org/10.1016/0038-1098(71)90001-9.
Smith W., Sorokin P.P., Gelles I.L., Lasher G.J. (1959) Electron-spin resonance of nitrogen donors in diamond. *Physical Review*, Vol. 115, No. 6, pp. 1546–1552, http://dx.doi.org/10.1103/PhysRev.115.1546.
Tallaire A., Achard J., Sussmann R.S., Silva F., Gicquel A. (2005) Homoepitaxial deposition of high-quality thick diamond films: Effect of growth parameters. *Diamond and Related Materials*, Vol. 14, No. 3–7, pp. 249–254, http://dx.doi.org/10.1016/j.diamond.2004.10.037.
Vavilov V.S., Gippius A.A., Zaitsev B.V., Deryagin B.V., Spitsyn B.V., Aleksenko A.E. (1980) Investigation of the cathodoluminescence of epitaxial diamond films. *Soviet Physics-Semiconductors*, Vol. 14, pp. 1078–1079.
Wang W., Moses T.M. (2011) Lab Notes: Gem-quality CVD synthetic diamonds from Gemesis. *G&G*, Vol. 47, No. 3, pp. 227–228.
Wang W., Moses T., Linares R., Shigley J.E., Hall M., Butler J.E. (2003) Gem-quality synthetic diamonds grown by the chemical vapor deposition method. *G&G*, Vol. 39, No. 4, pp. 268–283, http://dx.doi.org/10.5741/GEMS.39.4.268.
Wang W., Tallaire A., Hall M.S., Moses T.M., Achard J., Sussmann R.S., Gicquel A. (2005) Experimental CVD synthetic diamonds from LIMHP-CNRS, France. *G&G*, Vol. 41, No. 3, pp. 234–244, http://dx.doi.org/10.5741/GEMS.41.3.234.
Wang W., Hall M.S., Moe K.S., Tower J., Moses T.M. (2007) Latest-generation CVD-grown synthetic diamonds from Apollo Diamond Inc. *G&G*, Vol. 43, No. 4, pp. 294–312, http://dx.doi.org/10.5741/GEMS.43.4.294.
Wang W., Doering P., Tower J., Lu R., Eaton-Magana S., Johnson P., Emerson E., Moses T.M. (2010) Strongly colored pink CVD lab-grown diamonds. *G&G*, Vol. 46, No. 1, pp. 4–17, http://dx.doi.org/10.5741/GEMS.46.1.4.
Welbourn C.M., Cooper M., Spear P.M. (1996) De Beers natural versus synthetic diamond verification instruments. *G&G*, Vol. 32, No. 3, pp. 156–169, http://dx.doi.org/10.5741/GEMS.32.3.156.
Willems B., Martineau P.M., Fisher D., Van Royen J., Van Tendeloo G. (2006) Dislocation distributions in brown diamond. *Physica Status Solidi (a)*, Vol. 203, pp. 3076–3080, http://dx.doi.org/10.1002/pssa.200671129.
Woods G.S., Collins A.T. (1983) Infrared absorption spectra of hydrogen complexes in type I diamonds. *Journal of Physics and Chemistry of Solids*, Vol. 44, No. 5, pp. 471–475, http://dx.doi.org/10.1016/0022-3697(83)90078-1.

Sapphires from Thammannawa, Kataragama Area, Sri Lanka

Pannipitiye G. R. Dharmaratne, H. M. Ranjith Premasiri, and Dayananda Dillimuni

The February 2012 discovery of high-quality blue sapphires at Thammannawa near Kataragama in southeastern Sri Lanka has intensified gem mining and exploration in the surrounding area and all over the country. The deposit is hosted by the Kataragama klippe, and corundum mineralization is associated with pegmatitic intrusions and surrounding micaceous layers. Well-formed crystals from this primary deposit display flat faces and sharp edges with an unusually vitreous luster. The sapphires possess good transparency and a pure blue color that is characteristic of corundum from this deposit. Several kilograms of rough material have been produced so far, with some crystals larger than 200 g. Faceted blue sapphires of fine color and weighing more than 20 ct have been cut.

In February 2012, fine blue sapphires (e.g., figure 1) were discovered during the reconstruction of a two-lane road from the Lunugamwehera area to Kataragama in southeastern Sri Lanka (figure 2). Gravel for the roadbed was supplied from nearby land belonging to the Forest Conservation Department (FCD). After several days of work, a truck driver noticed glittery reflections in material that had been dumped the previous day. The driver quickly recognized the crystals as blue sapphires and filled a sack with them. He abandoned the truck and left a note for the vehicle's owner pointing him to a parcel of the gems in the battery box. Local farmers noticed the abandoned truck and soon found their own gems in the roadbed. As the news spread, thousands rushed to the site and hauled away bags full of the newly laid gravel and soil (figure 3). This lasted a day or two until the area was secured by police, the armed forces, and the National Gem & Jewellery Authority (or NGJA, the agency responsible for gems found on federal lands). By February 23, newspapers and TV stations were reporting the discovery (Fernando, 2012; Nizam, 2012).

Figure 1. This sapphire from the new Thammannawa deposit weighs 20.5 ct. Courtesy of Ajward Deen; photo by P.G.R. Dharmaratne.

While the road itself was being guarded, one enterprising individual thought to search for the original source of the gravel. This turned out to be only 1 km away, on the side of the same road, at a place called

See end of article for About the Authors and Acknowledgments.
Gems & Gemology, Vol. 48, No. 2, pp. 98–107,
http://dx.doi.org/10.5741/GEMS.48.2.98.
© 2012 Gemological Institute of America

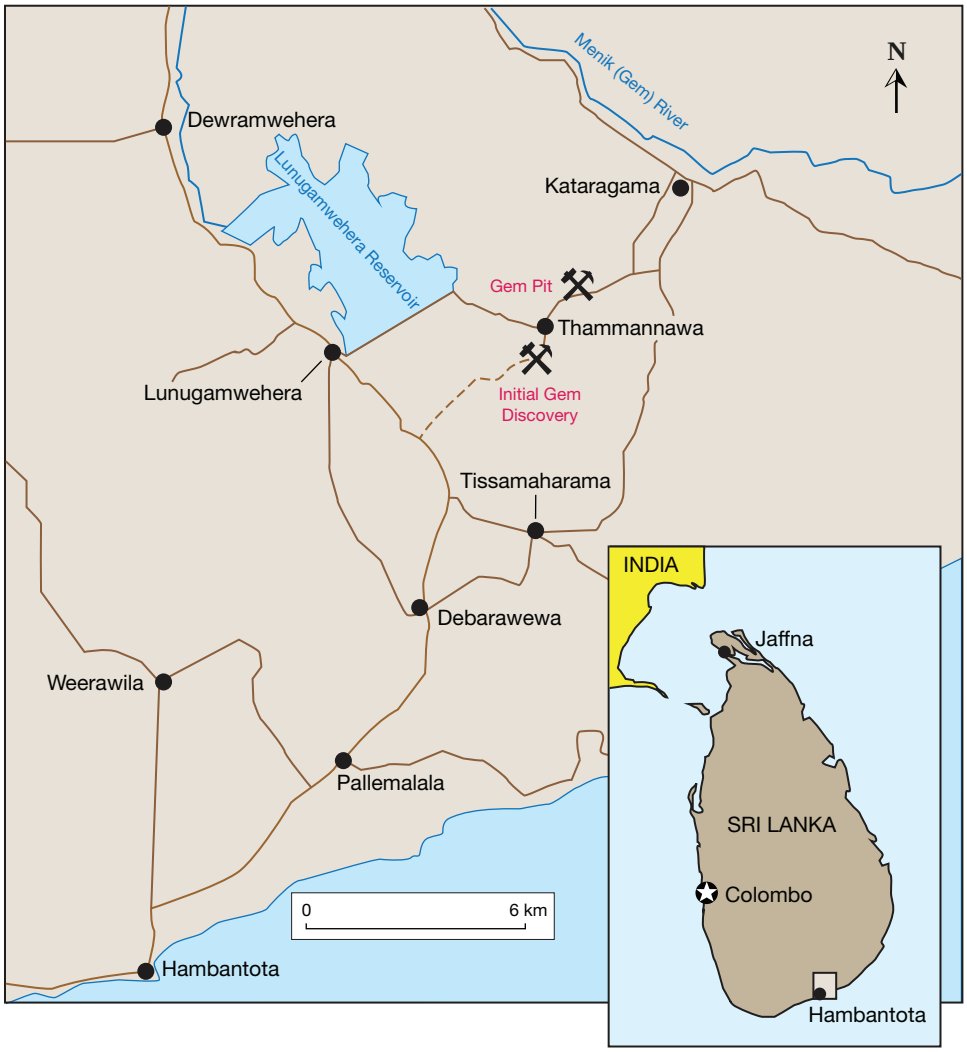

Figure 2. The Thammannawa deposit is located along the road from the Lunugamwehera area to Kataragama in southeastern Sri Lanka.

Thammannawa. Once again, thousands rushed to the scene in search of sapphires (figure 4), and some even used excavators and dump trucks to remove loads of earth. However, the NGJA soon secured this area as well. The entire excavated area measured only about 60 m^2. The NGJA and FCD divided this pit and the surrounding area into 49 blocks of about 10 perches (22 m^2) each. Mining rights for these blocks went up for public auction on February 24.

On February 27, these authors were permitted to study the new sapphire deposit with special permission, accompanied by a police escort. We were advised not to pick up anything, as the mining rights were privately owned. We also visited the road construction site where the gems were first discovered, which was still under heavy guard.

LOCATION AND ACCESS

The Thammannawa corundum deposit is located ~245 km from the capital city of Colombo at 6°22′14.08″N and 81°17′19.04″E. This falls on the southern boundary of the Monaragala District in Uva Province. The site is accessible by a gravel road and lies 4 km from the historical pilgrimage town of Kataragama (again, see figure 2). This road, which extends ~12 km from the Lunugamwehera area to Kataragama via Thammannawa, is being paved with asphalt.

Southeastern Sri Lanka is covered by low, dense dry-zone forest and shrubs. The mining site is situated within a forest and there are few settlements. Local inhabitants rely on the land for seasonal agriculture.

Figure 3. During the initial gem rush at the road construction site, people removed the gravel and soil in bags and dump trucks. Photo by Eranga Basnayake.

GEOLOGY

Regional Setting. Sri Lanka is mainly underlain by high-grade metamorphic rocks of Proterozoic age (figure 5). These rocks have been subdivided into three principal metamorphic complexes based on their age and tectonic setting (Kroner et al., 1991): the Highland Complex (granulite facies) and the Vijayan and Wanni Complexes (both upper amphibolite facies). The new sapphire discovery is hosted by rocks of the Highland Complex within the Kataragama klippe metamorphic complex (Silva et al., 1981).

Rocks of the Highland Complex have been subjected to multiple events of deformation and metamorphism. The age of the original metasediments is inferred to be ~2 billion years (Ga), with subsequent metamorphism and granitoid emplacement occurring 1,942–665 million years ago (Ma). Peak (granulite-grade) metamorphism took place during 665–550 Ma, resulting in the formation of charnockitic rocks (Milisenda et al., 1988; Holzl et al., 1991). Therefore, Highland Complex rocks are generally considered to span an age range of 0.67–2 Ga.

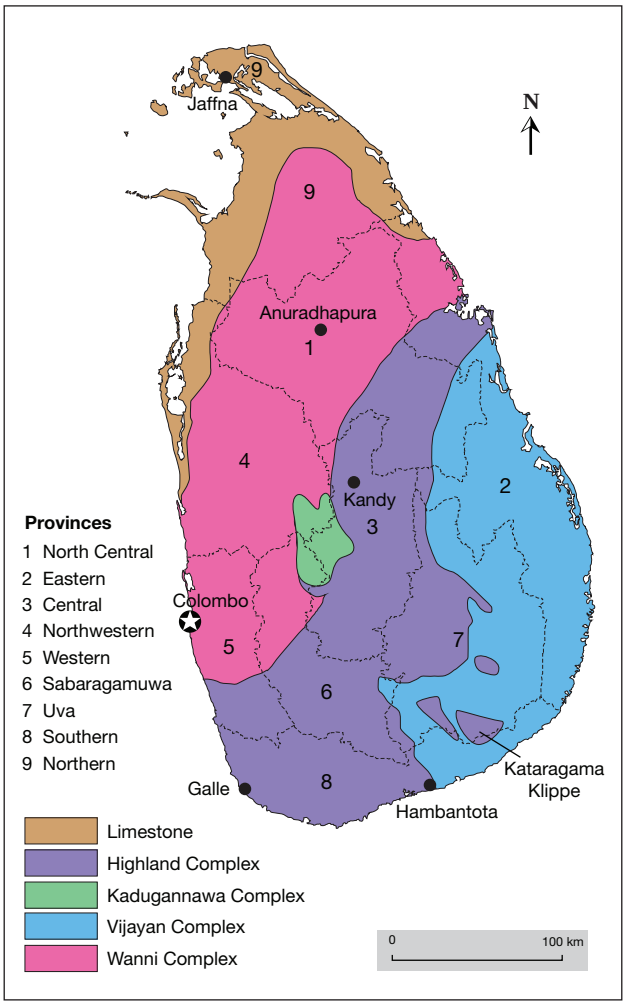

Figure 5. This simplified geologic map of Sri Lanka shows the location of the Kataragama klippe, one of the largest portions of the Highland Complex within the Vijayan Complex. Adapted from Cooray (1994).

Figure 4. The source of the gravel used at the road construction project proved to be this quarry, which was the scene of a second gem rush. Photo by Eranga Basnayake.

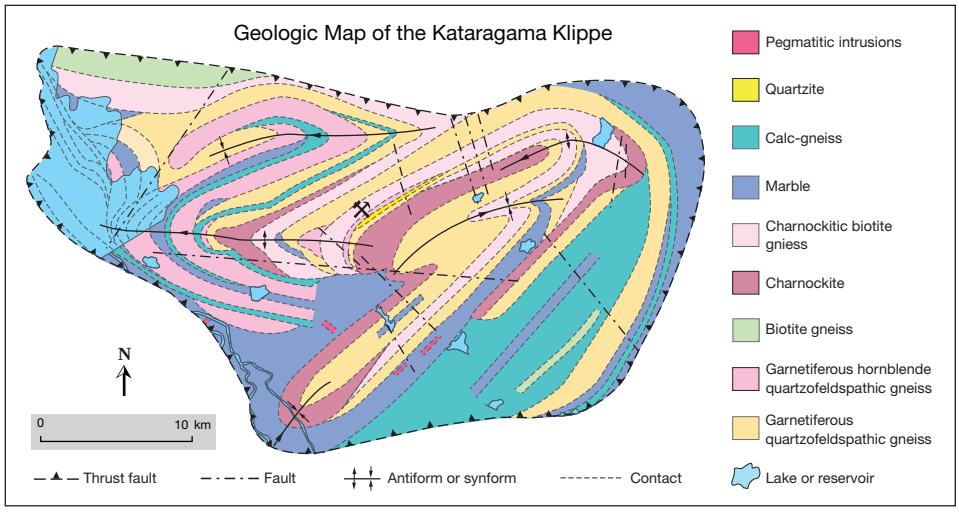

Figure 6. This geologic map of Kataragama klippe shows the new sapphire deposit is located within a band of charnockitic biotite gneiss. Source: Geological Survey and Mines Bureau (1997).

They have a layered appearance (ranging from millimeters to tens of meters wide) that is parallel to the main foliation of the rocks formed during the latest stage of pervasive metamorphism. The Kataragama area shows a series of large-scale antiform and synform structures trending east-west and northeast-southwest, and the klippe is separated from the surrounding Vijayan Complex rocks by thrust faults (figure 6).

In Brief

- A gem rush occurred in February 2012 after sapphires were discovered in a road construction site near Kataragama in southeastern Sri Lanka.
- Mining rights were auctioned on February 24 for 49 blocks covering the area.
- The sapphires are hosted by weathered pegmatitic intrusions associated with micaceous layers.
- Several kilograms of rough have been recovered, including lustrous well-formed crystals with transparent areas large enough to facet fine blue sapphires weighing more than 20 ct.

The major rock types in the Kataragama klippe are garnetiferous quartzofeldspathic gneiss ± hornblende, marble, calc-gneiss, charnockite and charnockitic biotite gneiss, and minor bands of quartzite (again, see figure 6). Late granitoid and pegmatitic intrusions of various sizes are locally found in the granulite-grade terrain; some crosscut the main geological structures, while others are parallel to the foliation of the host rocks.

Corundum Occurrence. Our field observations of the sapphire occurrence at Thammannawa revealed a complex, highly deformed geologic setting. The foliation of the rocks varies in several directions locally, but the general trend is 060°, dipping 50–60° northwest. Pegmatitic intrusions (figure 7) consisting of coarse-grained feldspar (kaolinized) and mica were surrounded by a micaceous layer that was foliated parallel to the contact with the intrusions. Quartz was absent from these rocks, though secondary silica formations such as chert and flint were seen in the area. Corundum mineralization was associated with the pegmatitic intrusions and mica layers, as indicated by our observations of a few small blue sapphire

Figure 7. Pegmatitic intrusions with associated micaceous layers host the corundum mineralization at Thammannawa. A Brunton compass (~7 cm wide) is shown for scale. Photo by H. M. R. Premasiri.

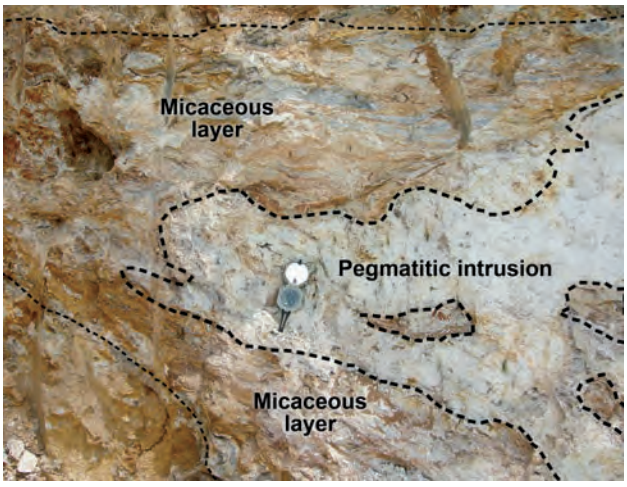

Figure 8. The known area of corundum mineralization (roughly outlined by dashed lines) is worked by backhoes in this view of the Thammannawa deposit. Photo by H. M. R. Premasiri.

crystals *in situ* and descriptions of the occurrence by local miners. This is also consistent with previous studies of Sri Lankan corundum mineralization, which have documented large crystals embedded in a feldspar matrix in the presence of biotite (Coomaraswamy, 1903; Hapuarachchi, 1989; Fernando et al., 2001; Hofmeister, 2001). Also present at Thammannawa were green tourmaline and garnet. The zone of intrusions and associated micaceous bands extended in the general foliation direction of the host rocks, and measured about 60 m thick.

Field geological evidence suggests that these rocks formed by a metasomatic process between pegmatitic fluid and the host rock. The corundum-bearing mineral assemblage is indicative of activity by pegmatitic fluid (e.g., Popov et al., 2007), and points to a metasomatic process for the origin of large euhedral sapphire crystals. Other than corundum, no noteworthy crystals or gem-quality minerals are known from the area.

MINING ACTIVITIES AND REGULATIONS

Gem mining in Sri Lanka has always been conducted by artisanal methods, using hand tools and water pumps. This tradition continues, and is supported by government and industry authorities to help insure the sustainability of gem mining activities and minimize damage to the environment. The use of backhoes and gravel-washing plants has been limited to isolated cases where the gravel beds were known to contain only low concentrations of gems or the same plot of land was worked by hand methods for many years. Therefore, the mining of secondary deposits (alluvial gem-bearing gravel layers) has continued in Sri Lanka for centuries. The less common primary gem deposits (*in situ*, often in weathered rocks) are commonly exhausted relatively quickly, and their discovery typically initiates gem rushes in which people dig with whatever equipment is available.

In Sri Lanka, gems found on private holdings or on government-owned land (forests, wildlife reserves, etc.) are considered de facto government property. In the case of private land, mining rights are given to the land owner and the government collects license fees in lieu of a royalty. However, in a gem rush situation the government imposes no immediate restriction, whether the land is private or government-owned. Invariably, though, the NGJA takes over the land and ensures it is kept under armed protection until the mining rights are auctioned to the public.

This same scenario unfolded at Thammannawa. The new deposit generated considerable excitement since the gems occurred as sharp-edged, well-formed crystals with a vitreous luster that is unprecedented in Sri Lankan sapphires. Because of the extraordinary publicity surrounding these gems, there was a frenzy of bidding at the auction for one-year mining rights. The auction raised a staggering 270 million rupees (US$2.45 million), or an average of US$18/m^2. However, some of the claims sold for as much as US$80/m^2, the highest price per square meter in the auction of gem mining rights during the NGJA's 40-year existence.

After the auction, the use of backhoes and dump trucks was allowed to resume (figure 8). Many of the miners continue to dig pits in their allocated land, but some abandoned their claims after encountering hard rock. The production of gems from the deposit is difficult to assess because the miners almost always keep their discoveries secret. According to some government officials, the total value of sapphires found at the road construction site and in the pit before the auction could have approached US$100 million.

In recent decades, successive administrations have introduced income tax concessions on rough gem sales to make trading more transparent. Only

Figure 9. These sapphire crystals and fragments (2.04–8.52 g) form some of the study samples used in this report. Courtesy of Udara Vijayamuni Zoysa; photo by D. Dillimuni.

about 2.5% of rough sales revenue is collected by the government as tax, whereas the tax applied to other businesses is often as high as 30%. Yet only a few gems—perhaps less than 10 specimens valued at over US$500,000 apiece—have been officially exported throughout the entire history of Sri Lanka, even though many gems over $1 million in value are discovered each year.

MATERIALS AND METHODS

Twenty-two sapphire crystals (2.0–289.6 g) and 11 faceted stones (1.00–6.48 ct) were studied for this report. According to the owners, the crystals were not heat treated, and our microscopic examination of the faceted stones showed no indications of heating. The samples were blue except for two yellow crystals; all were of good gem quality. Some were obtained at the site and others were received at the Allied Gemmological Institute & Laboratory for testing. The latter stones were loaned by the owner of the mining rights to block 6 (Udara Vijayamuni Zoysa), and by a reputable gem dealer in Ratnapura (Punsiri Tennekoon) who said they were from the Thammannawa deposit.

All 11 faceted sapphires were tested using a Topcon refractometer with a monochromatic filter. Specific gravity was determined hydrostatically on these same samples. Eighteen crystals and the 11 faceted stones were tested with both calcite and London dichroscopes and with prism- and diffraction-type hand spectroscopes. All rough and cut stones were checked for fluorescence with a standard UV lamp.

RESULTS

Visual Appearance. The study samples consisted of well-formed crystals or broken pieces of sapphire displaying bipyramidal or short barrel habits, mainly with a combination of hexagonal bipyramids and the

Figure 10. Weighing 4.5 g, this medium blue sapphire crystal displays a combination of hexagonal bipyramids with rhombohedral and basal pinacoids. Photo by Janaka Hemachandra.

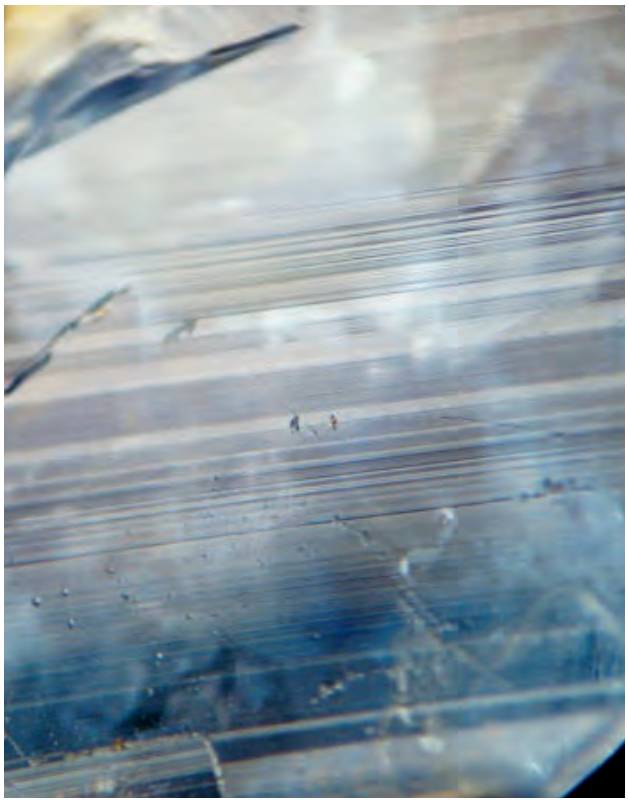

Figure 11. Thammannawa sapphire crystals show clearly defined horizontal striations on their bipyramidal faces. Photomicrograph by D. Dillimuni; magnified 10×.

basal pinacoid (figures 9 and 10). A few also showed rhombohedral and trigonal bipyramidal faces. Significantly, all of the crystals displayed lustrous crystal faces and perfectly sharp edges, with almost no signs of wear. Horizontal striations on bipyramidal faces were well defined (figure 11). When basal pinacoid faces were present, they displayed trigonal growth lines that evolved into hexagonal steps.

The samples were transparent with a glassy appearance, except for the largest specimen (~10 cm long), which was very dark blue and almost opaque. All the sapphire crystals displayed a strong pure blue color, somewhat different from the violetish blue commonly seen in Sri Lankan blue sapphire (figure 12). The crystals and cut stones also showed obvious dichroism, with a well-defined greenish blue seen perpendicular to the c-axis (figure 13). Observation with the dichroscope revealed that all the faceted samples had their table facet oriented perpendicular to the c-axis. Color zoning was clearly displayed in some crystals, parallel to the basal plane or the hexagonal pyramids. The color distribution in the faceted stones appeared even when viewed face-up, but closer examination revealed some irregular color patches with no particular orientation relative to the crystal structure.

Figure 12. These untreated sapphires (3.98–6.48 ct) show the pure blue color that is typical of stones from the Thammannawa deposit. Courtesy of Punsiri Tennekoon; photo by P. G. R. Dharmaratne.

Some of the crystals showed silky patches, but no asterism has been seen in sapphires from this area. Liquid-filled feathers, surface-reaching fractures, and large negative crystals were commonly visible to the unaided eye. Brown impurities in the fractures of some samples probably consisted of iron oxides/hydroxides.

Gemological Properties. Table 1 summarizes the properties of our Thammannawa samples and compares them to typical sapphires from elsewhere in Sri

Figure 13. Strong dichroism is observed with the London dichroscope in this 5.7 g sapphire. Photo by D. Dillimuni.

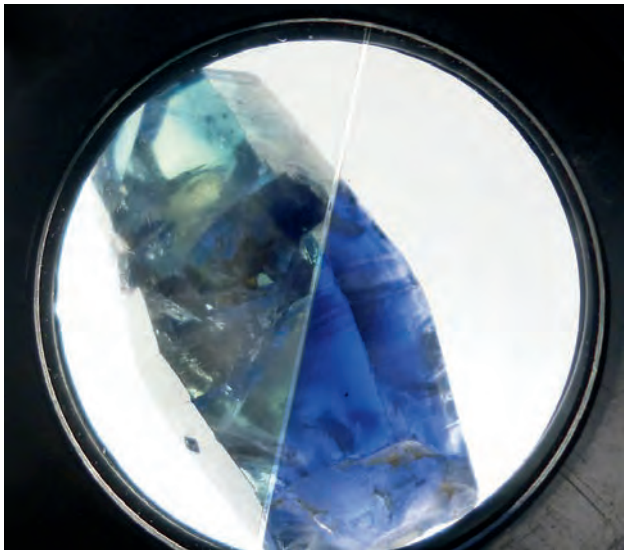

TABLE 1. Gemological properties of blue sapphires from Thammannawa and elsewhere in Sri Lanka.

Property	Thammannawa	Typical Sri Lanka
Color	Pure blue	Violetish blue
Color zoning	Straight and sharp zones parallel to the basal plane or hexagonal pyramid	Strong color zoning is common, but is less distinct in heat-treated stones. Some *(ottu)* have a colorless core with an outer layer or patch of blue color (Gunaratne, 1981; Hughes, 1997).
Optical phenomena	None	Asterism may be present
Refractive Indices	n_o = 1.760–1.762 and n_e = 1.768–1.770	n_o = 1.759–1.763 and n_e = 1.767–1.771
Birefringence	0.008	0.008
Specific Gravity	3.98–4.02[a]	3.98–4.02
Dichroism	Strong, in blue and greenish blue	Strong, in blue and greenish blue
Fluorescence		
Long-wave	Weak red (and strong orange from decomposed brown impurities in some crystals); colorless zones fluoresced weak orange	Inert to strong red to orange
Short-wave	Inert	Heat-treated specimens often show a zoned chalky blue-green reaction
Absorption spectra	Strong Fe absorption line at 450 nm	Weak to moderate Fe absorption line at 450 nm (Hughes, 1997)
Internal features	Short rutile needles, liquid-filled feathers, and negative crystals. Long rutile needles, translucent milky patches *(geuda)*, blue patches or zones *(ottu)*, and silk were not observed in any of the samples.	Short and long rutile needles, liquid-filled feathers, and negative crystals, translucent milky patches *(geuda)*, blue patches or zones *(ottu)*, and silk in asteriated samples

[a] *Crystals with large negative crystals had low SG values (~3.98), while all the faceted stones had a constant value of 4.00.*

Lanka. Microscopic examination showed that oriented short needles (probably rutile) are characteristic of the Thammannawa sapphires (figure 14). These inclusions formed weak silky patches in some samples, while others had needles that were more compact and coarse. In one case, part of a faceted stone showed a copper color with a metallic sheen due to a high concentration of these needles (figure 15). Liquid-filled

Figure 14. Fine rutile needles oriented in parallel layers form characteristic inclusions in the sapphires. Photomicrograph by D. Dillimuni; magnified 15×.

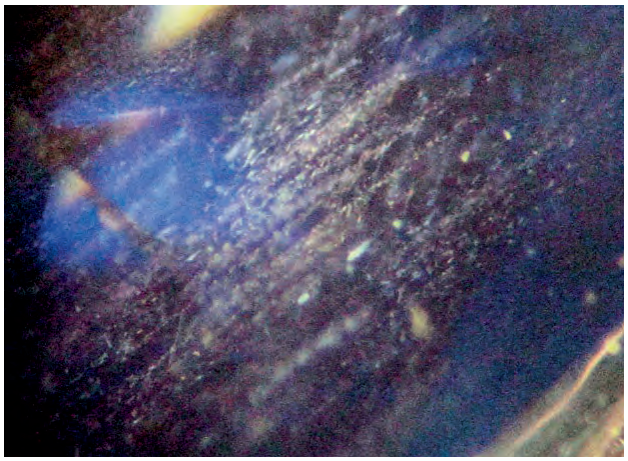

Figure 15. A portion of this sapphire contains a high concentration of rutile needles that produces a copper-colored metallic sheen. Photomicrograph by D. Dillimuni; magnified 20×.

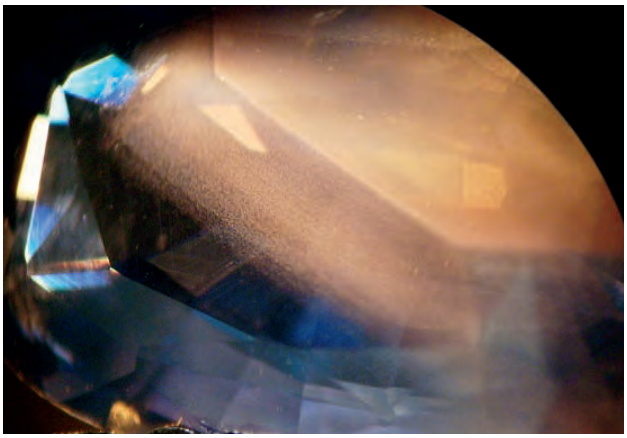

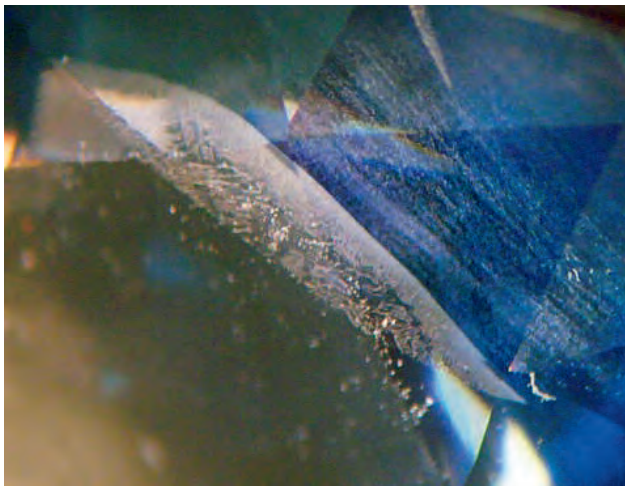

Figure 16. Liquid-filled feathers are common in the Thammannawa sapphires. Photomicrograph by D. Dillimuni; magnified 10×.

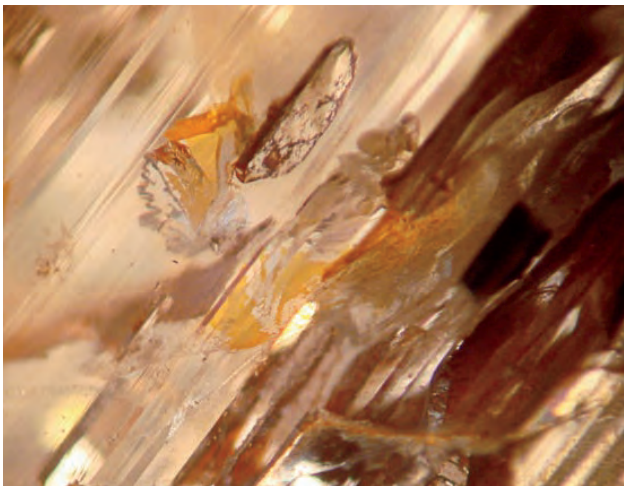

Figure 17. This yellow sapphire from Thammannawa contains a parallel arrangement of tabular negative crystals. Photomicrograph by D. Dillimuni; magnified 10×.

feathers were routinely observed in the sapphires from this deposit (figure 16). They were visible even in the rough specimens, on account of their smooth crystal faces. Negative crystals with tabular and columnar forms were also present as large isolated inclusions or grouped in parallel arrangement (figure 17).

DISCUSSION

Compared to other gem occurrences in Sri Lanka, the new deposit at Thammannawa has some characteristic features. Whereas other deposits on the island contain several gem varieties, only corundum has been found at this new locality—mainly blue and a few yellow sapphires. Star varieties, *geuda*, and corundum of other colors have not been found in this deposit. The crystals possess a bright vitreous luster and good transparency, with a glassy appearance; their sharp edges and lack of alluvial transport are unusual for Sri Lankan corundum. Also, their characteristically pure blue color is different from the violetish blue typically observed in sapphires from other parts of the country. Some of the stones displayed color zoning, but none showed the typical patches or concentrations of color that are amenable to heat treatment.

Although an absorption line at 450 nm is weak to moderate in typical Sri Lankan blue sapphires (Hughes, 1997), a strong line was observed in the Thammannawa specimens with both the prism and diffraction-type spectroscopes. UV-Vis-NIR spectra of Thammannawa sapphires obtained by Pardieu et al. (2012) confirmed the presence of this absorption line.

Consistent with their strong blue bodycolor, the samples exhibited a weak red fluorescence to long-wave UV radiation, an effect seen in some violet-blue sapphires from elsewhere in the country. The inclusions are also fairly characteristic to these stones: Short and fine rutile needles concentrated in layers and large well-formed negative crystals (sometimes several arranged in parallel) were seen with liquid feathers. A similar combination of inclusions is only typical of yellow sapphires from the Balangoda area in Sri Lanka. Additional mineral inclusions documented in Thammannawa sapphires by Pardieu et al. (2012) included dark opaque crystals resembling uraninite, graphite, and spinel—along with dark green and colorless crystals resembling spinel and zircon, respectively.

Figure 18. These pendants feature sapphires from Thammannawa that weigh 4.6–6.2 ct. Composite photo by Sherrif Rahuman.

CONCLUSION

The discovery of commercial quantities of gem corundum from a weathered primary deposit at Thammannawa near Kataragama has revived gem mining activities in an area of Sri Lanka previously known to contain only hessonite garnet. Mining in the auctioned lands is progressing rapidly, and the collected gravel is still being washed. Geologists are working to find additional desilicated pegmatitic intrusions and associated micaceous layers that have gem-bearing potential. So far, a limited amount of these sapphires have been mounted into jewelry (e.g., figure 18). Nevertheless, this deposit—and the possibility of similar occurrences in the same area of Sri Lanka—could provide additional high-quality material for the sapphire market in the future.

ABOUT THE AUTHORS

Dr. Dharmaratne (dharme27@yahoo.com) is senior professor, and Dr. Premasiri is senior lecturer in geology, at the University of Moratuwa in Sri Lanka. Mr. Dillimuni is a consultant gemologist and tutor at Allied Gemmological Institute & Laboratory in Colombo, Sri Lanka.

ACKNOWLEDGMENTS

For their assistance with this article, the authors thank Dr. C. B. Dissanayake (Institute of Fundamental Studies, Kandy, Sri Lanka), Dr. Rohan L. De Silva (CCS Project, National Grid, UK), Rosemary Dharmaratne (Colombo), Punsiri Tennekoon (Punsiri Gems, Ratnapura), Ranjith Aruna (National Gem & Jewellery Authority, Monaragala), Tissa Jayawardana (Ratnapura), Janaka Hemachandra (National Gem & Jewellery Authority, Colombo), Sherrif Rahuman (Colombo), Gamini Kumasaru (Department of Earth Resources Engineering, University of Moratuwa), Udara Vijayamuni Zoysa (Ministry of Education, Colombo), Eranga Basnayake (Balangoda, Sri Lanka), and Ajward Deen (A.M.S. Deen & Sons, Colombo).

REFERENCES

Coomaraswamy A.K. (1903) Occurrences of corundum *in-situ* near Kandy, Ceylon. *Geological Magazine*, Vol. 21, pp. 348–350.

Cooray P.G. (1994) The Precambrian of Sri Lanka: A historical review. *Precambrian Research*, Vol. 66, No. 1–4, pp. 3–18, http://dx.doi.org/10.1016/0301-9268(94)90041-8.

Fernando G.W.A.R., Hauzenberger C.A., Hofmeister W. (2001) Origin of corundums in Sri Lanka: Evidence from case studies of in-situ deposits. *Journal of the Geological Society of Sri Lanka*, Vol. 10, pp. 37–47.

Fernando T. (2012) Biggest blue sapphire gem deposit found. *The Daily Mirror*, Feb. 23, p. A-3.

Geological Survey and Mines Bureau (1997) Kataragama-Tissamaharama-Yala geology map, Sheet No. 21, scale 1:100,000.

Gunaratne H.S. (1981) Geuda sapphires: Their colouring elements and their reaction to heat. *Journal of Gemmology*, Vol. 17, No. 5, pp. 292–300.

Hapuarachchi D.J.A.C. (1989) Some observations on the origin of gem corundum in Sri Lanka. *Journal of the Geological Society of Sri Lanka*, Vol. 2, pp. 5–9.

Hofmeister W. (2001) Interpretation of some typical Vietnamese gem mineralizations. *Proceedings of the International Workshop on Material Characterization by Solid State Spectroscopy: Gems and Mineral of Vietnam*, Hanoi, April 4–10, pp. 1–9.

Holzl S., Kohler H., Kröner A., Jaeckel P., Liew T.C. (1991) Geochronology of the Sri Lankan basement. In A. Kröner, Ed., *The Crystalline Crust of Sri Lanka, Part 1*. Professional Paper No. 5, Geological Survey Department, Sri Lanka, pp. 237–258.

Hughes R.W. (1997) *Ruby & Sapphire*. RWH Publishing, Boulder, Colorado.

Kroner A., Cooray P.G., Vitanage P.W. (1991) Lithotectonic subdivision of the basement in Sri Lanka. In A. Kröner, Ed., *The Crystalline Crust of Sri Lanka, Part 1*. Professional Paper No. 5, Geological Survey Department, Sri Lanka, pp. 5–21.

Milisenda C.C., Liew T.C., Hofmann A.W., Kroner A. (1988) Isotopic mapping of age provinces in Precambrian high-grade terrains: Sri Lanka. *Journal of Geology*, Vol. 96, No. 5, pp. 608–615, http://dx.doi.org/10.1086/629256.

Nizam I. (2012) Gem rush expected today. *The Island*, Feb. 23, www.island.lk/index.php?page_cat=article-details&page=article-details&code_title=45936 [date accessed: Feb. 26, 2012].

Pardieu V., Dubinsky E.V., Sangsawong S., Chauviré B. (2012) Sapphire rush near Kataragama, Sri Lanka (February–March 2012). GIA News from Research, www.gia.edu/research-resources/news-from-research/Kataragama_US_version_0503.pdf [date accessed: May 21, 2012].

Popov V.A., Popova V.I., Polyakov V.O. (2007) Regular intergrowths of minerals in pegmatites from the Il'meny mountains. *Geology of Ore Deposits*, Vol. 49, No. 7, pp. 573–582, http://dx.doi.org/10.1134/S1075701507070136.

Silva K.P.L.E., Wimalasena E.M., Sarathchandra M.J., Munasinghe T., Dissanayake C.B. (1981) The geology and the origin of Kataragama Complex, Sri Lanka. *Journal of the National Science Council of Sri Lanka*, Vol. 9, No. 2, pp. 189–197.

CULTURED PEARL FARMING AND PRODUCTION IN THE FEDERATED STATES OF MICRONESIA

Laurent E. Cartier, Michael S. Krzemnicki, and Masahiro Ito

The current production of cultured pearls from the black-lipped pearl oyster (*Pinctada margaritifera*) in the Federated States of Micronesia (FSM) includes mostly beaded as well as blister and nonbead-cultured pearls in a wide array of colors. Pearl farming is carried out on four islands, with plans for commercial production in the near future. The sector is envisaged as a model for economic development and marine conservation. To successfully compete in the marketplace, pearl farmers in the FSM should focus on producing high-quality cultured pearls and explore market differentiation strategies such as the "Micronesian Blue" product. Gemologically, the FSM cultured pearls are indistinguishable from those of French Polynesia that are produced using the same mollusk species.

In Micronesia, a group of more than 2,000 small islands in the western tropical Pacific Ocean, *P. margaritifera* oyster shells have been used by local populations and sold to itinerant traders since the 18th century (Clarke et al., 1996). Martin (1996) noted that in the 1800s, German divers gathered 50 tonnes of oysters from Chuuk Lagoon. The Japanese occupation of Micronesia (1914–1944) prompted further interest in pearl oyster resources, and shells were fished and a trial cultured pearl farm established in nearby Palau. In 1986, the FSM gained sovereignty after nearly 40 years as a U.S.-administered trusteeship. That year, 8,595 kg of black-lipped oysters were harvested in Chuuk Lagoon (Smith, 1992). Until 1987, however, there were no serious efforts to develop a cultured pearl farming industry in the area (Clarke et al., 1996). In the past 25 years there have been numerous attempts to establish commercial and community-based pearling operations. Current efforts are promising, and a variety of cultured pearl colors, including "Micronesian Blue," are beginning to reach the international market (figures 1 and 2).

Black cultured pearl production from the *P. margaritifera* mollusk was valued at more than US$100

Figure 1. These earrings contain "Micronesian Blue" cultured pearls (~10.5 mm in diameter). Photo courtesy of Natsuko Shiraki, © Hasuna Co. Ltd., Tokyo.

See end of article for About the Authors and Acknowledgments.
GEMS & GEMOLOGY, Vol. 48, No. 2, pp. 108–122,
http://dx.doi.org/10.5741/GEMS.48.2.108.
© 2012 Gemological Institute of America

Figure 2. These bracelets are made with baroque-shaped cultured pearls (~7.3–9.0 mm) from the FSM. Photo courtesy of Natsuko Shiraki, © Hasuna Co. Ltd., Tokyo.

million in 2009 (Müller, 2009). This mollusk has a wide geographic distribution, including the Pacific Ocean, Indian Ocean, Red Sea, and off the coast of Mexico (Strack, 2006). However, commercial cultivation of this mollusk only takes place in French Polynesia, the Cook Islands, and Fiji, and is just beginning to emerge in the FSM. The industry as a whole is only 50 years old; the first successes in French Polynesia were reported in 1961 (Domard, 1962).

Pearl farming and associated economic activity has brought considerable development to remote regions of French Polynesia and the Cook Islands (Southgate and Lucas, 2008). At its peak in 2000, the French Polynesian cultured pearl sector employed 7,000 people (Murzyniec-Laurendeau, 2002). In recent decades, a number of other developing Pacific countries—through government and donor-funded projects—have attempted to emulate these successes in culturing black pearls from *P. margaritifera*. These include Kiribati, the Marshall Islands, Papua New Guinea, the Solomon Islands, and Tonga (Strack, 2006; Southgate and Lucas, 2008). The FSM is an ideal candidate for pearl farming projects because of its ecological similarity to the islands of French Polynesia. The country is highly dependent on foreign aid through the U.S. Compact of Free Association agreement, receiving a projected US$92.2 million in 2011 ("The Federated States of Micronesia…," 2010). Clearly, the production of high-value cultured pearls could foster indigenous economic development.

This article reviews various initiatives since 1987 to establish a Micronesian cultured pearl industry and evaluates the viability of community-based farming projects and marketing opportunities for "development pearls." It examines the implications of recent developments in the global black cultured pearl industry for the nascent FSM industry. The hatchery production of juvenile oysters is highlighted, as are a number of pearl oyster husbandry techniques and factors that influence the quality of the resulting cultured pearls. Finally, gemological characteristics of the bead-cultured pearls are presented. One of the authors (LC) visited the FSM pearl farms in October 2011, whereas another author (MI) has been working in the FSM on developing pearl farming and other aquaculture activities since 2001.

HISTORY AND INDUSTRY STRUCTURE

In 1987, the Pacific Fisheries Development Foundation and Pohnpei Research Division began evaluating the feasibility of a domestic cultured pearl industry. Since then a number of pilot projects and initiatives in the FSM have been started by local government, donors, and private citizens. Survey work and a feasibility study were briefly carried out on Ahnt Atoll but ceased in 1991 (Clarke et al., 1996). The primary focus of subsequent efforts was on Nukuoro Atoll, the only island in the FSM known to have a sufficient population of wild spat, thus eliminating the need for costly hatchery production of juvenile oysters. In 1994, Australia and the Pohnpei state government began funding a local project, and by 1995 there were 3,000 oysters seeded with round nuclei and 100 shells implanted with blister nuclei (Clarke et al., 1996). Low retention rates were attributed to the "poor condition of the oysters, the rudimentary working conditions and the relative inexperience of the local staff" (Clarke et al., 1996; p. 4). These factors, along with others detailed later in this article, have posed serious challenges to donor-funded community pearl farms in the FSM.

The Nukuoro farm was eventually incorporated in 2009 as Nukuoro Black Pearl Inc. (Leopold, 2011). The first significant harvest was sold locally in 2002, with 800 cultured pearls bringing US$10,000 (Sehpin, 2002). Three years later, financial irregularities were reported at Nukuoro (Sehpin, 2005). That same year saw the development of a bioeconomic model for small-scale pearl farms that was based on production and financial data from the Nukuoro farm, along with another farm in the Marshall Islands (Fong et al., 2005). However, pearl cultivation ceased in 2009. According to the Nukuoro municipal government, the oysters were left in the lagoon, and 10,000–20,000 have now reached an operable size but cannot be implanted due to lack of funding.

At present, pearl culturing takes place on four of the FSM's 607 islands, all within the state of Pohnpei: Pakin, Pohnpei (Nett Point), Pingelap, and Pweniou (a tiny islet off Pohnpei Island; figure 3). The first two farms each have 10,000 oysters, whereas the latter ones each have 3,000 oysters. All of these farms are in preparation for commercial pearl cultivation. Municipal government recently discontinued cultivation on a fifth island (Mwoakilloa) pending additional investment.

The waters in the FSM region, especially near Pohnpei, are rich in nutrients from nearby coastal mangrove forests. Water temperatures near Pohnpei's Nett Point farm vary between 27°C and 30°C, and salinity ranges from 35.0 to 35.5 parts per thousand. Testing at various sites within the Pohnpei lagoon has revealed that water currents, nutrient availability, and shelter vary greatly from site to site. Appropriate sites for pearl farming have been chosen taking these factors into account. The healthier the oyster, the lower the probability of disease, complications, or mortality and the higher the likelihood of harvesting high-quality cultured pearls.

The most encouraging efforts in support of pearl culturing in the FSM involve a project at the College of Micronesia (COM) Land Grant Program, which supplies hatchery-grown spat and technical assistance to the four operations mentioned above. In 2001, work began on a demonstration and training hatchery at the program's facilities at Nett Point on Pohnpei. The aim of the hatchery was to supply high-quality spat to islands that have insufficient natural oyster populations (Ito et al., 2004). This project has received funding from the U.S. Department of Agriculture (USDA), the U.S. Department of the Interior's Office of Insular Affairs, and the COM program. The ultimate goal is to "develop a self-sustaining pearl industry, integrating both community-based and commercial pearl farming operations" by 2016 (Ito, 2006). Investors have visited the FSM to explore the possibility of a large-scale commercial pearl farm, and such an enterprise would ensure the long-term viability of the hatchery, which is still being subsidized.

Figure 3. This map shows the location of past and present cultured pearl operations in the FSM. The hatchery that produces oyster spat is located at Nett Point on Pohnpei. The brood stock for this hatchery was initially collected from Ahnt, Pohnpei, and Pakin Islands. Pearl farms are presently in operation on Pakin, Pohnpei, Pingelap, and Pweniou (just off Pohnpei) Islands. Former farms on Mwoakilloa and Nukuoro are no longer producing any cultured pearls. Illustration by Augustin Hiebel.

Another project has received two rounds of funding from the Center for Tropical and Subtropical Aquaculture (CTSA) to investigate the development of pearl farming in the FSM (Haws, 2004), as well as to make hatchery production more efficient and to determine the spawning seasons of black-lipped pearl oysters (Haws et al., 2004). Most of the hatchery-based work was attempted in the Marshall Islands. This project has been discontinued due to a lack of funding. There was no overlap with the COM-based project, and the activities described in this article all stem from work at COM designed to produce cultured pearls marketed under the "Micronesian Blue" label.

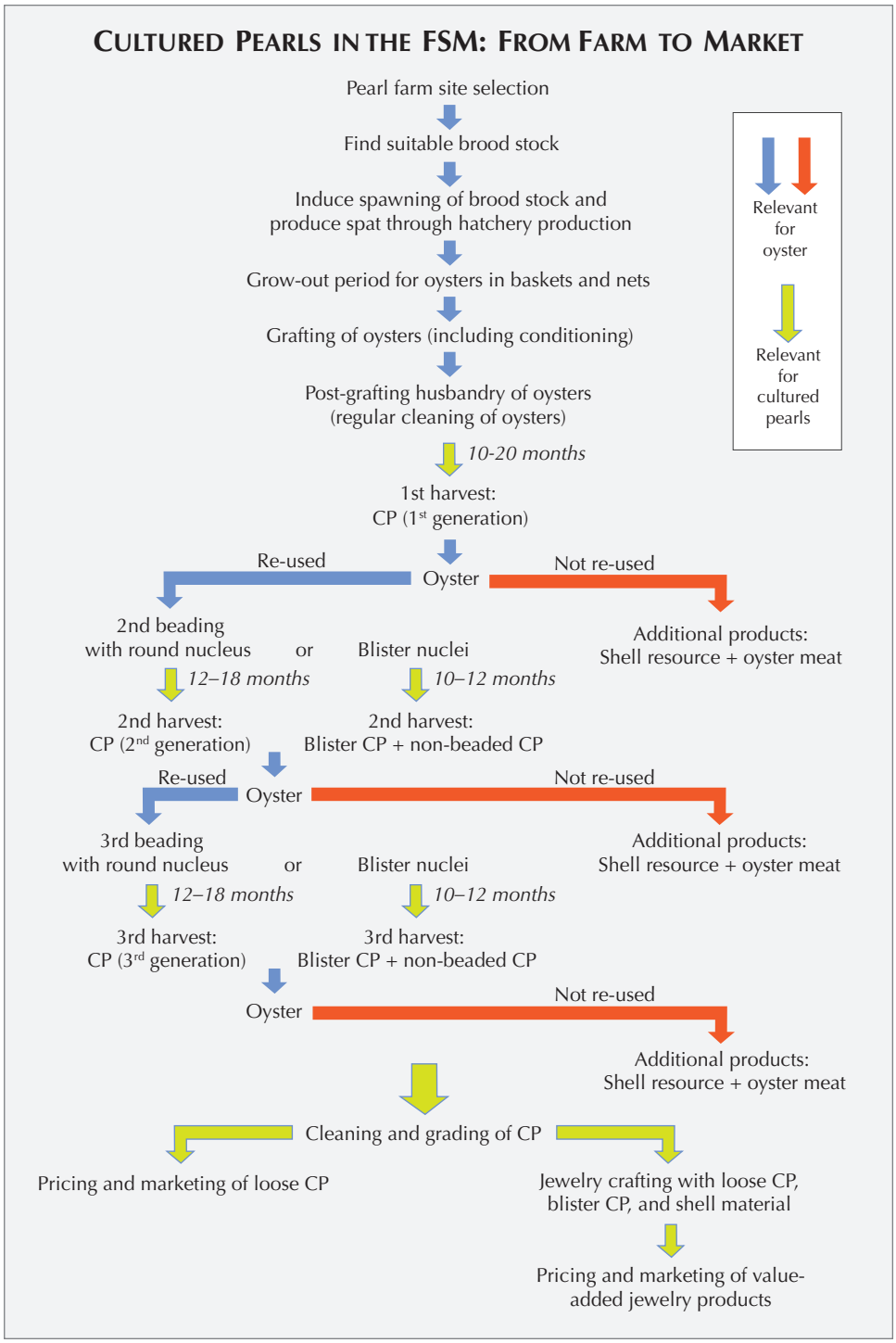

Figure 4. This diagram illustrates the different steps in setting up a pearl farm and obtaining cultured pearls (CP) in the FSM. It shows the potential of using the same oyster several times in the production of cultured pearl products and what resources can be obtained from this process. The periods indicated are from the time of seeding to the time of harvest. Modified after Haws (2002).

PEARL FARMING

The entire FSM pearling procedure, from farm site selection to marketing of the cultured pearls, is presented in figure 4.

Spat Production. Whereas the French Polynesian industry has relied on the collection of wild spat, the emerging FSM cultured pearl sector—apart from Nukuoro—relies on hatchery production using mature oysters (i.e., "brood stock"). Many Pacific islands have seen overfishing and a significant depletion of wild oyster stocks. Winds, currents, hydrology, and the placement of spat collectors and substrates also play major roles in determining the number of spat

that can be collected in the wild. Surveys have been conducted around the islands of Ahnt, Pakin, and Pohnpei to determine the feasibility of wild spat collection, but the populations were far too low. To address the shortage of wild spat in Micronesia, two hatcheries were set up in 2001: at Nett Point operated by COM (mentioned above) and on the southern part of Pohnpei Island run by the Marine and Environmental Research Institute of Pohnpei (Haws, 2004).

The key to high-quality hatchery-based spat production is careful selection of mature brood stock oysters collected in the wild. The brood stock strongly influences the color and quality of the cultured pearls. Brood stock for the Nett Point hatchery were collected by one of the authors (MI) and collaborators during multiple transect dives on the islands of Ahnt, Pohnpei, and Pakin from 2001 through 2004.

Whether spat is collected in the wild or produced in a hatchery, oyster reproduction follows very specific cycles that must be taken into account. Interestingly, the FSM seems to have no distinct spawning seasons. However, there are roughly two periods, March–June and September–December, when oysters release eggs and sperm and fertilization can take place. As in French Polynesia, this corresponds to seasonal changes in ocean water temperature and nutrient content (Southgate and Lucas, 2008). Full moon is usually a very good time to induce spawning in the hatchery setting, and this is done by stressing the oysters, such as by a rapid change in water temperature. Spawning in the wild is also induced by a change in environmental factors, though much less rapidly. One episode of spawning in a hatchery can yield 1–2 million oyster larvae per 1,000 liter tank. These larvae are fed various types of algae (figure 5), and they eventually develop into spat. Meanwhile, the water conditions are closely monitored. The combination of algal feed and water conditions is critical to producing strong, high-quality spat. Around day 17–19, spat collectors (e.g., 30 × 50 cm pieces of shade cloth attached to ½ in. PVC pipe frames, known as "Christmas tree" collectors) are placed in the tanks. Approximately 500–2,000 spat accumulate on the 60–70 collectors deployed in each tank. The spat are left there for 42–46 days, until they reach a size of 2–5 mm in antero-posterior shell length. Following this stage, they are transferred from the hatchery tanks into oceanic spat collectors or pearl oyster nets for nursery grow-out.

Figure 5. At the Nett Point hatchery, four species of algae are typically used to feed oyster larvae: Cheatoceros *(yellow),* Pavlova *(yellow-brown),* Rhodomonas *(orange), and* Tetraselmis *(green). Photo by L. Cartier.*

In Brief

- Efforts to produce black cultured pearls in the Federated States of Micronesia (FSM) date back to 1987.
- Farms on four islands in the state of Pohnpei (Pakin, Pohnpei, Pingelap, and Pweniou) are preparing for commercial pearl cultivation, with a total of 26,000 hatchery-reared oysters.
- These farms are projected to yield 6,500 cultured blister pearls and 2,000 loose bead-cultured pearls in 2012, with increasing production in the future.
- The cultured pearls show a range of colors; those with particularly distinct blue overtones are most prized, and branded "Micronesian Blue."

Nursery and Husbandry. Baskets with juvenile oysters are taken to the pearl farm (e.g., figure 6), and left on the seabed in shallow waters to reduce predation. Spat mortality is initially assessed by onsite counting approximately four months after fertilization, and the baskets are examined every six weeks for predators. Carnivorous snails and crabs are major causes of spat mortality. The young oysters are later transferred to lantern baskets (figure 7). When they are between 1.5 and 2.5 years in age they are removed from the baskets, drilled, and hung on chaplet lines (see figure 8). In most areas of the FSM, netting is not required at this stage because predation is less of a threat. Biofouling, the settling and growth of animals and plants

Figure 6. This photo shows the farming operation near Pweniou Island off Pohnpei. Photo by L. Cartier.

on the oysters, must be removed in 1–2 month intervals to ensure the proper health and growth of the pearl oysters (figure 9). Once the shell is deemed sufficiently large (10–12 cm in diameter) and healthy, the oyster can be grafted to induce the formation of a cultured pearl.

Grafting. The grafting operation requires a host and a donor oyster, and a skillful technician (e.g., Hänni, 2007). Whereas the donor oyster (which is sacrificed) is selected for the quality of its mantle, the host oyster is chosen for its vigor (Haws, 2002). An international grafting technician regularly visits the FSM to train locals in grafting techniques for both round and blister cultured pearls, with the aim that by 2013 they can meet the requirements of a nascent cultured pearl industry. The nuclei consist of Mississippi mussel shell material and range from 5.5 to 13.0 mm in diameter.

Figure 7. Two-year-old oysters in lantern baskets are examined at the Pweniou pearl farm. Inside the basket, technicians found two predatory snails. Photo by L. Cartier.

Typically, the first-generation operation is carried out to produce a loose cultured pearl. Cultured blister pearls are sought in older generations of pearl oysters, which can be regrafted two or three times. For the production of bead-cultured pearls, the seeded oysters are kept in the water between 10 and 20 months. An oyster deemed unsuitable for regrafting may then be seeded to produce several cultured blister pearls (figure 10). In this case, the oyster is left in the water 10–12 months. Because a pearl sac is already present, such oysters are very likely to bear "keshi" nonbead-cultured pearls as well. This strategy maximizes the resource: Rather than sacrificing the oyster, it is reused to produce cultured blister pearls that can be manufactured into simple jewelry.

PRODUCTION, PROCESSING, AND MARKETING

Loose cultured pearls and blister products are harvested several times a year, but the output remains small. Production from the COM project in the FSM during the past decade was around 15,000 round cultured pearls and 3,000 cultured blister pearls. The majority of them came from the Nett Point farm on

Figure 8. Grafted oysters are attached to ropes using the "ear-hanging" method, forming chaplets. Photo by L. Cartier.

Pohnpei. They were sold as samples from the COM project to selected Japanese jewelry designers and shops for promotional purposes.

The four farms linked to the COM program are projected to yield 6,500 cultured blister pearls and 2,000 loose bead-cultured pearls in 2012, with a steady expansion in the coming years. The cultured blister pearls are expected to come from Pohnpei (3,000 pieces), Pakin (2,000 pieces), and Pweniou (1,500 pieces), and they will be sold on the local and international markets. As pearl farming moves toward commercial operation in the near future, round cultured pearls will also enter the international market.

The FSM produces far fewer dark cultured pearls than French Polynesia, because it uses lighter-colored brood stock. They are cleaned and processed with nothing more than sea salt and a polishing cloth. Most cultured blister products are crafted into jewelry and sold locally. Two charity sales in Pohnpei in 2010 led to revenues of US$6,000 and $13,500. The entire local market in the FSM is estimated at only US$100,000 per year, and the country drew just 20,000 tourists in 2010. If the pearl sector is to grow, it must expand beyond the local market. Nearby Guam, for instance, is an important tourist destination.

The FSM pearl industry must also find suitable niches worldwide and generate greater income through marketing differentiation (Fong et al., 2005). Although not yet commercially available on the international market, "Micronesian Blue" cultured pearls are being sold at charity sales and were used in two Japanese jewelry collections. The FSM products are also being marketed as "development pearls" because of their contributions to the local economy and marine conservation. Additional marketing strategies are being examined to avoid the failures of numerous donor-funded projects to promote community-based pearl farming over the past three decades (Ito, 2011a).

QUALITY: THE KEY TO PEARL FARM VIABILITY

The greater the proportion of high-quality cultured pearls in a harvest and the lower the oyster mortality rates, the more likely a farm will be profitable. Haws (2002) calculated that 95% of a farm's earnings come from just 2% of the cultured pearls. Le Pennec et al. (2010) estimated that for 2,000 grafted oysters, only 3% yield "beautiful" cultured pearls; improving this rate to 4% would considerably increase farmers' incomes. Conversely, Fong et al. (2005) projected that for a farm with 25,000 seeded oysters, a 5% increase in mortality would raise production costs per cultured pearl by nearly 21%.

Figure 9. Regular cleaning of oysters, as shown here on Pakin Island, is vital to maintaining their health. This step also creates jobs for local villagers. Photo by L. Cartier.

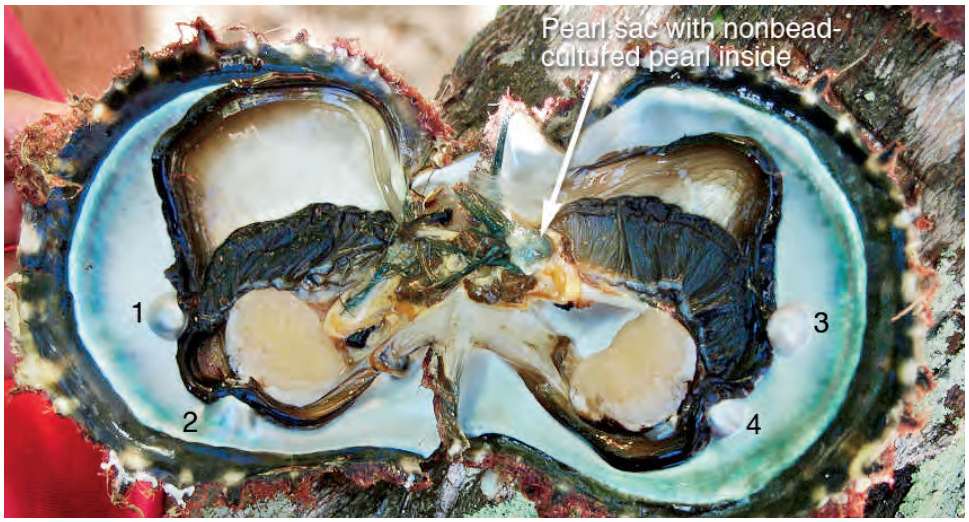

Figure 10. An oyster that yielded a first-generation cultured pearl was re-beaded to produce four cultured blister pearls. The remaining pearl sac produced a nonbead-cultured pearl. Photo by L. Cartier.

Le Pennec et al. (2010) noted that out of 1,000 oysters grafted in French Polynesia, 250–300 saleable cultured pearls (25–30%) are typically produced in the first generation. In a study of the Nukuoro farm and another farm in the Marshall Islands, Fong et al. (2005) found that 10,725 marketable cultured pearls (42.9%) were produced from a harvest of 25,000 first-seeded oysters. This success rate is surprisingly high given that mortality rates should be similar to those in other areas of Micronesia (see below) and that the two farms were not commercially successful. The lack of an industrywide grading system for cultured pearls also makes such comparisons difficult.

Improving Cultured Pearl Quality. Murzyniec-Laurendeau (2002) showed that in a sample harvest of 271,000 *P. margaritifera* cultured pearls from French Polynesia, circled goods (cultured pearls with concentric rings or grooves visible on the surface) accounted for 23% of the volume but only 6% of the value. If formation mechanisms of circled cultured pearls can be better understood, practices can be adapted to minimize their production in favor of more valuable cultured pearls. There is a surprising lack of collaboration between gemologists and scientists researching biomineralization, aquaculture, and oyster genetics. Greater synergy across disciplines would advance cultured pearl production and quality.

A three-year research project was initiated by COM in 2007 to understand how grafting techniques could be optimized to improve quality (Ito, 2009). The study also investigated formation mechanisms of circled cultured pearls and disproved the widely held idea that they result from nucleus rotation in the pearl sac (see also Caseiro, 1993). Ito (2009, 2011b) argued that if this were the case, non-linear patterns should be found on circled cultured pearls. However, Ito's (2011b) study of 4,011 samples found no evidence for this, and proposed a mantle cell proliferation mechanism of circled cultured pearl formation.

A great deal of experimentation has gone into understanding the optimal conditions for oysters and how the quality of harvested cultured pearls can be improved through certain pearling practices. A trial project was initiated by COM in 2005 to investigate the circling phenomenon in cultured pearls, and this study also offered an overview of mortality and rejection rates (figure 11). These rates were higher than in a normal pearl farming context, because the aim was scientific experimentation rather than commercial success; the total success rate was only 28%. Nucleus rejection rates for second-generation grafting of these trial oysters decreased to 10–15%, which is good by international comparison.

The harvesting success rates and qualities are highly dependent on farm site, nursery expertise, skills of the grafting technicians, and whether pearl farming was carried out for experimental or commercial purposes. The following practices are recommended in the FSM: Waiting until the oysters reach a good size (10–12 cm in shell diameter) before grafting, maintaining low stocking densities of oysters, extending the period between grafting and harvest, and regularly (every 6–8 weeks) removing any biofouling from the oysters.

ECONOMIC CONSIDERATIONS AND DEVELOPMENT STRATEGIES

The average price (at export) of black cultured pearls in French Polynesia has fallen by a factor of four in

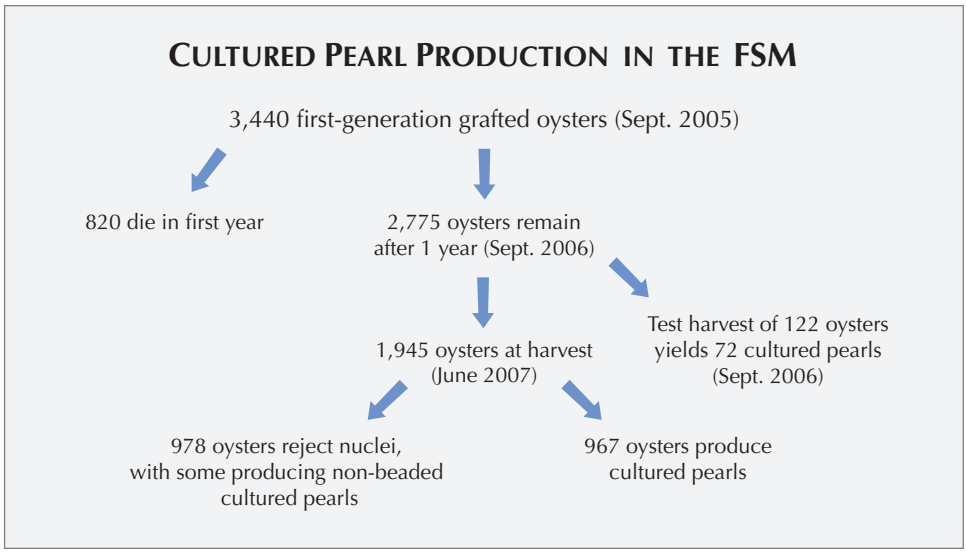

Figure 11. This chart shows the oyster mortality and rejection rates for a 2005–2007 trial project in the FSM. These figures are higher than those in other pearl farming regions, but do not reflect current rates in the FSM, which are much lower.

the past decade, from 1,800 CFP francs (US$19.68) to 460 CFP francs (US$5.03; Talvard, 2011). However, this depreciation is also the result of diminishing quality in the output of many pearl farms. Government authorities continue to carry out quality control of exported cultured pearls, and those of very low quality are destroyed. However, both the average size and average quality of these cultured pearls are lower than a decade ago. Such developments in the French Polynesian industry—which accounts for more than 95% of the world's black cultured pearls—are bound to also affect minor producers such as the Cook Islands, Fiji, Mexico, and the FSM.

A number of reports have noted the lack of large (>13 mm) high-quality black cultured pearls in the international market (Shor, 2007; Torrey and Sheung, 2008; Italtrend, 2010) and the fact that the average price of these larger goods has not decreased. Some reports suggest an overproduction of small black cultured pearls of low to medium quality, but obviously this cannot be generalized to include all types and qualities of these goods at present.

For two farms in the FSM and the Marshall Islands, both with 25,000 seeded oysters, Fong et al. (2005) calculated the average cost of producing a cultured pearl to be US$19.15. This was over a 20-year period, and both farms examined for that study have since ceased operation. In French Polynesia, as elsewhere, large pearl farms (>200,000 oysters) benefit from economies of scale (Poirine, 2003). Poirine and Kugelmann (2003) calculated with data from 2000 that the average cost per cultured pearl in French Polynesia for a large-scale farm was 902 CFP francs (US$9.93), compared to 1,889 CFP francs (US$20.79) for a small-scale farm of <25,000 oysters. Although pearl farming still has the potential to bring economic development to remote coastal communities, the long-term viability of these farms may be at risk due to challenging market factors, not to mention environmental and climate considerations.

Do small-scale farms have a future? The revenue models presented by Johnston and Ponia (2003) and Fong et al. (2005) do not reflect the economically unfavorable evolution of the black cultured pearl market in the past decade. The assumptions of their models render all small-scale pearl farms unprofitable if the recent global slump in black cultured pearl prices is taken into account. Yet other research in French Polynesia and the FSM suggests that there is a future for small-scale pearl farms that adopt alternative strategies, including:

- Maximizing revenue by marketing oyster meat and oyster shell resources (as jewelry or as raw material for medicinal purposes)
- Reducing spat costs through innovation in hatchery production
- Reducing oyster mortality
- Emphasizing cultured pearl quality over quantity
- Strategizing market differentiation through branding (e.g., Fiji)
- Adopting value-added activities such as jewelry crafting and developing synergies with tourism
- Emphasizing technology so that dependence on costly international assistance is minimized
- Making pearling a seasonal activity for local people, complemented by income from fishing, farming, or tourism

Technology Transfer. Even with these strategies, the transfer of technology to local inhabitants is essential. In several countries, the production of cultured blister pearls has been envisioned as an economic development strategy, and donors have funded such projects using *P. margaritifera* in Kiribati (Teitelbaum, 2007), Tanzania (Southgate et al., 2006), and Tonga (Teitelbaum and Fale, 2008). Yet none of these has achieved sustained commercial success, domestically or abroad. Typically, these types of internationally funded projects emphasized farming methods and handicraft-making techniques without training locals in sales and marketing (Ito, 2011a).

In contrast, current efforts in the FSM focus on training locals in all aspects of cultured pearl production and marketing. This ensures that the skills necessary for a pearl farming sector can be sustained locally without long-term foreign aid. Micronesians, not foreigners, are training local workers as technicians at the COM project's Nett Point hatchery on Pohnpei. This is widely regarded as a positive step in the development of aquaculture because it fosters local expertise and community collaboration, making the sector more likely to succeed. Overall, the project has four aims:

1. Standardizing hatchery and ocean grow-out protocols to realize mass spat and seedable oyster production
2. Training local technicians in hatchery-subsequent husbandry practices and grafting techniques
3. Training locals in basic jewelry manufacturing methods
4. Incorporating pearl farming into an integrated aquaculture and marine protected area development project and an ecosystem-based community fisheries management plan, with the goal of promoting alternative livelihood opportunities and local marine conservation

This project in the FSM is unique in the sense that the local grafting technicians being trained also have pearl farming and cultured pearl grading skills, and are themselves capable of training others. Indigenous youths who have learned basic jewelry design and manufacturing techniques (figure 12) then process the cultured blister pearls for sale locally and regionally (in Guam, for instance). Cultured blister pearl jewelry has recently sold in the local market for an average of US$20 per piece, an encouraging development (figure 13).

Figure 12. In a workshop on Pakin Island, local youths are taught how to drill shells containing cultured blister pearls so that they can be processed into jewelry. Photo by L. Cartier.

Management: The Key to a Successful Industry. After five decades of black cultured pearl farming and trading in French Polynesia, it has become clear that the management of both production and marketing is critical to ensuring long-term success. The striking differences in the industry development and

Figure 13. These pieces of cultured blister pearl and shell-derived jewelry, manufactured by indigenous youths, are sold in the local market. The diameter of the shell is ~10 cm. Photo by M. Ito.

government regulation between Australia (the main producer of white South Sea cultured pearls by value) and French Polynesia (the dominant source of black cultured pearls) have been examined by several authors (Tisdell and Poirine, 1998; Poirine, 2003; Müller, 2009). While French Polynesia, in Müller's words, adopted a "laissez-faire" approach to marine concessions, production, and trade, Australia chose to enforce strict quotas on output. Although the FSM pearl industry is unlikely to attain such international importance, questions regarding how the sector should be managed will need to be addressed as the sector develops.

While Poirine (2003) advocated economic regulation of the (Polynesian) cultured pearl sector through an auction system of limited marine concessions, another model has emerged in the FSM. Because most indigenous spat must be grown in a hatchery (Nukuoro notwithstanding), scientists control the oyster supply. Any pearl farm involved in the COM project that does not adhere to strict environmental and other guidelines must return its oysters to the Nett Point hatchery. The oysters remain the property of the hatchery, ensuring scientific oversight of the sector. Additional management models are currently under development.

Marine Conservation. Sound pearling practices have a positive impact on local fish stocks, since fry thrive around oyster farms and commercial fishing within these areas is prohibited (Pae Tai – Pae Uta, 2003). Unlike the extraction of many other gem resources, the cultivation of pearls depends directly on responsible environmental management. Low stocking densities have a positive influence on the health of oysters and are more likely to lead to high-quality harvests (Southgate and Lucas, 2008). Very high stocking densities can lead to mass mortality of oysters, as demonstrated on the island of Manihiki and the subsequent demise of the Cook Islands cultured pearl industry (Macpherson, 2000; Southgate and Lucas, 2008).

Pearl farming is one of the most profitable forms of aquaculture. With limited environmental impact and a high-value resource that can be produced in remote atolls, it has often been described as an ideal business model for developing Pacific coastal communities (Sims, 2003). In regions such as the FSM, which depend on artisanal fishing and subsistence farming and enjoy few if any alternative opportunities, pearl farming may reduce human pressures on the environment and generate cash income for local communities. Through alternative economic opportunities, such as pearl farming, pressures on rapidly diminishing fish stocks can be reduced. The income lost by abstaining from fishing in certain areas—Pakin or Pweniou islands, for instance—can be recouped by income from pearl farming. Marine protected areas (MPA) with no-fishing zones have been established in some parts of Pakin and Pweniou. In Pakin, for example, the model has been extended to become an integrated MPA in which pearl farming is carried out but fishing is not allowed. This innovative approach ensures that fish stocks can recover and gives locals access to alternative sources of income.

GEMOLOGY OF MICRONESIAN CULTURED PEARLS

Materials and Methods. For this study we examined 18 *P. margaritifera* cultured pearls obtained from Pohnpei's Nett Point farm by author LC (figure 14). The samples ranged from 3.86 to 13.00 ct, and measured approximately 8.1–12.1 mm in diameter. The selection was chosen to best represent the range of possible colors and qualities from the FSM's current cultured pearl production; three samples were of the "Micronesian Blue" variety.

In addition to visual examination and close microscopic inspection, all samples were analyzed by X-radiography using a Faxitron instrument (90 kV and 100 mA excitation) and Fuji film. On three samples (FSM_15, FSM_16, and FSM_17), we also measured

Figure 14. A range of colors and overtones were observed in the cultured pearl samples from the FSM (8.1–12.1 mm in diameter). Photo by M. S. Krzemnicki, © SSEF.

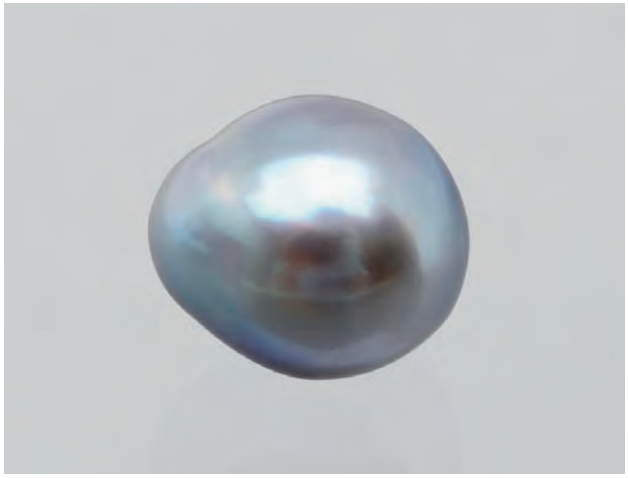

Figure 15. This light gray sample (8.4 mm in diameter) displays distinct blue and purple overtones characteristic of "Micronesian Blue" cultured pearls. Photo by M. S. Krzemnicki, © SSEF.

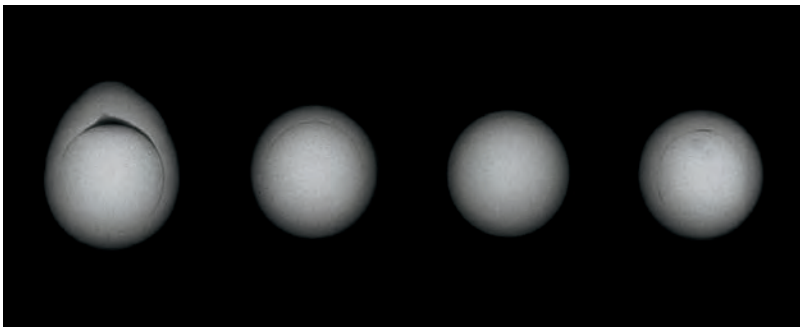

Figure 16. These X-radiographs of four bead-cultured pearls from Micronesia show varying nacre thicknesses, described here from left to right. Sample FSM_4 shows a small triangular cavity at the interface between the bead and nacre. FSM_10 has a medium nacre overgrowth (~1 mm), while FSM_14 shows a rather thin nacre layer (~0.5 mm), and FSM_16 has a thicker nacre overgrowth (~1.5 mm). Images by M. S. Krzemnicki, © SSEF.

UV-Vis reflectance spectra using a Varian Cary 500 spectrophotometer with a diffuse reflectance accessory. Furthermore, all 18 pearls were examined with a long- and short-wave UV lamp. Luminescence spectra of three cultured pearls (FSM_15, FSM_16, and FSM_18) were collected with an SSEF-developed UV-Vis spectrometer (based on an Avantes spectrometer) coupled with a luminescence accessory consisting of a mounting with three 365 nm LED lamps.

Results and Discussion. The cultured pearls' shape varied greatly from perfectly round to semi-round, button, drop, baroque, and circled. The color range included white, yellow, light gray to dark gray and brownish gray, and black (again, see figure 14). Most showed moderate to distinct overtones, with interference and diffraction colors dominated by green, purple, and particularly distinct blue hues (e.g., figure 15). The color distribution was partially uneven, especially in those showing circled features and surface imperfections such as dots, indentations, and bumps.

As the cultured pearls were taken directly from the production site prior to processing, the moderate to high luster represents their original state rather than their polished appearance. This was especially obvious under high magnification, which revealed fine fingerprint-like structures caused by the regular stacking of the aragonite platelets of the nacre.

X-radiographs (e.g., figure 16) revealed a distinct bead nucleus in the center of each sample, surrounded by nacre with a thickness of 0.5–3.9 mm. The off-shaped cultured pearls in particular showed distinct variations in nacre thickness, whereas the round to semi-round samples had typical (for *P. margaritifera* cultured pearls) nacre thickness of 0.8–1.4 mm.

UV-Vis spectra revealed a trough in reflectance at about 700 nm (figure 17), which is characteristic

Figure 17. The UV-Vis reflectance spectra of three P. margaritifera *cultured pearls from the FSM are compared to the spectrum of a yellow cultured pearl from* P. maxima. *The* P. margaritifera *samples show a distinct trough in reflectance at 700 nm that is characteristic for this species, but not seen in the* P. maxima *sample. The spectra are shifted vertically for clarity.*

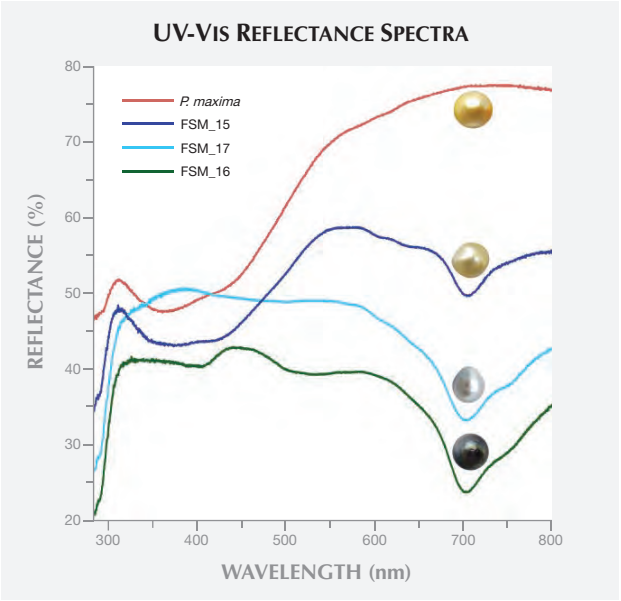

of the color pigments (porphyrins) in the shell and cultured pearls of *P. margaritifera* (Miyoshi et al., 1987; Karampelas et al., 2011). Interestingly, even the reflectance spectrum of the yellow cultured pearl (FSM_15) showed this feature. This is in contrast to yellow cultured pearls from the gold-lipped pearl oyster (*P. maxima*), which look very similar but do not show this trough. This supports the use of UV-Vis spectroscopy for separating yellow to "golden" cultured pearls from these two species (see also Elen, 2002).

The samples showed inert to distinct yellow reactions to long-wave UV radiation, and distinctly weaker fluorescence to short-wave UV. Often the reaction was not uniformly distributed, but correlated to the lighter gray surface regions of the cultured pearls. The luminescence spectra of three cultured pearls characterized by distinct yellow fluorescence (FSM_18), moderate yellow fluorescence (FSM_15), and essentially no reaction (FSM_16) to the long-wave UV lamp all revealed two broad luminescence bands that correlated in intensity with the visual strength of their fluorescence (figure 18). By comparison, gray to dark cultured pearls from *Pteria sterna* from the Sea of Cortez in Mexico show additional spectral features above 600 nm that correspond to the red luminescence commonly observed in them (Kiefert et al., 2004; Sturman, 2009).

Figure 18. The luminescence spectra of three cultured pearls from P. margaritifera *with distinct yellow (FSM_18), moderate yellow (FSM_15), and nearly no fluorescence (FSM_16) to long-wave UV radiation are compared to the spectrum of a brown* Pteria sterna *cultured pearl from Mexico, which fluoresced strong red to long-wave UV radiation. The strong luminescence intensity below 400 nm for all samples is due to the excitation wavelength of the LED light source.*

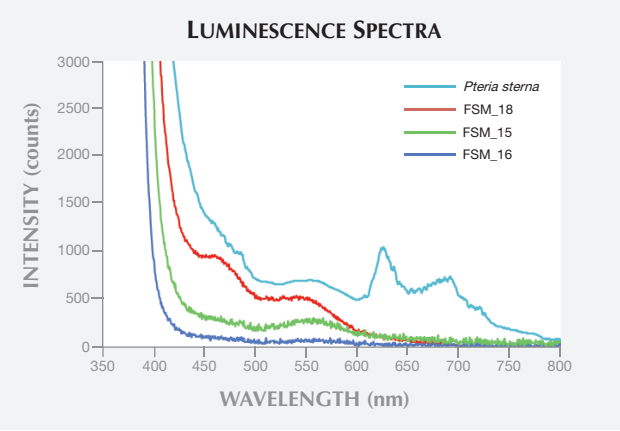

Figure 19. Blue overtones in "Micronesian Blue" cultured pearls (here, 12 mm in diameter) may be diagnostic of these products in the marketplace. Photo courtesy of Yuhei Hosono, © Le Collier, Tokyo.

Based on their observed and measured characteristics, our Micronesian samples were similar in many respects to cultured pearls produced in French Polynesia using the same species. The blue overtones, in some cases quite distinct, may serve to distinguish the "Micronesian Blue" cultured pearls in the international market (e.g., figure 19).

CONCLUSION

Pearl oyster farming is still in its infancy in the FSM, yielding small quantities of cultured pearls compared to the massive production in French Polynesia. Pearling activities and production are expected to expand in the FSM in the near future. Technical assistance through the COM program should ensure the supply of high-quality *P. margaritifera* oysters to support the nascent industry, as well as the adoption of responsible production practices.

Demand for the FSM's cultured pearls appears to be growing as they reach the international market, especially in Japan, where samples from initial harvests have been sold to selected jewelry designers who are marketing them as Micronesian cultured pearls. For the industry to succeed, a market differentiation strategy must be adopted. The decision to brand a portion of the production as "Micronesian Blue" cultured pearls is an important step in that direction.

Figure 20. This necklace features Micronesian cultured pearls (8.5–13.3 mm) of various colors. Photo courtesy of Yuhei Hosono, © Le Collier, Tokyo.

The FSM's cultured pearls come in a wide spectrum of colors and overtones (e.g., figures 14 and 20). Gemological and analytical instrumentation cannot conclusively separate these cultured pearls from those produced by *P. margaritifera* in French Polynesia and other areas. However, they are easily separated from *Pteria sterna* cultured pearls through UV-Vis reflectance spectroscopy. In addition, yellow cultured pearls from the FSM can be separated from yellow South Sea samples cultivated in the *P. maxima* oyster.

Through the careful selection of suitable brood stock, "Micronesian Blue" cultured pearls may become a high-value niche product on the international market in the near future. With an emphasis on quality and limited production, the FSM pearl sector has a realistic chance of economic success without foreign aid.

ABOUT THE AUTHORS

Mr. Cartier (laurent.cartier@unibas.ch) is a PhD candidate in environmental science at Basel University in Switzerland, and a project scholar at the University of Vermont, Burlington (www.sustainablepearls.org). Dr. Krzemnicki is director of the Swiss Gemmological Institute SSEF in Basel. Dr. Ito is director and chief scientist of aquaculture research and development at the College of Micronesia Land Grant Program in Pohnpei, Federated States of Micronesia.

ACKNOWLEDGMENTS

Mr. Cartier is deeply grateful for travel funding support from the Tiffany & Co. Foundation. He also thanks Dr. Ito and the entire Nett Point hatchery team for their great help and enthusiasm, and the people of Pakin Atoll for their wonderful hospitality. The authors thank Dr. Franz Herzog for discussions on the gemology of these cultured pearls.

REFERENCES

Caseiro J. (1993) L'huître Perlière de Polynésie. Biominéralisation, Paramètres et Processus de Croissance, Effets Chromatiques dans la Coquille et dans la Perle de *Pinctada Margaritifera*. PhD thesis, University of Lyon, France, 386 pp.

Clarke R.P., Sarver D.J., Sims N.A. (1996) Some history, recent developments and prospects for the black-lip pearl oyster, *Pinctada margaritifera* in Hawaii and Micronesia. Twenty-Sixth Regional Technical Meeting on Fisheries, *SPC/Fisheries 26*, August 5–9, Nouméa, New Caledonia.

Domard J. (1962) *Les Bancs Nacriers de la Polynésie Française. Leur Exploitation, Leur Conservation, Leur Reconstitution*. Commission du Pacifique Sud Conférence Technique des Pêches, Feb. 5–13, Nouméa, New Caledonia.

Elen S. (2002) Identification of yellow cultured pearls from the black-lipped oyster *Pinctada margaritifera*. *G&G*, Vol. 38, No. 1, pp. 66–72, http://dx.doi.org/10.5741/GEMS.38.1.66.

The Federated States of Micronesia—Millennium Development Goals & Status Report 2010 (2010) Palikir, Pohnpei, Dec. 15, www.undp.org.fj/pdf/MDG%20Report/FSM_MDG.pdf [date accessed: Dec. 8, 2011].

Fong Q.S.W., Ellis S., Haws M. (2005) Economic feasibility of small-scale black-lipped pearl oyster (*Pinctada margaritifera*) pearl fishing in the Central Pacific. *Aquaculture Economics & Management*, Vol. 9, No. 3, pp. 347–368, http://dx.doi.org/10.1080/13657300500234359.

Hänni H.A. (2007) A description of pearl farming with *Pinctada maxima* in South East Asia. *Journal of Gemmology*, Vol. 30, No. 7/8, pp. 357–365.

Haws M. (2002) The Basic Methods of Pearl Farming: A Layman's Manual. *Center for Tropical and Subtropical Aquaculture Publication No. 127*, 79 pp., www.ctsa.org/files/publications/CTSA_12763167286192394836 81.pdf [date accessed: Nov. 10, 2010].

Haws M. (2004) Development of Black-lip Pearl Oyster Farming in Micronesia. Center for Tropical and Subtropical Aquaculture Progress Report, www.ctsa.org/files/projects/2003_Final_Report_Black_Pearl_Farming6324467313314891801.pdf [date accessed: Aug. 23, 2011].

Haws M., Ellis S., Ellis E., Lewis T., Ueanimatang M., Muckenhaupt G., Hon D., Martin F., Carran J., Hemil M., Gallagher C., Silbanuz J., Fong Q., Nair M. (2004) Addressing Some Critical Bottlenecks to Commercially Viable Hatchery and Nursery Techniques for Black-lip Pearl Oyster Farming in Micronesia, and Population Genetics of the Black-lip Pearl Oyster (*Pinctada margaritifera*). Center for Tropical and Subtropical Aquaculture Progress Report, www.ctsa.org/files/projects/2004_Progress_Report_Black_Pearls6324460344680895241.pdf [date accessed: Aug. 12, 2011].

Italtrend (2010) Étude du Marché International de la Perle de Tahiti. Projet de Professionnalisation et de Pérennisation de la Perliculture, Tahiti, 126 pp.

Ito M. (2006) Development of pearl aquaculture and expertise in Micronesia. *World Aquaculture*, Vol. 37, No. 3, pp. 36–72.
——— (2009) Improving pearl quality by grafting and husbandry methods. *Aqua Tips*, Vol. 20, No. 1, pp. 1–8.
——— (2011a) Developing value-added product "half-pearls" from the blacklip pearl oyster *Pinctada margaritifera* in Pohnpei (the Federated States of Micronesia) Years 1 and 2. *Regional e-Notes*, September, Vol. 3, Issue 9, Center for Tropical and Subtropical Aquaculture, www.aquaculturehub.org/group/ctsa/forum/topics/september-issue-of-e-notes-micronesian-half-pearls-cnmi-shrimp?xg_source=activity [date accessed: Oct. 22, 2011].
——— (2011b) Circle and spot formation mechanisms and changes in luster, color, and roundness of cultured pearls by grafting methods in *Pinctada margaritifera*. *G&G*, Vol. 47, No. 2, p. 148, http://dx.doi.org/10.5741/ 10.5741/GEMS.47.2.79.
Ito M., Jackson R., Singeo S. (2004) Development of pearl aquaculture and expertise in Micronesia. *Journal of Shellfish Research*, Vol. 23, No. 1, p. 298.
Johnston B., Ponia B. (2003) Pacific Pearl Economic Model. Economic Models for Aquaculture and Agriculture Commodities. Queensland Department of Primary Industries and Fisheries, Brisbane, Australia, and Secretariat of the Pacific Community, Nouméa, New Caledonia.
Karampelas S., Fritsch E., Gauthier J.-P., Hainschwang T. (2011) UV-Vis-NIR reflectance spectroscopy of natural-color saltwater cultured pearls from *Pinctada margaritifera*. *G&G*, Vol. 47, No. 1, pp. 31–35, http://dx.doi.org/10.5741/GEMS.47.1.31.
Kiefert L., McLaurin Moreno D., Arizmendi E., Hänni H.A., Elen S. (2004) Cultured pearls from the Gulf of California, Mexico. *G&G*, Vol. 40, No. 1, pp. 26–38, http://dx.doi.org/10.5741/GEMS.40.1.26.
Le Pennec M., Anastas M., Bichet H., Buestel D., Cochard J.C., Cochennec-Laureau N., Coeroli M., Conte E., Correia P., Fougerousse-Tsing A., Langy S., Le Moullac G., Lo C., Peltzer L., Pham A. (2010) *Huître Perlière et Perle de Tahiti*. HQ Imaging, Faaa, French Polynesia.
Leopold M. (2011) Nukuoro Black Pearl Inc., Marketing Plan. http://docs.docstoc.com/pdf/7932852/e29b45cf-95ad-4bf3-9543-66ff72effaf2.pdf [date accessed: Oct. 21, 2011.]
Macpherson C. (2000) Oasis or mirage: The farming of black pearl in the northern Cook Islands. *Pacific Studies*, Vol. 23, No. 3–4, pp. 33–55.
Martin J. (1996) Atoll hopes for black pearl revival. *Pacific Magazine*, January/February, pp. 44–45.
Miyoshi T., Yasunori M., Komatsu M. (1987) Fluorescence from pearls and shells of black lip oyster, *Pinctada margaritifera*, and its contribution to the distinction of mother oysters used in pearl culture. *Japanese Journal of Applied Physics*, Vol. 26, No. 7, pp. 1069–1072, http://dx.doi.org/10.1143/JJAP.26.1069.
Müller A. (2009) Cultured pearls: Past, present, future. *Abstracts of Lectures: European Gemmological Symposium*, June 4–7, Bern, Switzerland.
Murzyniec-Laurendeau S. (2002) La Perle de Tahiti: La fin de la Crise. Master of Advance Studies thesis, University of French Polynesia, 125 pp.
Pae Tai – Pae Uta (2003) Étude d'Impact sur l'Environnement pour la Filière Perlicole dans l'Archipel des Tuamotu. Papeete, French Polynesia, 202 pp.
Poirine B. (2003) Managing the commons: An economic approach to pearl industry regulation. *Aquaculture Economics & Management*, Vol. 7, No. 3–4, pp. 179–193.
Poirine B., Kugelmann S. (2003) Etude Économique des Determinants de la Rentabilité des Fermes Perlières en Polynésie Française. IRIDIP Report, University of French Polynesia.
Sehpin M.P. (2002) Nukuoro's first pearl sale in FSM. *The Kaselehlie Press*, June 13–26, www.fsmgov.org/press/nw062802.htm [date accessed: Dec. 15, 2011].
——— (2005) Governor calls for audit of Nukuoro government. *The Kaselehlie Press*, April 28, www.fm/news/kp/2005/04_7.htm [date accessed: Sept. 10, 2011].
Shor R. (2007) From single source to global free market: The transformation of the cultured pearl industry. *G&G*, Vol. 43, No. 3, pp. 200–226, http://dx.doi.org/10.5741/GEMS.43.3.200.
Sims N. (2003) The green pearl issue. *Pearl Oyster Information Bulletin*, No. 16, pp. 1–3, www.spc.int/DigitalLibrary/Doc/FAME/InfoBull/POIB/16/POIB16.pdf [date accessed: Apr. 13, 2011].
Smith A.J. (1992) Federated States of Micronesia Marine Resources Profiles. *Forum Fisheries Agency Report No. 92/17*, Pacific Islands Forum Fisheries Agency, Honiara, Solomon Islands, www.spc.int/DigitalLibrary/Doc/FAME/FFA/Reports/FFA_1992_017.pdf [date accessed: Dec. 15, 2011].
Southgate P.C., Lucas J.S. (2008) *The Pearl Oyster*. Elsevier, Oxford.
Southgate P., Rubens J., Kipanga M., Msumi G. (2006) Pearls from Africa. *SPC Pearl Oyster Information Bulletin*, No. 17, pp. 16–17, www.spc.int/DigitalLibrary/Doc/FAME/InfoBull/POIB/17/POIB17.pdf [date accessed: Apr. 13, 2011].
Strack E. (2006) *Pearls*. Rühle-Diebener-Verlag, Stuttgart, Germany.
Sturman N. (2009) News from Research: A large naturally colored blister pearl. GIA, www.gia.edu/research-resources/news-from-research/large_natural_blister_pearl.pdf [date accessed: Apr. 28, 2012].
Talvard C. (2011) La perliculture en 2010. *Points Forts de la Polynésie Française*, No. 10, 8 pp.
Teitelbaum A. (2007) *Pearl Oyster Products Jewelry Making Workshop*. South Tarawa, Kiribati, June 26–July 2, www.spc.int/aquaculture/index.php?option=com_docman&task=doc_download&gid=27&Itemid=3 [date accessed: Dec. 12, 2011].
Teitelbaum A., Fale P.N. (2008) Support for the Tongan pearl industry. *SPC Pearl Oyster Information Bulletin*, No. 18, pp. 11–14, www.spc.int/DigitalLibrary/Doc/FAME/InfoBull/POIB/18/POIB18.pdf [date accessed: Apr. 13, 2011].
Tisdell C., Poirine B. (1998) Socio-economics of pearl culture: Industry changes and comparisons focusing on Australia and French Polynesia. *Economics, Ecology and the Environment Working Paper 24*, University of Queensland, Brisbane, Australia, http://espace.library.uq.edu.au/eserv/UQ:121809/WP24.pdf [date accessed: Dec. 15, 2011].
Torrey R.D., Sheung B. (2008) The pearl market. In P.C. Southgate and J.S. Lucas, Eds., *The Pearl Oyster*, Elsevier, Oxford, pp. 357–365.

For online access to all issues of GEMS & GEMOLOGY from 1981 to the present, visit:

store.gia.edu

THANK YOU DONORS

GIA appreciates gifts to its permanent collection, as well as gemstones, library materials, and other non-cash assets to be used in education and research activities. These contributions help GIA further its public service mission while offering donors philanthropic benefits. We extend sincere thanks to all 2011 contributors.

CIRCLE OF HONOR*

$100,000 and higher

The Aaron Group
Dr. Suman Agrawal
Almaza Jewelers (Ziad H. Noshie)
American Pearl Company
Amsterdam Sauer
Robert and Marlene Anderson
Aurafin Oro America
Banks International Gemology Inc. (Daniel & Bo Banks)
The Bell Group/Rio Grande
Allan Caplan
Chatham Created Gems Inc. (Thomas H. Chatham)
PierLuigi Dalla Rovere
The De Beers Group
Debbie and Mark Ebert
Fabricjewelry
Dallas R. Hales
Dr. H. Tracy Hall
Dr. Gary R. and Barbara E. Hansen
James Y. Hung, M.D.
Inta Gems Inc.
J.O. Crystal Company Inc. (Judith Osmer)
Jewel America Inc. (Zvi & Rachel Wertheimer)
Kazanjian Bros Inc.
KCB Natural Pearls (K.C. Bell)
Wi iam F. & Jeanne H. Larson
Stephen Lentz
Sophie Leu
Honoring Betty H. Llewellyn
Marshall and Janella Martin
Roz & Gene Meieran
Nancy B. & Company
Dr. Kurt Nassau
John & Laura Ramsey
R. Ed Romack
Art Sexauer
Shades of the Earth (Laura & Wayne Thompson)
Ambaji Shinde
S.H. Silver Company (Stephen & Eileen Silver)
Dr. Geoffrey A. Smith
D. Swarovski & Co.
Touraine Family Trust
United States Pearl Co. (James & Venetia Peach)
Robert H. Vanderkay
Vicenza Fair

2011 D0NORS*

$50,000 to $99,999

Thomas Cacek
Steven & Betty Lou Neely

$10,000 to $49,999

Cos Altobelli
Jerry Bearman
Dudley Blauwet
Kenneth Brown Family Estate
Farooq Hashmi
Chris Johnston
Mark Mauthner
Joseph Tenhagen
In Memory of Dorothy Wade
Benjamin Zucker

$5,000 to $9,999

G. Scott Davies
House of Onyx
In Memory of RTL: A Visionary and Friend

$2,500 to $4,999

Dayananda Kulathunga
Erica Courtney Inc.
Galit Levian
In Memory of Phyllis Parsons

$1,000 to $2,499

Brad Farrar
German Sanchez

$500 to $999

Aucoin Hart Jewelers
Carol & Larry Greenfield
Alexandra Hart
Dr. Jaroslav Hyršl
Jewelry Television
Kristi Koivula
Modern Postcard
In Memory of Richard and Alyce Ulmer

Under $500

AIDC Inc.
Aurora Gems
Margo Bedman
Hannes Brunner
John Chapman
Terry Coldham
Cosmos Gems (Leonardo Silva Souto)
In Memory of Robert Crowningshield
David Epstein
Frederick Fisher
Gem Press
Gary Gosnell
Kizer-Cummings
In Memory of My Father, Ronald V. Leroux
Gavin Linsell
Vernetta McCarthy
Mauricio Serrano Jewelry
Marcus Origlieri
Mani Pirouzbakht
R. T. Boyd Ltd.
Natalie Ratnavira—Ratnavira Family
Sacred Earth Minerals (Greg Turner)
Jurgen Schnellrath
Ruben D. Shabekov
Gerard Smith, G.G.
thebeautyintherocks.com (Mauro Pantò)
Kyaw Thu
Paul Wickstrom

* All are cumulative donations

If you are interested in making a donation and receiving tax benefits information, please contact:

MCKENZIE SANTIMER
call (760) 603-4150
fax (760) 603-4056 | e-mail mckenzie.santimer@gia.edu

Recent Advances in CVD Synthetic Diamond Quality

Sally Eaton-Magaña and Ulrika F. S. D'Haenens-Johansson

Synthetic diamond growth was first documented in 1952 by William Eversole of the Union Carbide Corporation, but it took another two decades before GIA issued the first grading report for a laboratory-made diamond (Crowningshield, 1971). Virtually all single-crystal synthetic diamonds are made by two very different processes. High-pressure, high-temperature (HPHT) synthesis mimics some of the key conditions for natural diamond formation, with pressures of 5–6 GPa and temperatures of 1400–1600ºC applied to a carbonaceous source material. The second method, chemical vapor deposition (CVD), involves growing synthetic diamond as thin-film layers at moderate temperatures and low (i.e., below atmospheric) pressures. One of the main advantages of the CVD procedure over HPHT is the superior flexibility of synthetic diamond size and geometry produced. Furthermore, intentional doping with impurity elements can be controlled by the addition of gases containing those atoms.

Diamond, with its superlative physical properties, is of great interest for both scientific and technological reasons. CVD synthesis uses technology similar to that employed for producing silicon-based computer chips and electronics. In fact, many of the technological improvements in synthetic diamond quality are fueled by industrial applications, with commercial gem production a largely ancillary concern (Balmer et al., 2009).

Most current research efforts are focused on maximizing growth control and rates, improving purity, and understanding defect incorporation (e.g., Silva et al., 2008; Butler et al., 2009). The processes occurring in the gas phase and on the surface are complex and acutely sensitive to even minute changes to various parameters, such as surface orientation and smoothness, hydrocarbon-to-hydrogen ratio, substrate temperature, plasma density, and impurities present (e.g., Martineau et al., 2004; Silva et al., 2008).

As a result of this research effort, the quality of CVD products has advanced greatly over the last decade. Gem-quality CVD synthetic diamond (e.g., figures 1 and 2), once considered a "holy grail," is now routinely produced thanks to several technical and experimental improvements.

Figure 1. This 0.87 ct as-grown CVD synthetic diamond plate is near colorless and shows polycrystalline growth at the edges. Photo by Wuyi Wang.

Improvements in Growth Chemistry

In CVD synthesis, the feed gases are typically composed of hydrocarbons in a hydrogen-rich environment. The CVD reactor (figure 3) contains an energy source, such as microwave plasma, that splits the molecules into their constituent atoms or into molecular fragments (figure 4). For instance, methane (CH_4) dissociates into CH_3 and H. The carbon-based radicals diffuse down to the cooler substrate stage and react with the surface to create synthetic diamond and non-diamond carbon (Butler et al., 2009). The temperature is typically held at 700–1000ºC. A high concentration of hydrogen in the reactor drives the gas-phase and surface chemical reactions toward diamond. The precursor gas (e.g., CH_4) is therefore heavily diluted in H_2, with a typical mixing ratio of 0.1–8% by volume.

Figure 2. The 0.20 ct CVD synthetic diamond in this pendant was manufactured by Apollo Diamond Inc. and has SI_2 clarity and K color. Photo by Wuyi Wang.

All CVD techniques require a means to activate the gas-phase hydrogen and carbon-containing precursor molecules, and they are classified accordingly. Activation can occur using thermal methods (such as a hot filament), electric discharge (direct currents, radio frequencies, or microwaves), or a combustion flame. The vast majority of single-crystal CVD synthetic diamonds are grown using microwave-plasma CVD reactors.

Researchers have found that relatively minor changes to the growth parameters can yield large improvements. Such modifications include a redesigned substrate stage that helps maintain a stable microwave plasma and prevents plasma concentrations at the edges of the substrate, raising the growth rate 10-fold (Yan et al., 2002). A pressure increase from 60 to 200 torr (from ~1/12 to 1/4 of atmospheric pressure) in the reactor improves the growth rate five-fold, while also reducing defects (Yan and Vohra, 1999). Researchers have also raised the microwave power to generate a high-density plasma. This allows uniform heating of the diamond substrate and raises the H/CH_3 concentration ratio within the reactor, which affects crystal size (Liang et al., 2009).

Intentional and unintentional addition of impurities can affect the growth rate, quality, and color of the synthetic diamond. A small amount of oxygen in the reactor gases can prevent the formation of cracks, thus maintaining single-crystal rather than polycrystalline growth (Tallaire et al., 2004; Friel et al., 2009). Additionally, minute quantities of nitrogen in the feed gases can enhance the growth rate eight-fold (Butler and Oleynik, 2008) while promoting crystallization on the {100} face (Tallaire et al., 2006). However, nitrogen incorporated into the CVD synthetic diamond creates a yellowish or light brown color, necessitating further treatment (Martineau et al., 2004; Liang et al., 2009).

Improvements in Substrate Material

For single-crystal growth, the CVD film must be deposited on diamond—typically high-quality, HPHT-grown plates. Type Ib synthetic diamond traditionally served as the CVD substrate, but this resulted in lower-quality CVD material due to the high concentration of single-substitutional nitrogen in this

Figure 3. This schematic diagram shows some of the key components of a 2.45 GHz ASTeX-microwave-plasma CVD reactor. Depending on the reactor size, the growth parameters, and the desired synthetic diamond quality, the growth area may vary in diameter between 2 and 20 cm. Adapted from Martineau et al. (2004).

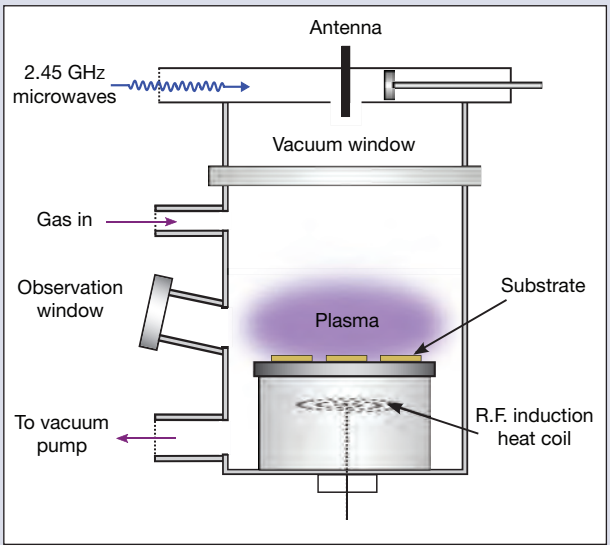

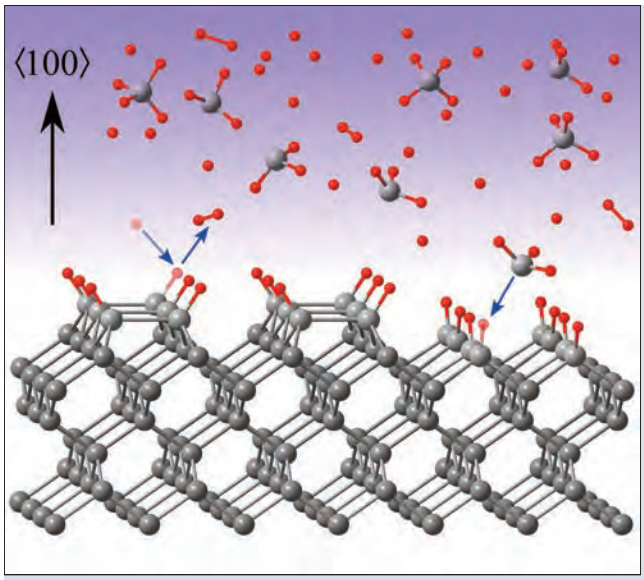

Figure 4. This drawing shows the simplified chemical reactions that occur during CVD synthetic diamond growth on a {100} hydrogen-terminated surface showing 2 × 1 reconstruction (Butler et al., 2009). Carbon and hydrogen atoms are represented by gray and red spheres, respectively. The microwaves activate the gaseous reactants, resulting in a mixture of atomic hydrogen (H), molecular hydrogen (H_2), and hydrocarbon species (e.g., CH_4 and CH_3). Two events are illustrated: an incident H atom removing hydrogen from a C-H bond on the surface, leaving an exposed carbon atom; and a CH_3 molecule moving toward a separate exposed carbon site, where it may react to form the next synthetic diamond layer.

substrate. The lattice mismatch in the crystal structure between the type Ib substrate and the growing material (Lang et al., 1991) creates stress and additional opportunities for secondary nucleation (i.e., polycrystalline growth) and the generation of dislocations (Martineau et al., 2009). Type IIa HPHT-grown substrates are now available and offer several advantages over type Ib material, resulting in fewer defects in the CVD synthetic diamond (Twitchen et al., 2009).

Growth quality is influenced by the crystallographic orientation of the substrate growth plane, which should be oriented in the {100} direction for best results. An angular deviation greater than 2° from this direction leads to a significant decline in the quality of the CVD-grown synthetic diamond (Berdermann et al., 2004), making careful polishing and surface preparation of the substrate important for CVD synthesis.

Improvements in Post-Growth Treatment

As-grown brown CVD synthetics have three broad bands centered at 270 nm (due to substitutional nitrogen), 370 nm, and 550 nm (Liang et al., 2009). Post-growth treatment rearranges the defects and impurities to improve optical and mechanical properties such as color, hardness, and fracture toughness. Both HPHT and careful low-pressure, high-temperature (LPHT) annealing can reduce the brown color in the as-grown CVD synthetic diamond, and each method has its own advantages (e.g., Meng et al., 2008). HPHT annealing is more commonly used, as the stabilizing pressure applied reduces the risk of graphitization. Although graphitization can be problematic with LPHT annealing, it can be conveniently performed within the CVD reactor after growth. Recently, researchers have succeeded in annealing single-crystal diamond at low pressures and at temperatures of 1400–2200°C within a hydrogen plasma, without significant graphitization (Meng et al., 2008; Liang et al., 2009). Depending on the treatment temperature chosen, there was a significant variation in annealing time, with the synthetic diamond held at the highest temperature for only 30 seconds. Notably, the CVD samples used by those authors were carefully chosen and prepared prior to treatment.

High-temperature annealing can decrease the 270 and 370 nm absorption bands, while the intensity of the band near 550 nm remains unchanged (Liang et al., 2009). On average, the color is improved by three grades.

Future Potential

With improvements in gas-phase chemistry and growth parameters, the greater availability of high-purity HPHT synthetic diamond as a starting material, and the effective application of post-growth treatments, the quality of CVD synthetic diamonds has improved considerably. Spectroscopic measurements verify that their purity is comparable to or even higher than that of typical type IIa natural diamond.

With all the recent progress in CVD synthesis, it continues to evolve as a major player on the engineering and gemological landscapes. We project that CVD synthetic diamond sizes will continue to

increase and the available colors will expand beyond colorless, pink, and brown to include type IIb blue samples doped with boron. The use of CVD synthetic diamond as a coating material for natural diamond may become more widespread, though it has already occurred for research purposes (e.g., Koivula and Kammerling, 1991). Regardless of the advancements in CVD growth, well-equipped gem labs are still able to confidently identify these synthetic diamonds.

Drs. Eaton-Magaña (smagana@gia.edu) and D'Haenens-Johansson are research scientists at GIA, in Carlsbad and New York, respectively.

The authors thank Dr. James E. Butler for his suggestions on the manuscript.

References

Balmer R.S., Brandon J.R., Clewes S.L., Dhillon H.K., Dodson J.M., Friel I., Inglis P.N., Madgwick T.D., Markham M.L., Mollart T.P., Perkins N., Scarsbrook G.A., Twitchen D.J., Whitehead A.J., Wilman J.J., Woollard S.M. (2009) Chemical vapour deposition synthetic diamond: Materials, technology and applications. *Journal of Physics: Condensed Matter*, Vol. 21, No. 36, article 364221 [23 pp.], http://dx.doi.org/10.1088/0953-8984/21/36/364221.

Berdermann E., Ciobanu M., Hartmann W., Martemiyanov A., Moritz P., Pomorski M., Rebisz M., Voss B., Darmstadt G. (2004) Characterisation of single-crystal CVD-diamond detectors. http://gsi-heavy-ion-researchcenter.org/informationen/wti/library/scientificreport2004/PAPERS/INSTMETH-35.pdf [date accessed: May 14, 2012].

Butler J.E., Oleynik I. (2008) A mechanism for crystal twinning in the growth of diamond by chemical vapour deposition. *Philosophical Transactions of the Royal Society A: Mathematical Physical and Engineering Sciences*, Vol. 366, pp. 295–310.

Butler J.E., Mankelevich Y.A., Cheesman A., Ma J., Ashfold M.N.R. (2009) Understanding the chemical vapor deposition of diamond: Recent progress. *Journal of Physics: Condensed Matter*, Vol. 21, No. 36, article 364201 [20 pp.], http://dx.doi.org/10.1088/0953-8984/21/36/364201.

Crowningshield R. (1971) General Electric's cuttable synthetic diamonds. *G&G*, Vol. 13, No. 10, pp. 302–314.

Friel I., Clewes S.L., Dhillon H.K., Perkins N., Twitchen D.J., Scarsbrook G.A. (2009) Control of surface and bulk crystalline quality in single crystal diamond grown by chemical vapour deposition. *Diamond and Related Materials*, Vol. 18, No. 5–8, pp. 808–815, http://dx.doi.org/10.1016/j.diamond.2009.01.013.

Koivula J.I., Kammerling R.C., Eds. (1991) Gem News: Bluish gray synthetic diamond thin films grown on faceted diamonds. *G&G*, Vol. 27, No. 2, pp. 118–119.

Lang A.R., Moore M., Makepeace A.P.W., Wierzchowski W., Welbourn C.M. (1991) On the dilatation of synthetic type Ib diamond by substitutional nitrogen impurity. *Philosophical Transactions: Physical Sciences and Engineering*, Vol. 337, No. 1648, pp. 497–520, http://dx.doi.org/10.1098/rsta.1991.0135.

Liang Q., Yan C.-S., Meng Y., Lai J., Krasnicki S., Mao H.-K., Hemley R.J. (2009) Recent advances in high-growth rate single-crystal CVD diamond. *Diamond and Related Materials*, Vol. 18, No. 5–8, pp. 698–703, http://dx.doi.org/10.1016/j.diamond.2008.12.002.

Martineau P.M., Lawson S.C., Taylor A.J., Quinn S.J., Evans D.J.F., Crowder M.J. (2004) Identification of synthetic diamond grown using chemical vapor deposition (CVD). *G&G*, Vol. 40, No. 1, pp. 2–25, http://dx.doi.org/10.5741/GEMS.40.1.2.

Martineau P.M., Gaukroger M.P., Guy K.B., Lawson S.C., Twitchen D.J., Friel I., Hansen J.O., Summerton G.C., Addison T.P.G., Burns R. (2009) High crystalline quality single crystal CVD diamond. *Journal of Physics: Condensed Matter*, Vol. 21, No. 36, article 364205 [11 pp.], http://dx.doi.org/10.1088/0953-8984/21/36/364205.

Meng Y.-F., Yan C.-S., Lai J., Krasnicki S., Shu H., Yu T., Liang Q., Mao H.-K., Hemley R.J. (2008) Enhanced optical properties of chemical vapor deposited single crystal diamond by low-pressure/high-temperature annealing. *Proceedings of the National Academy of Sciences*, Vol. 105, No. 46, pp. 17620–17625, http://dx.doi.org/10.1073/pnas.0808230105.

Silva F., Achard J., Bonnin X., Brinza O., Michau A., Secroun A., De Corte K., Felton S., Newton M., Gicquel A. (2008) Single crystal CVD diamond growth strategy by the use of a 3D geometrical model: Growth on (113) oriented substrates. *Diamond and Related Materials*, Vol. 17, No. 7–10, pp. 1067–1075, http://dx.doi.org/10.1016/j.diamond.2008.01.006.

Tallaire A., Achard J., Silva F., Sussmann R.S., Gicquel A., Rzepka E. (2004) Oxygen plasma pre-treatments for high quality homoepitaxial CVD diamond deposition. *Physica Status Solidi (a)*, Vol. 201, No. 11, pp. 2419–2424, http://dx.doi.org/10.1002/pssa.200405164.

Tallaire A., Collins A.T., Charles D., Achard J., Sussmann R., Gicquel A., Newton M.E., Edmonds A.M., Cruddace R.J. (2006) Characterisation of high-quality thick single-crystal diamond grown by CVD with a low nitrogen addition. *Diamond and Related Materials*, Vol. 15, No. 10, pp. 1700–1707, http://dx.doi.org/10.1016/j.diamond.2006.02.005.

Twitchen D.J., Summerton G.C., Friel I., Hansen J.O., Guy K.B., Gaukroger M.P., Martineau P.M., Burns R.C., Lawson S.C., Addison T.P.G. (2009) High crystalline quality synthetic diamond. U.S. Patent No. 20090127506.

Yan C.S., Vohra Y.K. (1999) Multiple twinning and nitrogen defect center in chemical vapor deposited homoepitaxial diamond. *Diamond and Related Materials*, Vol. 8, No. 11, pp. 2022–2031, http://dx.doi.org/10.1016/S0925-9635(99)00148-X.

Yan C.S., Vohra Y.K., Mao, H., Hemley R.J. (2002) Very high growth rate chemical vapor deposition of single-crystal diamond. *Proceedings of the National Academy of Sciences*, Vol. 99, No. 20, pp. 12523–12525, http://dx.doi.org/10.1073/pnas.152464799.

Nano-Polycrystalline Diamond Sphere: A Gemologist's Perspective

Elise A. Skalwold

Synthetic nano-polycrystalline diamond (NPD) is one of the latest and most exciting results of scientific efforts to synthesize a mineral that has held the fascination of humankind for ages. Unlike other forms of polycrystalline diamond, it is completely transparent. Owing to the material's unique structure, it is also much tougher than natural diamond and previous synthetics, either single-crystal or polycrystalline. This represents a significant breakthrough for industrial purposes and for high-pressure research into the nature and properties of minerals, including diamond.

Naturally occurring polycrystalline diamond (PCD) is highly included. Two types of granular aggregates, referred to as *bort* and *carbonado*, are generally opaque, dark, and unattractive (Orlov, 1973), though some examples have been fashioned into interesting jewelry (Wang et al., 2009). Another form of polycrystalline diamond, of interest for its structure and strength as a model for possible synthesis, consists of the rare naturally occurring fibrous spheres known as *ballas* diamond, found in the Urals, Brazil, and South Africa. Natural aggregates have varying compositions and structural strength, making them inferior to synthesized PCD (Lux et al., 1997).

Gemologists regularly assess diamonds based on certain standard properties. The recently developed NPD sphere invites one to consider those characteristics in a different light and perhaps look with renewed wonder at that which is possible through science and understanding.

The NPD Sphere

A sphere fashioned from diamond: Its very existence seemingly breaks the rules at the heart of our gemological training. How would one cut and polish such a shape out of the world's hardest material, one that also cleaves? Yet this object is actually the fruit of understanding those rules.

The creation of a 7.5 mm NPD orb, described as the world's "first spherical diamond" (Yamada and Yashiro, 2011), was announced in October 2011 by one of Japan's largest newspapers ("Ehime University dazzles…," 2011). This development was quickly followed by a second sphere measuring 5.09 mm (figure 1). Dr. Tetsuo Irifune, the director of Ehime University's Geodynamics Research Center (GRC), kindly offered this author the opportunity to study the latter, a nearly perfect sphere created to study the elastic properties of NPD (Yamada and Yashiro, 2011). In 2003, Dr. Irifune and his colleagues first reported success in producing small NPD pieces measuring approximately 1 mm (Irifune et al., 2003; Sumiya and Irifune, 2008). Today, larger sizes are being manufactured at the GRC as 1 cm (14.5 ct) brownish yellow rods suitable for shaping into forms used in a variety of applications (Irifune and Hemley, 2012).

Figure 1. As this photo demonstrates, NPD is completely transparent. When placed over text on a piece of paper, the 5.09 mm sphere reverses and transmits the letters so that they are clearly legible. Photo by E. A. Skalwold.

The adamantine NPD sphere is deceptively nondescript at first glance, until one considers that it is not a single crystal but a group of nano-sized synthetic diamond crystals packed so tightly that the

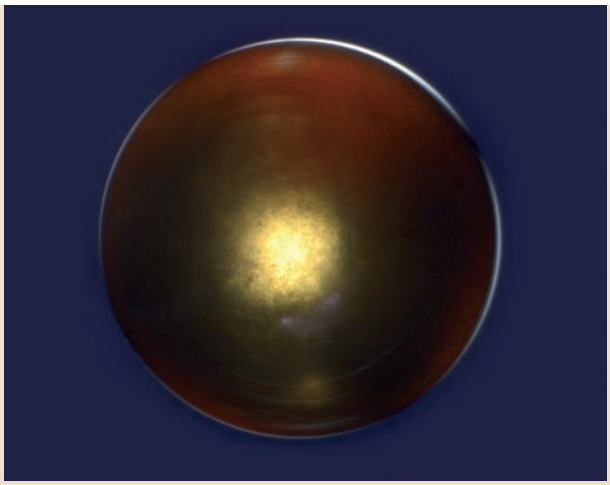

Figure 2. The 5.09 mm NPD sphere displays uniform birefringence between crossed polarizers. Photo by S. D. Jacobsen.

material is tougher than either PCD or single-crystal diamond (SCD)—and essentially flawless and completely transparent (again, see figure 1). This transparency stems in part from a manufacturing process that creates atomic bonding between individual nano-size crystals, interlocking them and thus minimizing the scattering of light waves along grain boundaries, while also minimizing voids and impurities that might contribute to scattering (T. Irifune, pers. comm., 2012). Earlier synthetic PCDs required the addition of metals such as cobalt, which produced a less transparent and weaker material (Irifune et al., 2003). But NPD contains only trace impurities: 100–200 ppm hydrogen, 10–30 ppm oxygen, 50–100 ppm nitrogen as aggregates (dispersed nitrogen <0.5 ppm), and <1 ppm boron (Sumiya et al., 2009).

Although diamond is optically isotropic, natural diamond often displays a birefringence pattern caused by lattice strain. In NPD, the crystals' random orientation results in a similarly isotropic solid, but with a uniform birefringence. Observation of the sphere between crossed polarizers revealed this very condition (figure 2). This is quite different from SCD, where birefringence often exposes a specimen's synthetic origin—or, in the case of natural diamond, reveals underlying strain associated with inclusions or structural weakness or even evidence of treatment. In fact, laboratory analysis detected no large lattice strain in NPD (Sumiya et al., 2009). The sphere's brownish yellow color has been attributed to lattice defects in each synthetic nano-diamond crystallite, which are analogous to those found in brown type IIa diamond and result from plastic deformation brought on by high-pressure, high-temperature (HPHT) growth (Sumiya et al., 2009). It is unknown what causes NPD's reddish orange fluorescence observed under long-wave UV radiation (a slightly weaker reaction is seen under short-wave UV).

What is the significance of the prefix "nano"? Consider that the diameter of a human hair is somewhere between 50,000 and 100,000 nm. NPD is actually a mixture of two forms of synthetic diamond: 10–20 nm equigranular crystallites and 30–100 nm lamellar crystalline structures (Sumiya and Irifune, 2005). Both are formed during a sintering process used to convert pure graphite directly into cubic synthetic diamond in a matter of minutes (Irifune et al., 2003). How is this possible? The GRC utilizes a 6,000-tonne multi-anvil apparatus (figure 3) to achieve the required pressure of 15 gigapascals (2.18 million psi) and temperature of 2,300–2,500°C (Irifune et al., 2003; Irifune and Hemley, 2012). Interestingly, lower temperatures in the 1,600–

Figure 3. The GRC's large-volume, multi-anvil press uses a 6,000-tonne hydraulic ram to synthesize NPD rods up to 1 cm long. The two young GRC staff members are wearing traditional costumes from a famous Japanese novel set in Matsuyama, the city where the facility is located. Photo courtesy of T. Irifune.

Figure 4. Using pulsed lasers, it is possible to fashion nearly any shape from NPD, including the 7.5 and 6.0 mm round brilliants shown here. The NPD rods range from 6.5 to 8.0 mm in diameter. Photo courtesy of T. Irifune.

2,200°C range produced some areas of hexagonal synthetic diamond—or *lonsdaleite*, an allotrope of diamond associated with meteoritic impact, which is a naturally occurring HPHT event (Irifune et al., 2003; Sumiya and Irifune, 2005; Ohfuji and Kuroki, 2009). The lamellar structures observed in NPD apparently originate in a lonsdaleite phase produced during the sintering process. This phase and the euhedral granular structures present in NPD are directly related to the crystallinity of the graphite starting material (Ohfuji and Kuroki, 2009).

While diamond is considered the hardest material in nature, diamond crystals do not have the same hardness in all crystallographic directions. In addition to its transparency, NPD is tougher than natural diamond, and it is uniformly as hard as the hardest direction of any single-crystal diamond. The NPD grown by the GRC group also has better hardness than other forms of synthetic polycrystalline diamond and displays superior mechanical properties at high temperature (Sumiya and Irifune, 2007a,b). How? As explained above, within NPD the crystallites are solidly bonded to each other, essentially interlocking. This reduces or nearly eliminates breakage along grain boundaries (Sumiya and Harano, 2012), while the lamellar structure adds toughness against fracturing within the grains (Sumiya and Irifune, 2008). Because the crystals are randomly oriented, there is no particular cleavage direction in NPD, whereas SCD cleaves along planes parallel to its octahedral faces and less easily along its dodecahedral faces (Field, 1992). This weakness becomes problematic during high-pressure research, and also puts at risk diamonds set in rings exposed to sharp blows. That makes NPD an interesting possibility for jewelry subjected to heavy wear.

The unique nature of NPD allows it to be fashioned into a virtually unlimited variety of shapes with uniform properties in all directions, including spheres and round brilliant gems (e.g., figure 4). But NPD's hardness and toughness pose a daunting problem when it comes to cutting and polishing, a necessity for many kinds of applications such as the diamond anvil cell. This instrument uses two diamonds oriented culet to culet, not only for applying pressure but also as windows for viewing a sample under study.

While an SCD specimen can be cut with lasers, the polishing is accomplished with diamond abrasives. Not so for NPD, whose polycrystalline nature dictates that the hardest direction of many of its crystallites will always be exposed to the surface, making abrasives far less effective. Pulsed lasers are the only method for successfully cutting and fine finishing NPD. These lasers work by converting diamond to graphite, which can then be removed by several means. Researchers found that micromachining with a nano-pulsed near-ultraviolet laser produces a smooth undamaged surface on NPD, but generates micro-cracks and micro-cleavages during processing of single-crystal diamond (Odake et al.,

2009). A later study by Okuchi et al. (2009) concluded that the most efficient method involves three types of pulsed lasers used in combination: near-infrared for rough shaping, and ultraviolet and femtosecond lasers for fine finishing.

Future Possibilities

The development of high-quality nano-polycrystalline synthetic diamond has been made even more fascinating by the opportunity to observe a sphere of the material firsthand. With its superior hardness and toughness, NPD can be fashioned into a virtually endless array of shapes using lasers. Its implications for the gem industry presently lie within research applications. Nevertheless, improvements in color and production efficiency may soon make NPD a beautiful and sought-after synthetic gem material.

Ms. Skalwold (elise@nordskip.com) is a gemologist, author, and editor involved in research and curating at Cornell University in Ithaca, New York. *She is grateful to Dr. Tetsuo Irifune for generously providing the NPD sphere for study and for his insights regarding its nature. She also thanks Dr. Steven D. Jacobsen of the Department of Earth & Planetary Sciences at Northwestern University (Evanston, Illinois), for facilitating this opportunity, and John I. Koivula, analytical microscopist at GIA in Carlsbad, for sharing his gemological wisdom during a visit to Northwestern's laboratory. Finally, she is deeply indebted to Dr. William A. Bassett, professor emeritus of geology at Cornell University, for his ongoing intellectual support and collaboration in exploring the world of mineral physics.*

References

Ehime University dazzles with spherical diamond (2011) *Daily Yomiuri Online*, Oct. 22, http://www.yomiuri.co.jp/dy/national/T111021005302.htm [date accessed: April 7, 2012].

Field J.E., Ed. (1992) *The Properties of Natural and Synthetic Diamond*. Academic Press, London, 710 pp.

Irifune T., Hemley R.J. (2012) Synthetic diamond opens windows into the deep earth. *EOS, Transactions, American Geophysical Union*, Vol. 93, No. 7, pp. 65–66, http://dx.doi.org/10.1029/2012EO070001.

Irifune T., Kurio A., Sakamoto S., Inoue T., Sumiya H. (2003) Ultrahard polycrystalline diamond from graphite. *Nature*, Vol. 421, pp. 599–600, http://dx.doi.org/10.1038/421599b.

Lux B., Haubner R., Holzer H., DeVries R.C. (1997) Natural and synthetic polycrystalline diamond, with emphasis on ballas. *International Journal of Refractory Metals and Hard Materials*, Vol. 15, No. 5–6, pp. 263–288, http://dx.doi.org/10.1016/S0263-4368(97)87503-8.

Odake S., Ohfuji H., Okuchi T., Kagi H., Sumiya H., Irifune T. (2009) Pulsed laser processing of nano-polycrystalline diamond: A comparative study with single crystal diamond. *Diamond and Related Materials*, Vol. 18, No. 5–8, pp. 877–880, http://dx.doi.org/10.1016/j.diamond.2008.10.066.

Ohfuji H., Kuroki K. (2009) Origin of unique microstructures in nano-polycrystalline diamond synthesized by direct conversion of graphite at static high pressure. *Journal of Mineralogical and Petrological Sciences*, Vol. 104, No. 5, pp. 307–312, http://dx.doi.org/10.2465/jmps.090622i.

Okuchi T., Ohfuji H., Odake S., Kagi H., Nagatomo S., Sugata M., Sumiya H. (2009) Micromachining and surface processing of the super-hard nano-polycrystalline diamond by three types of pulsed lasers. *Applied Physics A: Materials Science & Processing*, Vol. 96, No. 4, pp. 833–842, http://dx.doi.org/10.1007/s00339-009-5326-8.

Orlov Y.L. (1973) *The Mineralogy of the Diamond*. Wiley-Interscience Publishers, New York, 235 pp.

Sumiya H., Harano K. (2012) Distinctive mechanical properties of nano-polycrystalline diamond synthesized by direct conversion sintering under HPHT. *Diamond and Related Materials*, Vol. 24, pp. 44–48, http://dx.doi.org/10.1016/j.diamond.2011.10.013.

Sumiya H., Irifune T. (2005) Synthesis of high-purity nano-polycrystalline diamond and its characterization. *SEI Technical Review*, No. 59, pp. 52–58.

——— (2007a) Microstructure and mechanical behaviors of nano-polycrystalline diamonds synthesized by direct conversion sintering under HPHT. *Materials Research Society Symposium Proceedings*, Vol. 987, pp. 03–01.

——— (2007b) Hardness and deformation microstructures of nano-polycrystalline diamonds synthesized from various carbons under high pressure and high temperature. *Journal of Materials Research*, Vol. 22. No. 8, 2345–2351, http://dx.doi.org/10.1557/jmr.2007.0295.

——— (2008) Microstructure and mechanical properties of high-hardness nano-polycrystalline diamonds. *SEI Technical Review*, No. 66, pp. 85–91.

Sumiya H., Harano K., Arimoto K., Kagi H., Odake S., Irifune T. (2009) Optical characteristics of nano-polycrystalline diamond synthesized directly from graphite under high pressure and high temperature. *Japanese Journal of Applied Physics*, Vol. 48, No. 12, Article no. 120206 [3 pp.].

Wang W., Lu R., Moses T. (2009) Photoluminescence features of carbonado diamonds. News from Research, July 21, http://www.gia.edu/research-resources/news-from-research/carbonado-diamonds.pdf [date accessed: April 7, 2012].

Yamada A., Yashiro M., Eds. (2011) The first spherical diamond. *Deep Earth Mineralogy Global COE Newsletter*, No. 9, p. 2.

DIAMOND

Large Artificially Irradiated Yellow

Natural diamonds that have been laboratory-irradiated to obtain a more desirable color are quite common today. Recently the New York laboratory examined a 50.86 ct emerald-cut diamond with a Fancy Vivid yellow color (figure 1), a desirable grade that would fetch a high price in the market—provided the color was natural.

The diamond was very clean, receiving a clarity grade of VVS_2. It was evenly colored and had no apparent color zoning, though a very weak brown graining was observed with diffuse lighting. Initial gemological observations did not seem to indicate irradiation, but spectroscopic data proved otherwise.

UV-visible absorption spectroscopy showed a "cape" spectrum common for this color of diamond. Mid-infrared absorption spectroscopy proved it was a type Ia diamond, but also revealed very weak bands at ~5165 and 4935 cm^{-1} (H1c and H1b), which aroused some concern as to the origin of color. Using a custom-made high-resolution UV-Vis spectrometer, we detected a very weak absorption peak at ~595 nm, indicative of artificial radiation treatment in this type of diamond (G.R. Crowningshield, "Spectroscopic recognition of yellow bombarded diamonds," Winter 1957–58 *G&G*, pp. 99–104, 117). Also observed was strong absorption at ~503 nm (H3), the center responsible for the yellow color. The brown graining suggested that the stone originally had a brown color and underwent irradiation and subsequent annealing to achieve the Fancy Vivid yellow appearance.

Figure 1. Spectroscopic analysis showed that this 50.86 ct Fancy Vivid yellow emerald-cut diamond had been artificially irradiated.

The successful treatment of this stone resulted in a color found in large natural-color diamonds, such as a 127 ct cape diamond from the Kimberley mine in South Africa that was also recently graded by GIA.

GIA's laboratory frequently encounters artificially irradiated diamonds, but they are usually much smaller. GIA previously graded this 50.86 ct diamond in 1992 and identified it as treated. It remains one of the largest artificially irradiated diamonds seen in the laboratory.

Paul Johnson

Multi-Treated Yellowish Green

While radiation-induced defects are commonly responsible for green color in diamond, either artificially or by natural processes, the color is often not very saturated. Recently examined in the Carlsbad laboratory was a 0.99 ct diamond (figure 2) with a Fancy Deep yellowish green color that resulted from a multistep process involving irradiation and HPHT treatments. Multi-treatment processing has been documented for orange, pink, and red

Figure 2. This 0.99 ct diamond's saturated yellowish green color resulted from a multistep process involving HPHT treatment and irradiation.

Editors' note: All items were written by staff members of GIA laboratories.

Gems & Gemology, Vol. 48, No. 2, pp. 132–141, http://dx.doi.org/10.5741/GEMS.48.2.132.

© 2012 Gemological Institute of America

diamonds (see, e.g., W. Wang et al., "Treated-color pink-to-red diamonds from Lucent Diamonds Inc.," Spring 2005 *G&G*, pp. 6–19; and Winter 2005 Lab Notes, pp. 341–342), but only recently has GIA seen multi-treated saturated green diamonds.

Microscopic examination of the yellowish green diamond revealed brown graining and an etched cleavage. Strong green emission was observed with fiber-optic illumination, indicating the presence of the H3 defect. When examined in immersion, the diamond displayed a subtle green zone near the culet.

The FTIR absorption spectrum revealed that this was a type Ia diamond with resolvable A- and B-aggregated nitrogen impurities, hydrogen-related defects, and nitrogen-aggregate platelets. The FTIR spectrum also showed evidence of both HPHT treatment and post-HPHT irradiation; H1a defects (1450 cm^{-1}) resulting from irradiation were particularly prominent. UV-Vis-NIR spectroscopy showed absorption features at 595, 666, and 741 (GR1) nm, confirming that artificial irradiation had imparted a significant green color component.

Because of the observed brown graining and the indications of treatment, we infer that this stone started as a brown type Ia diamond that was HPHT-treated to a saturated yellow to greenish yellow color. Next, artificial irradiation was used to intensify the green component, creating an unusually saturated color. This type of product could fill the market gap for highly saturated green diamonds.

Nathan Renfro and Christopher M. Breeding

Natural Green, Artificially Irradiated for Color Enhancement

Some gem diamonds are naturally irradiated, giving rise to very rare blue to green hues. Laboratory irradiation with a high-energy beam is one common form of diamond treatment used to induce a blue to green color. The New York laboratory recently encountered an intense green diamond that originally had a naturally light green color which was enhanced by artificial irradiation.

Figure 3. This 0.83 ct cushion-cut diamond was color graded as Fancy Intense green. Its naturally light yellow-green color had been enhanced by artificial irradiation.

This 0.83 ct cushion cut (5.64 × 5.59 × 3.16 mm) was color graded as Fancy Intense green (figure 3). The color was evenly distributed. It was identified as a type Ia diamond with a high concentration of aggregated nitrogen and weak hydrogen-related absorption. UV-Vis spectroscopy showed a strong GR1 absorption (zero-phonon line at 741.2 nm), as well as weak 594 nm, weak H3 (ZPL at 503.2 nm), and moderate N3 (ZPL at 415.3 nm) absorptions. Records revealed that this stone had been tested previously by GIA's laboratory, but was color graded as Light yellow-green. Gemological and spectroscopic features at that time confirmed that it was a natural diamond and attributed the green color to natural irradiation and related GR1 absorptions. In the resubmitted Fancy Intense green diamond, however, the absorption intensity of GR1 had nearly doubled (using N3 intensity as an internal reference, which should remain stable). Based on this, we believe that the color improvement from light yellow-green to intense green was due to artificial irradiation. This conclusion was also supported by other spectroscopic data.

Naturally and artificially irradiated diamonds share many gemological and spectroscopic features. When a naturally light blue to green diamond is irradiated to enhance its color saturation, this can be very difficult to detect. Successful identification of this diamond was achieved through extensive spectroscopic analysis and careful documentation of its grading history.

Wuyi Wang, Siau Fung Yeung, and Ivana Kayes

Pink Diamonds with 478 nm Peak

Pink diamonds are rare in nature and command a high price accordingly. They can be either type IIa (with no detectable nitrogen) or type Ia (nitrogen-bearing). A broad band at ~550 nm observed in the visible absorption spectrum is usually responsible for the pink color. A typical type IaAB pink diamond—from the Argyle mine, for example—shows a characteristic visible spectrum with absorptions at 415 nm (N3) and 496/530 nm (H3), in addition to the broad band at ~550 nm. Other causes of pink coloration include concentrations of pink color in glide planes (type IaA diamonds) and occasionally nitrogen-vacancy (N-V) centers.

The New York laboratory examined three natural pink brilliants with unusual spectral features: a 0.35 ct Fancy Light pink pear, a 1.16 ct Fancy Light pink cushion, and a 0.80 ct Faint pink round (figure 4). These diamonds were submitted at different times starting in mid-2010. All were type Ia, but their UV-Vis spectra showed an absorption at 478 nm, a peak attributed to the N2 optical center typically seen in the spectra of yellow "cape" diamonds. The presence of a cape spectrum and an absorption at ~550 nm raised our suspicions of a coating. Although GIA has identified many coated pinks with this type of spectrum, these three brilliants showed no evidence of coating, and pink graining was visible throughout each stone (figure 5). We concluded that these were natural-color pink diamonds with very rare spectral features often attributed to cape diamonds.

Figure 4. These three natural-color pink diamonds showed a UV-Vis absorption peak at 478 nm, a feature normally associated with yellow "cape" diamonds. From left to right, they consist of a 0.35 ct Fancy Light pink, a 1.16 ct Fancy Light pink, and a 0.80 ct Faint pink.

Figure 5. Pink graining is visible through the pavilion facets of the 0.80 ct round brilliant. Magnified 50×.

The 550 nm absorption band, which is responsible for pink coloration in many natural diamonds, may occur with varying aggregations and concentrations of nitrogen. As these diamonds show, there is not necessarily any correlation between the formation of this optical center and the natural aggregation process of nitrogen in diamond.

Marzena Nazz and Paul Johnson

Rough Diamonds with a Green Coating

Faceted diamonds, both colorless and fancy-color, are sometimes surface-coated to improve their color appearance. In the New York laboratory, we recently encountered two rough diamonds that had been coated green.

Submitted for color origin testing, the two crystals (figure 6) showed rounded octahedral shapes and weighed 15.77 ct (14.83 × 9.76 × 14.54 mm) and 14.42 ct (12.18 × 11.37 × 13.74 mm). Under the microscope, they displayed a green surface-related coloration with uneven distribution (figure 7), similar to the appearance of naturally colored rough diamonds with strong green radiation stains. Yet the coatings were easily detected because the green color was restricted to the surface, rather than penetrating slightly into the crystal. In addition, the coating on the 14.42 ct crystal had partially worn off, revealing the underlying yellow bodycolor. When they were scratched with a pointer probe, the coating easily came off.

These coated rough diamonds serve as a reminder that some of the older, simpler treatments never go away, so it is always important to look for them. An unsuspecting buyer could easily be fooled by the general appearance of these crystals.

Emiko Yazawa

Figure 6. These rough diamond crystals (15.77 and 14.42 ct) were coated to mimic the appearance of naturally irradiated green diamonds.

Figure 7. A closer view of this diamond crystal (magnified 20×) shows the uneven distribution of the strong green surface coloration.

Jewelry Mounted with Red FELDSPAR from China

Two fine orangy red gems mounted in jewelry were recently submitted to the New York laboratory for identification. One specimen was a modified cushion cut measuring 14.70 × 10.90 × 7.75 mm, and the other was a modified heart measuring 16.85 × 15.30 × 9.10 mm (figure 8). The stones had refractive indices of 1.557–1.567 and were inert to long- and short-wave UV radiation, properties that identified them as feldspar. Specific gravity could not be measured because of the mountings, so their identity was confirmed using Raman spectroscopy. Microscopic examination of the cushion cut revealed bands of fine particles and short aligned needles, dotted with small reflective platelets. The heart shape showed general turbidity in fiber-optic lighting, but had no discrete inclusions.

Despite the economic importance of red feldspar in some markets, particularly in Asia, we rarely see this material submitted to the laboratory for identification. This is quite interesting, given the controversy over the color origin of red feldspar from certain deposits (see, e.g., A. Abduriyim et al., "Research on gem feldspar from the Shigatse region of Tibet," Summer 2011 *G&G*, pp. 167–180). The natural color of material from Oregon is generally undisputed, although treated samples have been seen. These samples are easily distinguishable, however, by their unusually high copper concentrations or atypical inclusion scenes. With Chinese material, there is no practical means of identifying whether the color is natural or induced by copper diffusion.

Using quantitative chemical analysis, it is possible to distinguish red feldspar from different localities (see figure 9, and also G. R. Rossman, "The Chinese red feldspar controversy: Chronology of research through July 2009," Spring 2011 *G&G*, pp. 16–30). Therefore, it is also possible to establish whether the color of a red feldspar is natural, as is the case for most material from Oregon, or undetermined, as with Inner Mongolian and Tibetan material. LA-ICP-MS analyses of the two samples yielded chemical compositions of $An_{48.9}Ab_{47.8}Or_{3.3}$ and $An_{51.0}Ab_{46.0}Or_{3.0}$, which correlate well with andesine-labradorite from China. Copper was detected in both samples. In light of their Chinese origin, we could not be certain that their color was natural. For their identification reports, we followed the lab's policy in stating that "color origin cannot currently be determined."

Emily V. Dubinsky and Ren Lu

Figure 8. These two orangy red gems (left—10.90 mm wide, and right—15.30 mm wide) were identified as plagioclase (andesine-labradorite). The origin of their color—natural or induced by copper diffusion—could not be determined.

Figure 9. The chemical compositions of gem-quality plagioclase from various localities, determined by quantitative LA-ICP-MS analysis, are clearly separated in this ternary plot. The compositions of the two red feldspars described in this study, shown as red squares, are consistent with material from China.

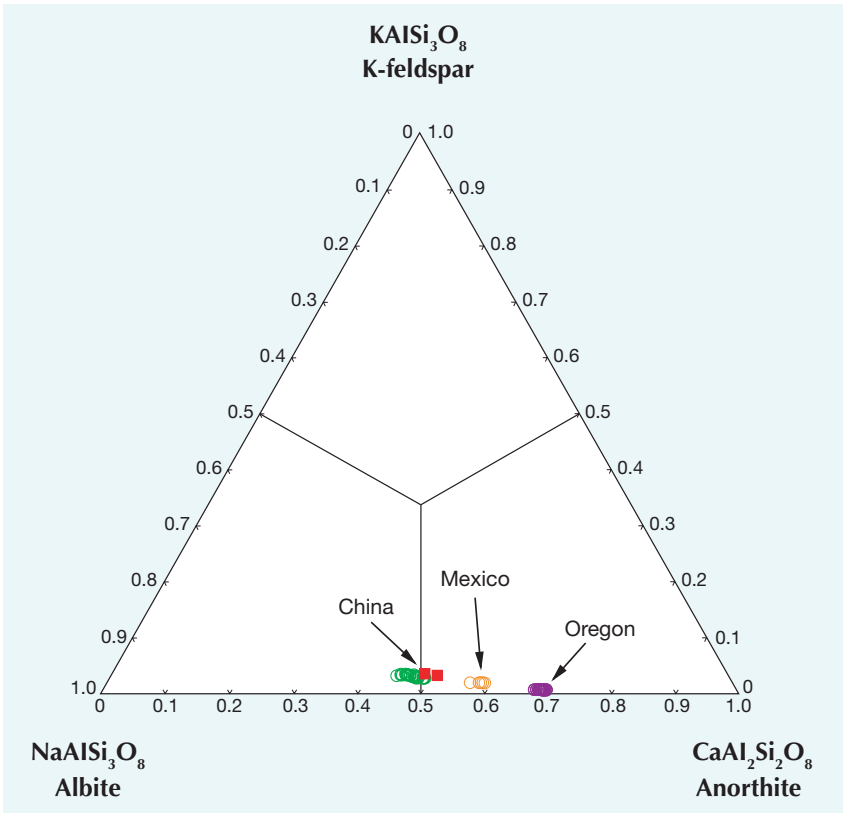

HIBONITE Crystal

Recently examined at the Carlsbad laboratory was a 3.1 g partially polished hexagonal crystal (figure 10) that proved to be a very rare collector mineral.

Initial microscopic observations revealed stepped etch features and numerous fractures and cleavages throughout. The sample contained dark brown mineral inclusions and some negative crystals, but their contents were not resolvable through the rough surface. A partially polished surface gave a spot RI of 1.79, though it was a vague reading as the polish was rather poor, and the hydrostatic SG was 3.80. Raman analysis revealed prominent features at 900 and 872 cm^{-1}, but the spectra did not match any samples in GIA's reference database.

The crystal's color and morphology were similar to those of hibonite specimens reportedly from Myanmar (T. Hainschwang et al., "Hibonite: A new gem mineral," Summer 2010 *G&G*, pp. 135–138). To confirm the identity, quantitative chemical data collected with LA-ICP-MS and its Raman spectrum were very consistent with those reported by Hainschwang et al. While the crystal we examined was much larger, only very small areas were clean enough to potentially yield faceted stones.

This was the first example of hibonite examined at the Carlsbad laboratory, and it illustrates the importance of familiarity with the gemological literature. Because of the increasingly specialized nature of gemology, a literature search may be the only resource to help identify an unusual gem material.

Nathan Renfro

Figure 10. This 3.1 g crystal was identified as the rare mineral hibonite.

Unusual Green Color in a JADEITE Bangle

The Carlsbad laboratory recently examined a jadeite bangle that showed an unusual band of green color (figure 11). While mottled white jade with irregular green patches or zones of color is not uncommon, these colored areas are usually due to naturally occurring chromium or artificially introduced green dye.

A spectroscope is useful for differentiating the cause of green color in jadeite; both chromium and dye show distinctive features in the red region of the spectrum. However, when this bangle was examined with a spectroscope, neither feature was observable in the red region, suggesting that the green color was not caused by either chromium or dye.

Under magnification the piece displayed a natural fibrous to granular structure. The green color followed a finer and denser zone that crosscut the bangle. This textural anomaly had the appearance of an irregular shear zone that occurred in the jadeite rock during its formation, causing a localized change in structure. All of the mineral grains, including those in the irregularly textured zone, appeared tightly interlocked and showed no indications of repair or manufacture.

Figure 11. This 58.3 g (70.70 × 12.93 mm) polymer-impregnated jadeite bangle showed a prominent green band caused by an optical flash effect.

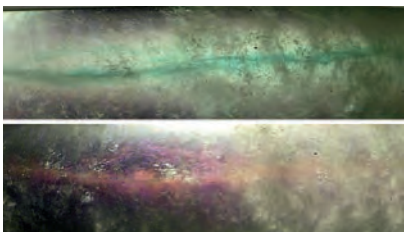

Figure 12. The impregnated bangle showed a green flash in brightfield lighting (top) and an orange flash in darkfield conditions (bottom). This color variation confirmed that a flash effect—not dye or chromium—was the cause of the bangle's green color band.

The green color proved to be due to a vivid flash effect that was visible when the observer's line of sight was nearly parallel to the textured zone against a light background (figure 12, top). When the same part of the bangle was examined against a black background, the flash effect displayed an orange color (figure 12, bottom). This color variation between brightfield and darkfield conditions proves that the green color was an optical effect, and not caused by dye or traces of natural chromium in the jadeite. With FTIR spectroscopy, polymer impregnation was confirmed by the presence of a strong absorption band centered around 3000 cm^{-1} that completely saturated the detector of the instrument.

While a flash effect due to polymer impregnation in jadeite has been previously reported (Spring 2010 Lab Notes, pp. 54–55), this was the first time the lab had seen a prominent green color caused by the flash effect. The fact that this effect strongly resembled the green color expected in jadeite added to the intrigue of this bangle.

Nathan Renfro

Greenish Blue Imitation OPAL

The Carlsbad laboratory recently examined a semitransparent, vibrant greenish blue 6.89 ct modified oval brilliant (figure 13) similar to material being sold as synthetic opal under the trade name "PeruBlu."

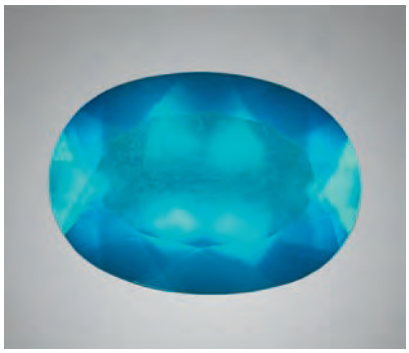

Figure 13. This 6.89 ct greenish blue modified oval brilliant is an imitation opal.

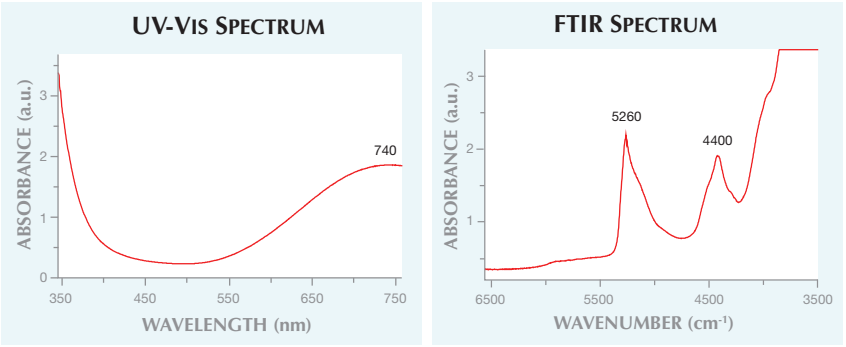

Figure 15. The UV-Vis absorption spectrum of the imitation opal shows broad absorption centered at 740 nm and a large transmission window at ~500 nm (left). Prominent features at ~5260 and 4400 cm^{-1} are seen in the IR spectrum (right).

While the sample appeared generally clean under low magnification, a closer look with a standard gemological microscope revealed wispy clouds and an artificial-looking, fine-grained, granular appearance that is not common to natural opal and caused a hazy quality. Pinpoint inclusions with faint optical halos (figure 14) were scattered throughout the sample. It had an RI of 1.339, with an additional faint shadow edge at 1.350, indicating the material might be composed of multiple components. The very low RI quickly ruled out natural opal. The hydrostatic SG of 1.54 was also well below the range expected for natural opal. In cross-polarized light, the sample displayed strong anomalous double refraction as prominent "snake bands." It was inert to long- and short-wave UV radiation.

Figure 14. Microscopic examination of the imitation opal with shadowed illumination showed a granular pattern and small pinpoint inclusions surrounded by an optical halo. Image width 0.80 mm.

UV-Vis spectroscopy revealed a strong absorption band centered at 740 nm and general absorption in the UV region, leaving a large transmission window centered at approximately 500 nm (figure 15, left). This spectrum was consistent with the observed greenish blue color. In addition to Si, EDXRF qualitative chemical analysis detected significant amounts of Cu along with very minor amounts of K and Cl. It is likely that the greenish blue color is caused by copper absorption. Since many Cu-colored minerals display a greenish blue color, the presence of Cu in this sample was not surprising.

Raman spectroscopy produced a featureless trace, consistent with an amorphous material. FTIR spectroscopy (figure 15, right) revealed prominent absorption features at ~5260 and ~4400 cm^{-1}. These absorptions are quite similar to those seen in the early version of MexiFire synthetic opal (G. Choudhary and R. Bhandari, "A new type of synthetic fire opal: Mexifire," Fall 2008 *G&G*, pp. 228–233). Except for its color, the appearance and the low RI and SG properties were also consistent with those reported for the MexiFire product, which has much different gemological properties than natural Peruvian opal (e.g., Winter 2003 GNI, p. 332).

Because the RI and SG values fell below any published values for natural common opal (e.g., R. Webster and P. G. Read, *Gems: Their Sources, Description, and Identification*, 5th ed., Butterworth-Heinemann, Oxford, UK, 2002), it is the lab's opinion that this sample is more properly described as an imitation, rather than a synthetic. This marked the first time the Carlsbad laboratory has encountered this material, even though a similar product has been available since 2007 (A. Abduriyim and T. Kobayashi, "Synthetic opal called 'MexiFire' and 'PeruBlu,'" *Gemmology*, Vol. 39, No. 464, 2008, pp. 2–3).

Nathan Renfro and Amy Cooper

PEARL

Cultured Freshwater Pearl Necklace Resembling Natural Saltwater Pearls

Recently, the New York laboratory received what appeared to be a typical antique-style pearl necklace with a small gold fishhook clasp. The knotted 20-inch (50.8 cm) necklace was comprised of graduated near-round to semibaroque white cultured pearls (3.38–7.08 mm; figure 16, left). The lab receives numerous pieces like this each month, and the overwhelming majority of the specimens prove to be natural saltwater pearls from mollusks of the *Pinctada* genus (e.g., figure 16, right). The rest are generally bead-cul-

Figure 16. The necklace on the left, composed of non-bead cultured freshwater pearls (3.38–7.08 mm), resembles a typical natural saltwater pearl necklace (see example on the right; 3.40–5.25 mm).

tured saltwater pearls or a mixture of these and natural saltwater pearls.

This necklace caught our attention when most of the cultured pearls' micro X-radiographs displayed dark linear irregular central features typical of the growth structures in freshwater non-bead cultured pearls (figure 17). The EDXRF spectrum and strong white fluorescence to X-rays revealed noticeable traces of manganese, confirming a freshwater origin. Despite all outward appearances, this necklace was composed of non-bead cultured freshwater pearls.

In many ways this piece was atypical of white freshwater cultured pearl strands, which tend to have a neutral white color and uniform size and shape, typically button, oval, or semi-baroque (figure 18). The present necklace was created using rounder graduated cultured pearls of a creamier color on a knotted string—all very typical of natural saltwater strands. In fact, the lab has begun to see freshwater pieces apparently intended to imitate older natural saltwater strands, either through their assembly or through physical modification of the cultured pearls to make them appear old and worn.

The last few years have seen increasing demand for natural saltwater pearls. Most consumers and many dealers in the jewelry industry have little experience with natural saltwater pearls due to their rarity and high cost. Items such as this necklace are a reminder to take extra caution when dealing with apparent natural saltwater pearl strands, since their cultured freshwater counterparts occupy the opposite end of the value spectrum.

Chunhui Zhou and Akira Hyatt

Large Freshwater Cultured Blister Pearl

The practice of culturing blister pearls dates back to ancient China, where small lead images of Buddha were placed inside the shells of freshwater mussels. Today blister pearls are cultured in various types of mollusks. Blister pearls also form naturally and can be quite large, such as a 97.80 ct sample examined by GIA's Bangkok laboratory (N. Sturman, "A large naturally colored natural blister pearl," GIA News from Research, www.gia.edu/research-resources/news-from-research/index.html, June 10, 2009).

A very large cultured blister pearl (figure 19) was recently submitted to the New York laboratory for identification. The baroque-shaped cream-colored specimen measured approximately 60.58 × 56.64 × 26.80 mm and weighed 517 ct. One side of it was fairly flat and displayed severed growth rings (figure 20), clear evidence of having been cut away from the shell, while the other side was nacreous and exhibited noticeable orient.

In addition to its extraordinary size, this cultured blister pearl had an-

Figure 17. X-radiographs of the client's necklace revealed the linear growth structure typical of non-bead cultured freshwater pearls (left, ~5 mm in diameter) rather than the concentric growth structure found in natural saltwater pearls (right, ~4 mm each).

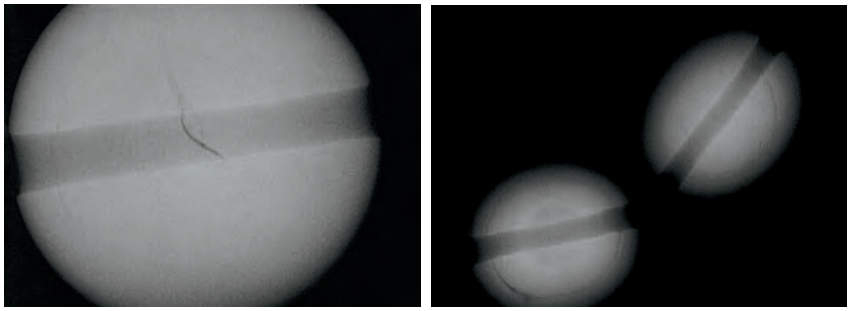

Figure 18. Most non-bead cultured freshwater pearl strands (here, with a maximum diameter of 3.60–4.50 mm) have a neutral white color and uniform size and shape.

Figure 19. This massive freshwater cultured blister pearl (shown with a 13 mm South Sea cultured pearl for comparison) weighs 517 ct and measures 60.58 × 56.64 × 26.80 mm.

other unusual feature: At least 10 distinct small cultured pearls were embedded in it, visible on the side where it had been cut from the shell (again, see figure 20). Within each one, X-radiography revealed the growth structures typical of nonbead-cultured freshwater pearls (e.g., figure 21).

The sample's strong yellow fluorescence to X-rays and EDXRF spectrum confirmed that it had a freshwater origin, in that it contained noticeable traces of manganese. A considerable amount of lead was also found in various parts of the blister's surface, which is not typical of either freshwater or saltwater pearls. Bioaccumulation in a polluted water environment can contribute to heavy metal concentrations in mollusk shells and tissues (S. K. Gupta and J. Singh, "Evaluation of mollusc as a sensitive indicator of heavy metal pollution in aquatic system [*sic*]: A review," *The IIOAB Journal,* Vol. 2, No. 1, 2011, pp. 49–57).

The unusual aggregate structure suggested that the large cultured blister pearl may have resulted from normal culturing gone awry. Typically, multiple freshwater pearls are cultured in a single mussel at one time. In this case, it appears that the secretion of nacre had grown out of control for some reason—possibly the result of the lead contamination—engulfing the small individual cultured pearls.

Although this is not the first freshwater cultured blister pearl we have seen, its large size, unusual structure, and anomalous lead content make it a unique and interesting specimen.

Chunhui Zhou and Akira Hyatt

Figure 20. A close-up view of the sawn flat side of the cultured blister pearl reveals numerous embedded small cultured pearls. Image width ~26 mm.

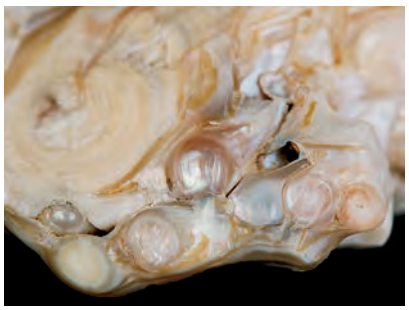

Figure 21. This X-radiograph image shows the outlines of some of the small nonbead-cultured pearls in the specimen. Image width ~16 mm.

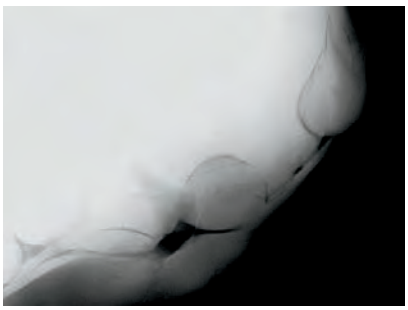

Luminescent STRONTIUM-CALCIUM ALUMINATE Doped with Rare-Earth Elements

In January 2012 the New York laboratory received for identification two unusual manufactured products, submitted within one week of each other. One was a yellowish green decorative vessel (figure 22) carved in the style of Asian jade or serpentine, with detailed patterns in relief; it measured approximately 20.20 × 8.00 × 7.50 cm and weighed 583.20 g. The other was a yellowish green and orangy brown piece of "rough" measuring approximately 11.0 × 7.2 × 6.7 mm and weighing 0.89 g (figure 23).

The carved vessel gave a spot RI of 1.65, and the rough piece's hydrostatic SG was 3.48; neither displayed any features in the desk-model spectroscope. Both showed a very strong yellowish green fluorescence to long- and short-wave UV radiation, and a strong green phosphorescence that lasted for more than 10 minutes. The same phosphorescence reaction was achieved using a strong fiber-optic light and in a light box using daylight-equivalent 6500 K bulbs. Microscopic examination of both samples revealed a uniform, granular texture with tiny, evenly distributed hexagonal grains and a pitted surface. Some dark brown stains were observed along fractures. LA-ICP-MS analysis showed that both pieces had essentially the same chemical composition, with major amounts of Sr, Al,

Figure 22. This 583.20 g carved vessel, composed of strontium-calcium aluminate doped with rare-earth elements, displayed a strong green phosphorescence reaction, as shown on the right.

and Ca, as well as minor amounts of Eu, Dy, and B. Raman spectroscopy also recorded similar features for both, with a main peak at 464 cm^{-1} and several minor peaks. Additional LA-ICP-MS data and the full Raman spectra are available in the *G&G* Data Depository at www.gia.edu/gandg.

Figure 23. This 0.89 g piece of strontium-calcium aluminate showed the same phosphorescence reaction as the carving in figure 22.

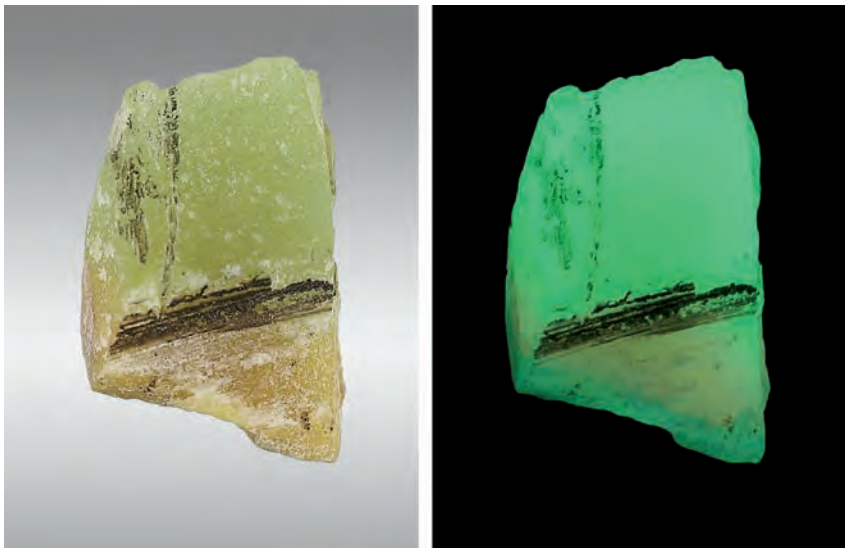

Many of these properties were consistent with a manufactured product represented at the 2002 Tucson gem show as "Nightglow Stone" (Winter 2002 Gem News International, pp. 358–360), which consisted of strontium aluminate doped with Eu^{2+} and Dy^{3+} to produce a very strong green phosphorescence. That material was reportedly produced by a sintering method, and the granular appearance of these two pieces was consistent with such a preparation. In 2005, a "night glowing pearl" coated with a similar material was also submitted to GIA for an identification report (see Spring 2005 Lab Notes, pp. 46–47), demonstrating a persistent interest in producing glowing gem materials.

Rare earth–doped strontium aluminate phosphors hold promise for the development of long-lasting phosphorescence applications, an important area of research. Chemical variations in the strontium aluminate host, as well as the type of activator, have yielded different afterglow colors and intensities. Various preparation techniques have been used, often with the addition of B_2O_3, which is regarded as an excellent flux to facilitate the diffusion process and reduce the synthesis temperature (Y.-L. Chang et al., "Characterizations of Eu, Dy co-doped $SrAl_2O_4$ phosphors prepared by the solid-state reaction with B_2O_3 addition," *Journal of Alloys and Compounds*, Vol. 461, 2008, pp. 598–603). The sintering temperature and the particle size of the phosphor also play important roles in determining the luminescence quality of the material (S. Hamdan et al., "Morphology and composition of strontium calcium aluminate matrix doped with Dy^{3+}," *Materials Science and Technology*, Vol. 27, No. 1, 2011, pp. 232–234).

Luminescent materials have many practical applications, such as emergency signage and alternative lighting sources. They are also being used to make interesting decorative objects.

Claire Ito

Figure 24. This 0.50 ct HPHT-grown synthetic diamond (left) was produced by AOTC. DiamondView images display strong blue to green fluorescence (middle) and intense blue phosphorescence (right). The middle image clearly shows the cuboctahedral growth pattern typical of HPHT-grown synthetic diamonds.

Near-Colorless HPHT-Grown SYNTHETIC DIAMONDS from Advanced Optical Technology Co.

Manufacturers of HPHT-grown synthetic diamonds have generally focused on fancy colors due to the ease of incorporating color-inducing impurities along with the faster growth rates that result in larger polished products. The majority of colorless to near-colorless HPHT synthetic specimens have been grown solely for research purposes by companies such as General Electric, De Beers, and Sumitomo Electric Industries. Near-colorless HPHT synthetics, though very rare, have also been marketed to the gem trade by Advanced Optical Technology Co. (AOTC).

Recently, three near-colorless and three faintly colored HPHT-grown AOTC synthetic diamonds were submitted to GIA's New York laboratory for grading services. These products can be purchased through AOTC's trade-only website or through their consumer-oriented brand, D.NEA, and each synthetic bears the inscription "AOTC-created." The diamonds are said to be manufactured using BARS- or toroid-type presses. AOTC also loaned us 24 colorless, near-colorless, and faintly and lightly colored HPHT-grown synthetic diamonds.

All 30 of the samples were faceted as round brilliants, ranging from 0.21 to 0.57 ct (e.g., figure 24, left). Most received colorless to near-colorless grades, with six classified as F and 17 falling in the G–J range. The remaining seven were very faint to light blue. Clarities ranged from VVS_1 to I_2, with no correlation between the color and clarity grades. The poorer clarities resulted from elongated opaque or metallic flux-metal inclusions. Graining was not evident, and only subdued interference colors (gray/blue), characteristic of HPHT synthetics, were observed.

Infrared absorption spectroscopy revealed that they were mixed type IIa/IIb, with only traces of boron detected. Nitrogen and boron impurities in diamond produce yellow and blue colors, respectively. It is the careful balance between the relative concentrations of these two impurities, at low concentrations, that gave rise to the near-colorless appearance of most of the samples. Although color zoning was not noticeable, the growth sector–dependent impurity uptake was obvious in DiamondView fluorescence images (e.g., figure 24, center). The samples exhibited strong blue to green fluorescence and intense, long-lived (1–6 minutes) blue phosphorescence (figure 24, right). This behavior differed from that seen using a standard UV lamp. The samples were inert to long-wave (366 nm) radiation, but showed very faint to strong yellow fluorescence to short-wave (254 nm) excitation. In the latter case, we observed strong greenish yellow phosphorescence with a persistent blue component.

Photoluminescence (PL) spectroscopy revealed that no one emission peak was characteristic of all the synthetic diamonds. Nitrogen vacancies (575.0 and 637.0 nm) and a peak at 658 nm were observed in some samples, independent of the press-type used. The latter peak has been reported in nickel-containing HPHT-grown synthetic diamonds, but was here noted in samples attributed to Ni-free toroid press production. An additional group of three peaks at 706.9, 709.1, and 712.2 nm was usually detected in the samples containing 658 nm peaks. The defect(s) responsible for these peaks have not been established. Nickel-related emissions (484 and 882.6/884.3 nm doublet) were identified in most of the BARS-grown synthetics. Nickel impurities, often observed in HPHT synthetic diamonds grown using Ni catalysts, are rare in natural diamonds. A weak H3 center (503.2 nm) was detected in three of the samples. One specimen (toroid press production, I color, I_2 clarity) did not show distinctive PL features.

This line of HPHT-grown synthetics can be confidently identified by careful analysis of data from a combination of advanced testing techniques, especially fluorescence imaging and PL spectroscopy.

Ulrika F. S. D'Haenens-Johansson, Kyaw Soe Moe, Paul Johnson, Shun Yan Wong, and Wuyi Wang

PHOTO CREDITS:
Jian Xin (Jae) Liao—1, 3–6, 8, 16, 18–20, 22–24 (left); Robison McMurtry—2, 11, 12; Jason Darley—7; C. D. Mengason—10, 13; Nathan Renfro—14; Chunhui Zhou—17, 21; Sood-Oil (Judy) Chia—22, 23; Jian Xin (Jae) Liao—24 (left) Kyaw Soe Moe—24 (center and right).

G&G
Gem News International

Editor
Brendan M. Laurs (blaurs@gia.edu)

Contributing Editors
Emmanuel Fritsch, *CNRS, Team 6502, Institut des Matériaux Jean Rouxel (IMN), University of Nantes, France* (fritsch@cnrs-imn.fr)
Michael S. Krzemnicki, *Swiss Gemmological Institute SSEF, Basel, Switzerland* (gemlab@ssef.ch)
Franck Notari, *GGTL GemLab–GemTechLab, Geneva, Switzerland* (franck.notari@gemtechlab.ch)
Kenneth Scarratt, *GIA, Bangkok, Thailand* (ken.scarratt@gia.edu)

COLORED STONES AND ORGANIC MATERIALS

Burmese amber update. Amber from Myanmar's Hukawng Valley, also called Burmite, has been produced intermittently in commercial quantities from the 20th century to the early part of the 2000s (Summer 2001 Gem News International [GNI], pp. 142–143). In March 2012, Mark Smith (Thai Lanka Trading Ltd., Bangkok) informed GIA about a surge in this amber's availability in the Bangkok market since early 2011, notably as clean faceted stones. The color ranges from light yellow to orange and rarely red, which is most valued by the Burmese. However, the yellow material is appreciated for its strong fluorescence to long-wave UV radiation (figure 1). Mr. Smith indicated that most of the faceted stones weigh 5–20 ct, although the largest he obtained was 32 ct and he knew of samples weighing 40–50 ct. Considering the low specific gravity of amber, pieces of this weight are quite large. Mr. Smith estimated that several thousand carats of faceted stones have been cut since early 2011. The material is polished in both Myanmar and Bangkok.

Burmite is known for the presence of insects and other biological materials, which indicate a Cretaceous age of ~100 million years (see Summer 2001 GNI entry). While most of the recent production is fairly clean, some stones contain ~1 mm spheres that are probably composed of plant matter, and a few have insect inclusions. Mr. Smith obtained one notable example: a 27.55 ct cabochon with a well preserved scorpion (~8 mm long) and various insects resembling wasps, ants, and a tick; some of these are visible in figure 2. Although faked specimens consisting of molded amber or acrylic with modern scorpions are common, genuine scorpions are extremely rare in Burmese amber; Mr. Smith knew of only a few documented specimens.

Figure 1. These two faceted pieces of Burmese amber (4.80 ct total weight) show the range of color of the material seen recently in the Bangkok market (top). The lighter colored amber shows strong fluorescence to long-wave UV radiation (bottom). Photos by Prasit Prachagool.

Brendan M. Laurs

Editor's note: Interested contributors should send information and illustrations to Brendan Laurs at blaurs@gia.edu or GIA, The Robert Mouawad Campus, 5345 Armada Drive, Carlsbad, CA 92008.

Gems & Gemology, Vol. 48, No. 2, pp. 142–155, http://dx.doi.org/10.5741/GEMS.48.2.142.

© 2012 Gemological Institute of America

Figure 2. This 27.55 ct cabochon of Burmese amber contains a complete scorpion (on the left) and a variety of insects. Photo by Prasit Prachagool.

Aquamarine from San Bernardino County, California. Southern California's gem pegmatites are world-famous for their production of tourmaline, beryl, spodumene, quartz, and other minerals since the late 19th and early 20th centuries. The pegmatites are associated with the Peninsular Ranges Batholith, and extend from Riverside County into northern Baja California (e.g., J. Fisher, "Mines and minerals of the Southern California pegmatite province," *Rocks & Minerals*, Vol. 86, 2011, pp. 14–35, http://dx.doi.org/10.1080/00357529.2011.537167). Further north, San Bernardino County is not known to host many pegmatites, although two localities containing uranium-bearing minerals were documented several decades ago (D. F. Hewett and J. J. Glass, "Two uranium-bearing pegmatite bodies in San Bernardino County, California, *American Mineralogist*, Vol. 38, 1953, pp. 1040–1050). However, no gem mineralization has been noted from those pegmatites in the literature.

It was quite a surprise, then, when in 2006 a local prospector named Dave Schmidt found an aquamarine-bearing pegmatite on BLM (Bureau of Land Management) land north of Yucca Valley in San Bernardino County. He filed a claim, calling it the California Blue mine. He worked the ~1 m thick dike by hand and collected many loose crystals of aquamarine and topaz, but few matrix specimens. In November 2011, he partnered with mineral collector Paul Geffner to mine the deposit for a one-week period using an excavator. They found four aquamarine-bearing cavities that yielded matrix specimens (figure 3) and loose crystals of gem-quality aquamarine (bluish green to greenish blue), topaz (colorless and rarely pale blue), and quartz (colorless to smoky), as well as non-gem spessartine, fluorite, albite ("cleavelandite"), and microcline.

Rough and cut specimens of the aquamarine were exhibited at the 2012 Tucson gem shows by Rick Kennedy (Earth's Treasures, Santa Clara, California). He indicated that since the California Blue mine has been worked primarily for mineral specimens, fewer than 10 aquamarines have been faceted so far. The best cut stone weighed 7.35 ct and showed an attractive greenish blue color (again, see figure 3). A few pieces of smoky quartz have also been cut.

In March 2012, another one-week mining project at the California Blue mine yielded several more aquamarine crystals of good color and clarity, as well as ~80 g of facet/cabochon-quality aquamarine and ~40 g of colorless facet-grade topaz. Mr. Schmidt will continue developing the mine in the near future, and also plans to host fee digging on the property within the next year.

Brendan M. Laurs

Trapiche aquamarine from Namibia. In August 2010, GIA was informed about a new find of trapiche aquamarine from the Erongo Mountains in Namibia by Jo-Hannes Brunner (Pangolin Trading, Windhoek, Namibia). The material was reportedly recovered from a small pocket that contained matrix specimens and crystal clusters, as well as a few loose crystals up to 10 cm long. The crystals were typically semitransparent with etched prism faces, but they displayed a variety of interesting patterns when sliced parallel and perpendicular to the c-axis (e.g., figure 4). Mr. Brunner subsequently donated several rough and cut samples to GIA, and four specimens were examined for this report.

The samples consisted of a crystal (43.60 mm long), an oval cabochon (6.13 ct), a rectangular step cut (8.20 ct), and

Figure 3. These rough and cut aquamarine specimens are from a new find in San Bernardino County, California. The cut stone weighs 7.35 ct and the specimen is 7.9 cm wide. Photo by Jeff Scovil.

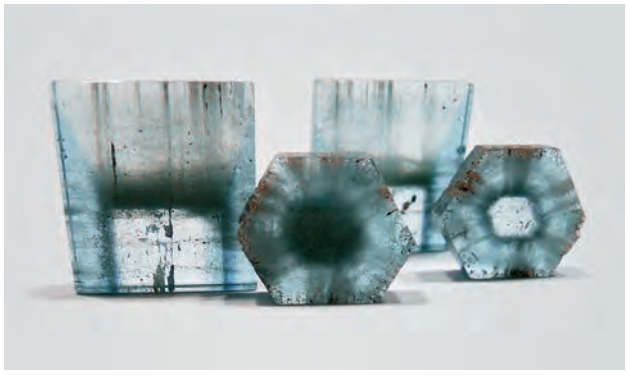

Figure 4. Interesting patterns are created by dense crystallographically oriented clouds in these slices of aquamarine (20–30 mm wide) from Namibia's Erongo Mountains. The rectangular slices are cut parallel to the c-axis, while the hexagonal plates are sliced perpendicular to the c-axis and display trapiche structure. Photo by Jo-Hannes Brunner.

a hexagonal tablet (8.84 ct). They were semitransparent to transparent, and ranged from grayish blue to bluish grayish green. Basic gemological testing identified them as beryl, and this was confirmed by Raman spectroscopy.

The tablet showed an interesting trapiche structure formed by distinct hexagonal color zoning and some subtle radial arms (figure 5, left); two of them extended all the way from the core to the surface. The arms were composed mostly of clouds of minute crystals and particles (figure 5, right). Also present were negative crystals close to the surface, as well as grayish material in surface cavities that consisted of residue from the polishing compound.

Trapiche aquamarines have been reported previously from the Erongo Mountains (Fall 2008 GNI, pp. 275–276), but those samples had a much stronger radial pattern and lacked the hexagonal zoning shown by the present samples.

Trapiche growth structure, though best known in emerald, has also been documented in ruby, sapphire, tourmaline, quartz, and andalusite. In both beryl and corundum, the trapiche phenomenon has been attributed to skeletal (dendritic) growth, in which the edges and corners grow faster than the adjacent crystal faces (I. Sunagawa, *Crystals—Growth, Morphology and Perfection*, Cambridge University Press, Cambridge, UK, 2005).

Riccardo Befi (rbefi@gia.edu)
GIA, New York

Champagne/Imperial garnet from Lindi Province, Tanzania. The Lindi Province in Tanzania is well known as a source of pyrope-spessartine and almandine-spessartine (see Spring 2006 GNI, pp. 66–67, and Summer 2008 GNI, pp. 165–166). A new deposit in the same area recently yielded some additional production, marketed as Champagne or Imperial garnet at the 2012 Tucson gem shows. Several samples were loaned to GIA by Michael Puerta (International Gems H.K. Ltd., Hong Kong; see figure 6, left), who visited the Lindi area with Farooq Hashmi (Intimate Gems, Glen Cove, New York) in late 2011. According to them, this new garnet has been mined since mid-2011, and they know of one Tanzanian supplier who exported 360+ kg of rough material after one month of mining. The garnet is similar to the previous Lindi pyrope-spessartine except for being slightly darker and available in smaller pieces. They reported that it was produced as a byproduct of placer gold mining near the town of Ruangwa, where they obtained 15–20 kg of rough material. Additional samples were loaned and donated to GIA by Steve Ulatowski (New Era Gems, Grass Valley, California; see figure 6, right). At the Tucson show he had 22 kg of the new garnet, in pieces that mostly ranged from 1 to 3 g, and ~2,000 carats of faceted stones weighing 1–8 ct. He noted that during his buying trips to Tanzania since December 2011, he has seen bigger and better pieces of this garnet, and in greater quantities.

The samples loaned by Mr. Puerta were characterized for this report. The garnets were light reddish orange in daylight-equivalent light and orangy red under incandescent light. Color was evenly distributed. The samples had RIs ranging from 1.750 to 1.755 and hydrostatic SGs of

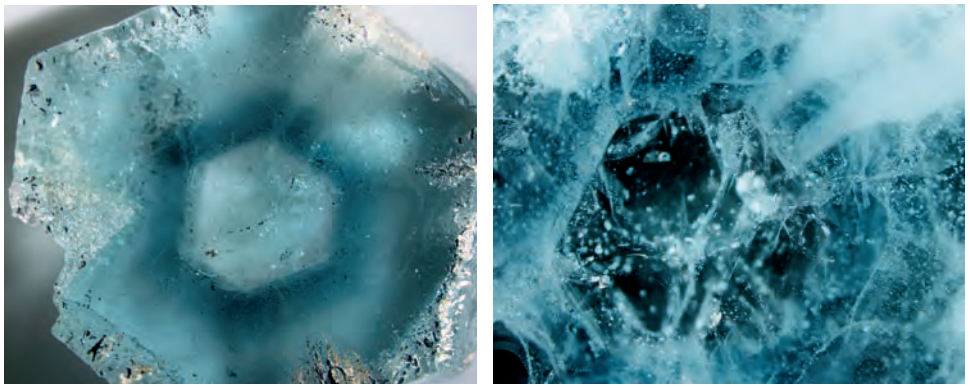

Figure 5. This hexagonal tablet of aquamarine displays an indistinct trapiche structure (left, magnified 10×). A closer view shows two of the trapiche arms (consisting mainly of clouds of minute particles) that radiate outward from the more transparent central core (right, 15×). Photomicrographs by R. Befi.

Figure 6. Pyrope-spessartine from Lindi Province, Tanzania, was available at the 2012 Tucson gem shows. The left photo shows examples from the new production (2.64–9.59 ct, faceted, courtesy of Michael Puerta; photo by Robert Weldon). The samples in the right photo (some donated to GIA by Steve Ulatowski; GIA Collection nos. 38516–38518; photo by Jeff Scovil) consist of material from older production, except for the cut stones in the center and right (7.38 and 2.23 ct), which are from the new mine.

3.77–3.83, and they were inert to long- and short-wave UV radiation. These properties are consistent with pyrope-spessartine, although slightly different from the previous Lindi pyrope-spessartine reported in the Spring 2006 GNI entry (which was pink in both incandescent light and daylight, with RI of 1.756 and an SG of 3.85). Microscopic examination showed three-dimensional networks of oriented needles, a few of them iridescent (figure 7, left). In some samples these needles formed dense concentrations (figure 7, center), while others had star-like arrays (figure 7, right). Raman analysis identified these needles as rutile, and they were often associated with clouds. In addition, short, reflective ribbon-shaped films were seen in all samples (figure 8); a long ribbon in one stone appeared brownish in certain orientations. A few unidentified dark crystals were observed in another sample. A banded strain pattern was visible in cross-polarized light.

Quantitative chemical analyses of three of the samples by laser ablation–inductively coupled plasma–mass spectrometry (LA-ICP-MS) correlated to a compositional range of $Prp_{45–51}Sps_{22–26}Alm_{16–23}Grs_{8–10}$, and also showed the presence of several trace elements, including Ti, V, Cr, Zn, Ga, Ge, Sr, Zr, Cd, and several rare-earth elements. Vis-NIR absorption spectra were very similar to malaya garnets (pyrope-spessartine) reported from Madagascar a decade ago (see K. Schmetzer, "Pink to pinkish orange malaya garnets from Bekily, Madagascar," Winter 2001 *G&G*, pp. 296–308), with features associated with Mn^{2+}, Fe^{2+}, Fe^{3+}, and V^{3+}. Mid-IR spectroscopy showed bands related to Fe^{2+} and hydrous components. (For additional photomicrographs and

Figure 7. Three-dimensional networks of oriented rutile needles were common in the Lindi garnets; a few needles appeared iridescent (left, magnified 75×). The needles were also present as dense concentrations (center, 23×) and in star-like patterns (right, 65×). Photomicrographs by K. S. Moe.

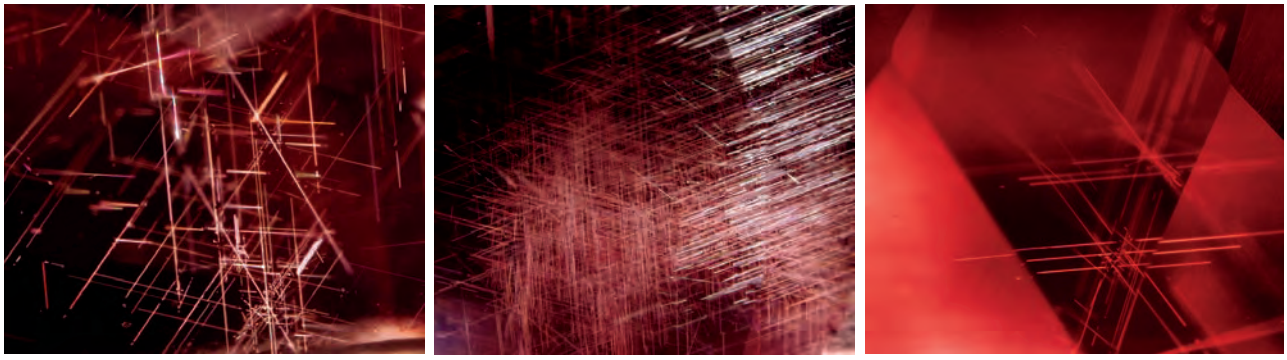

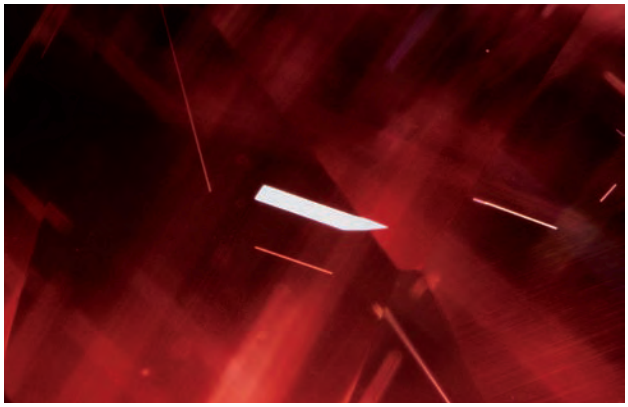

Figure 8. Short reflective ribbon-shaped films were seen in many of the garnets. Photomicrograph by K. S. Moe; magnified 63×.

the mid-IR and Vis-NIR spectra of the new and old Lindi garnets, see the *G&G* Data Depository at gia.edu/gandg.)

Kyaw Soe Moe (kmoe@gia.edu)
GIA, New York

Rainbow moonstone from Zambia. During the 2012 Tucson gem shows, Scott Davies (American-Thai Trading, Bangkok) displayed some new transparent rainbow moonstone that was reportedly mined in Zambia (e.g., figure 9). Since he first saw the rough material in August 2011, Mr. Davies has cut about 1,000 carats of it, as both faceted stones and cabochons. Although large cabochons of this moonstone can be very colorful, loupe-clean faceted stones have been more in demand by his customers. The largest such stone he cut weighed 2.65 ct, and it remains difficult to facet loupe-clean material larger than 1 ct. Mr. Davies donated eight specimens to GIA, consisting of four cabochons ranging from 2.08 to 4.24 ct, three faceted samples weighing 0.61–0.71 ct, and one partially faceted 8.33 ct sample.

Gemological testing of the eight stones gave the following properties: color—near-colorless with strong blue, orange, yellow, green, violet, and pink adularescence; RI—1.55 (spot) for the cabochons and 1.554–1.560 for the faceted samples; hydrostatic SG—2.66–2.70; and fluorescence—inert to weak blue to long-wave UV radiation and weak red to short-wave UV. Energy-dispersive X-ray fluorescence (EDXRF) analyses revealed major amounts of Al, Si, and Ca, and traces of Na, Cr, Fe, Ga, and Sr. These properties are generally consistent with plagioclase (M. O'Donoghue, Ed., *Gems*, 6th ed., Butterworth-Heinemann, Oxford, UK, 2006, pp. 238–258). LA-ICP-MS chemical analysis of a faceted sample gave a compositional range of $Ab_{45.9–51.5}An_{53.0–47.3}Or_{1.2–1.2}$ (expressed as mol.% albite:anorthite:orthoclase), which falls near the border between andesine and labradorite in the plagioclase series.

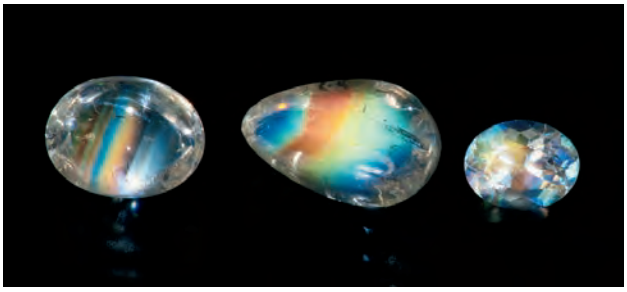

Figure 9. These rainbow moonstones are reportedly from Zambia; the largest weighs 2.82 ct. Gift of Scott Davies; GIA Collection nos. 38521–38523. Photo by Robert Weldon.

Microscopic examination showed polysynthetic twinning—which is commonly seen in plagioclase—in all the samples. Parallel arrays of ribbon-like inclusions with jagged edges were spatially oriented along the twin planes (e.g., figure 10, left). These ribbons showed intense blue or green iridescence in certain directions. One sample also contained two dark green crystals that were identified by Raman spectroscopy as actinolite (e.g., figure 10, right).

The moonstones' rainbow adularescence was best seen when looking parallel to the lamellar twin planes (figure 11, left). In addition, darkfield lighting illuminated narrow bands of sharply defined blue adularescence that were parallel to the polysynthetic twin lamellae (figure 11, center). These bands were defined by thin planes of fine particles. When the viewing direction was shifted, thicker areas between the polysynthetic twin planes showed fuzzy blue

Figure 10. Parallel arrays of ribbon-like inclusions with jagged edges showed iridescence in certain directions (left, 45×). Dark green actinolite inclusions (right, 90×) were observed in one of the samples. Photomicrographs by K. S. Moe.

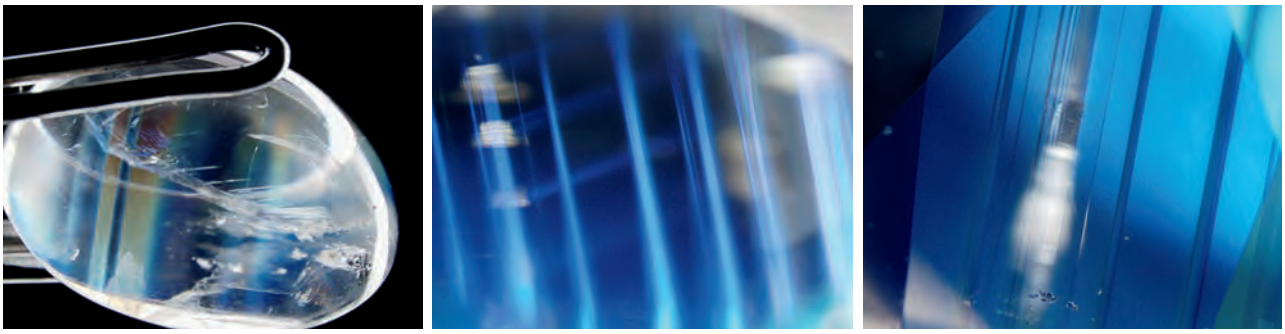

Figure 11. The rainbow phenomenon was best seen parallel to the lamellar twin planes (left, 15×). Thin, sharp blue bands (center, 50×) and thick, fuzzy blue bands (right, 60×) were observed from different viewing directions with fiber-optic lighting. Photomicrographs by W. L. Win.

adularescence (figure 11, right). The adularescent blue glow in these thicker layers was apparently caused by reflection of light between the thin planes of fine particles.

Wai L. Win (wwin@gia.edu) and Kyaw Soe Moe
GIA, New York

Morganite from Ethiopia. At the 2012 Tucson gem shows, Hussain Rezayee (Rare Gems & Minerals, Beverly Hills, California) showed GIA several faceted morganite samples (e.g., figure 12), reportedly mined near the town of Shakiso in southern Ethiopia. The stones ranged from light pink to orangy pink, and included two large ovals weighing 146.58 and 110.65 ct. Nine of the morganites were selected for examination at GIA based on their internal features, and Mr. Rezayee kindly donated them to the GIA Collection.

The samples weighed 1.10–7.75 ct, had RIs of 1.585–1.600, SG values of 2.73–2.80, and were inert to long- and short-wave UV radiation. Microscopic examination revealed two-phase fluid inclusions typical of morganite, along with a few solid and negative crystals. Raman analysis identified the solid crystals in a 2.65 ct specimen (figure 13) as mica and plagioclase (showing polysynthetic twinning). Numerous shapes of fluid inclusions were observed, including long curved inclusions with tails and well-formed hexagonal crystals (figure 14, left and center). The 2.65 ct stone contained a movable bubble filled with CO_2 (identified by Raman analysis). Also observed were negative crystals, with or without CO_2, and fluid inclusions associated with a roiled growth structure. A 4.75 ct sample contained a fluid inclusion that homogenized during photomicrography due to the heat from the microscope's lamp. The heating caused the gas bubble to disappear, and then it reappeared a few seconds after the lamp was switched off. Bands of clouds and needles were also found in many samples (figure 14, right). Some possessed partially healed feathers associated with wispy clouds. All nine morganites showed high-order interference colors in cross-polarized light.

Raman spectroscopy confirmed these specimens as beryl, and detected the presence of H_2O at 3600 and 3660 cm^{-1} (types I and II, respectively). The mid-IR spectrum revealed a 7060 cm^{-1} band caused by type II H_2O molecules. These and other unassociated water molecules also caused OH-stretching bands in the 4500–3000 cm^{-1} region. Bands in the 5700–5000 cm^{-1} range were caused by type I and II water molecules, while a small band at 2672 cm^{-1} was related to deuterated water, and a relatively strong absorption at 2356 cm^{-1} was due to CO_2.

Manganese is the chromophore in pink beryl, and a high-resolution UV-Vis-NIR spectrum showed Mn^{2+}-related broad bands with absorption maxima at 490 and 540 nm (see, e.g., D. L. Wood and K. Nassau, "The characterization of beryl and emerald by visible and infrared absorption spectroscopy," *American Mineralogist*, Vol. 53, 1968, pp. 777–800). A 370 nm band near the spectral cutoff was caused by Fe^{3+}, a common characteristic of beryl. Additional absorption bands were detected at 834, 920, 937, 956, and 978 nm. EDXRF spectroscopy showed the expected Al and Si as major elements, along with minor V, Cs, Fe, Zn,

Figure 12. These morganites were reportedly mined near the town of Shakiso in southern Ethiopia. The large ovals weigh 146.58 and 110.65 ct, and the small oval on the far right is 3.60 ct. Photo by Robert Weldon.

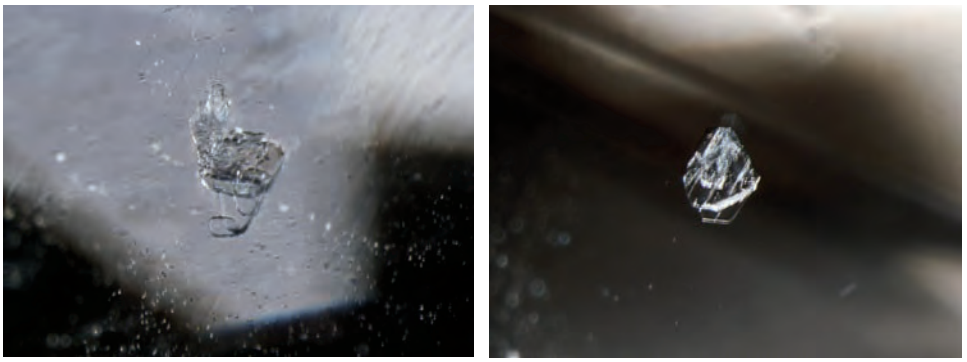

Figure 13. These inclusions, observed in the 2.65 ct morganite, were identified as mica (left, magnified 90×) and plagioclase (right, 110×). Photomicrographs by K. S. Moe.

As, and Rb, and traces of Mn, Ga, and Ti. (For additional photomicrographs and mid-IR and UV-Vis-NIR spectra, see the *G&G* Data Depository at gia.edu/gandg.)

Mr. Rezayee estimated that since 2010, approximately 200–300 kg of the rough Ethiopian morganite have been processed into cabochons and carvings. He also knew of about 1,000 carats that have been faceted in sizes up to ~150 ct. The morganite is reportedly being produced by artisanal miners from the same region of southern Ethiopia that yields emerald, tourmaline, and aquamarine.

Kyaw Soe Moe

Large natural-color freshwater cultured pearls with drilled beads. Since mid-2011, the Gübelin Gem Lab has received several high-quality necklaces and undrilled freshwater cultured pearls (FWCPs) for grading that were near round to round and averaged 12–18 mm. These resembled the "Ming" and "Edison" FWCPs described in recent reports (e.g., H. A. Hänni, "Ming pearls: A new type of cultured pearl from China," *Journal of the Gemmological Association of Hong Kong*, Vol. 32, 2011, pp. 23–25; Spring 2012 GNI, pp. 54–55).

The samples' bodycolor ranged from grayish violet to violet-gray (e.g., figure 15); some displayed strong pink and green overtones. All had a nacreous appearance, either clean or with slight blemishes. Some had a "hammered" effect, while others showed polish lines in the microscope. Each FWCP was inert to UV radiation as well as X-rays.

EDXRF analysis indicated an MnO concentration above 300 ppmw in most of the FWCPs (but as low as ~100 ppm in some samples) and a relatively low SrO concentration (<0.1wt.%). The SrO/MnO ratio of <12 identified them as freshwater products. Unlike the vast majority of FWCPs, which are cultured without a bead, X-radiographs showed nuclei composed of drilled beads (figure 16). Drilled beads have also been used in the cultivation of some Japanese FWCPs (i.e., Kasumiga cultured pearls). The nacre thickness varied from 1.0 to 2.5 mm or more.

UV-Vis-NIR diffuse reflectance spectra revealed bands similar to those observed in some FWCPs from *Hyriopsis sp.* (S. Karampelas et al., "Role of polyenes in the coloration of cultured freshwater pearls," *European Journal of Mineralogy*, Vol. 21, No. 1, 2009, pp. 85–97, http://dx.doi.org/10.1127/0935-1221/2009/0021-1897). Raman (figure 17) and photoluminescence spectra showed bands due to aragonite and polyenic pigments known as parrodienes. Raman spectroscopy also detected vaterite, a $CaCO_3$ polymorph previously reported in some FWCPs with low luster (A. Soldati et al., "Structural characterization and chemical composition of aragonite and vaterite in freshwater cultured pearls," *Mineralogical Magazine*, Vol. 72, No. 2, 2008, pp. 579–592, http://dx.doi.org/10.1180/minmag.2008.072.2.579, and references therein). In these samples, however, the luster was very good.

Figure 14. Various fluid inclusions were found in the morganite samples. Two-phase inclusions containing CO_2 bubbles showed long curved shapes (left, magnified 50×) and hexagonal forms (center, 85×). Also seen were bands of clouds (right, 25×). Photomicrographs by K. S. Moe.

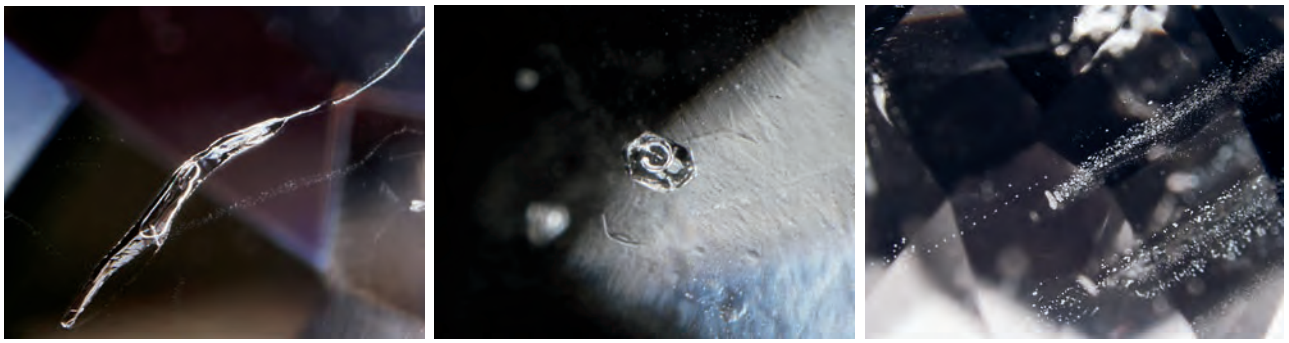

Figure 15. These undrilled violet-gray freshwater cultured pearls contain drilled bead nuclei. The largest measures 15.4 mm. Photo by S. Karampelas.

Some Chinese traders have indicated that such goods are produced from a crossbred mollusk in China that is probably similar to that used for the Kasumiga FWCPs, and their cultivation lasts more than one year and sometimes up to three. They also added that the new large, high-quality Chinese FWCPs can fetch more than US$1,000 per piece, but their supply is still very limited.

Stefanos Karampelas (s.karampelas@gubelingemlab.ch)
Gübelin Gem Lab, Lucerne, Switzerland

Figure 16. Digital X-radiography of one of the cultured pearls in figure 15 reveals a drilled bead 11 mm in diameter, and a nacre thickness of 2.2 mm. Image by S. Karampelas.

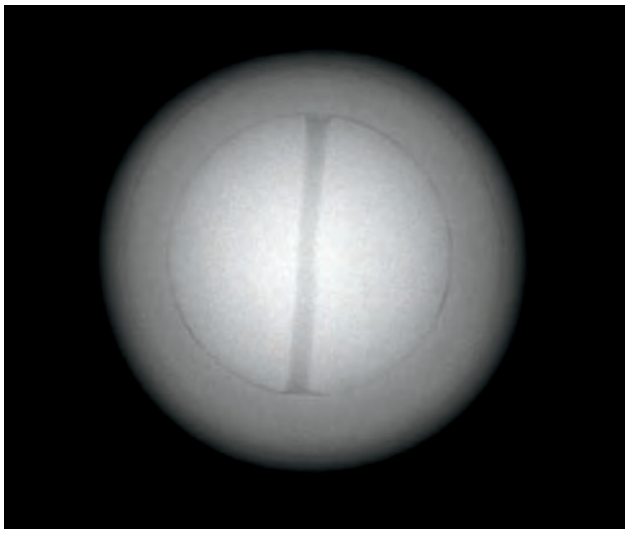

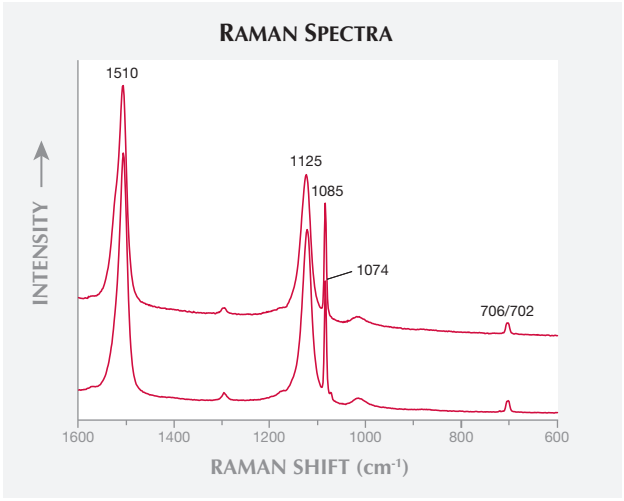

Figure 17. Raman spectra of two FWCPs from 1600 to 600 cm^{-1} (using 514 nm laser excitation) show bands due to simple polyenes at ~1510 and 1125 cm^{-1}. Aragonite bands are present at ~1085 cm^{-1} and at 706/702 cm^{-1} (displayed as a single band at about 704 cm^{-1} due to the resolution). Small features are present at ~1295, 1175, and 1010 cm^{-1}, and an additional small band (probably due to vaterite) is observed in the bottom spectrum at ~1074 cm^{-1}. Spectra are shifted vertically for clarity.

Ruby and sapphire rush near Didy, Madagascar. In April 2012, a gem rush occurred in northeastern Madagascar at coordinates 18°20′16″ S, 48°33′53″ E, located ~25 km south of Didy village, which is situated 50 km south of Ambatondrazaka. The authors investigated the new find on April 18–27.

The rush began after some parcels of fine blue sapphires were sold into the local market in early April in Moramanga, Ambatondrazaka, and subsequently in the capital city of Antananarivo by gold miners and people working for a local logging company in the area. The deposit appears to be situated inside the Ankeniheny–Zahamena corridor, a temporary protected area where mining is not allowed. However, thousands of Malagasy miners and hundreds of buyers rushed to the area, and the government was unable to control illegal mining in this jungle region.

The drive from Ambatondrazaka to Didy was made challenging by patches of deep mud. Soon after our arrival in Didy, we were notified by local security forces that all foreigners had to return to Ambatondrazaka in an effort "not to motivate the local population to work on the illegal mining site." One of us (NR) continued to the mining area. From Didy, the journey started with a three-hour boat trip up a local stream, followed by 10–15 hours' walk through dangerous and dense jungle terrain.

The mining site was inhabited by an estimated 5,000–10,000 people. Miners worked the gem gravels with hand tools in shallow pits (figure 18). The gravels were localized along a stream at a depth of <1 m. Gems were also report-

Figure 18. Malagasy miners dig shallow pits in a streambed surrounded by thick jungle in search of sapphires and rubies. Photo by N. Rakotosaona.

edly found on the adjacent hillside. Most of the production consisted of blue sapphire (figure 19), without any milky or geuda-type material that is commonly found at other Malagasy deposits. The new deposit also was producing orangy pink sapphires and orangy red rubies, often containing some blue areas that are reminiscent of corundum from Winza, Tanzania.

More than 400 foreign buyers (mostly from Sri Lanka) opened buying offices in Ambatondrazaka. Both in that town and in Didy, we saw several clean and attractive blue sapphires weighing up to 4 g, and heard about fine stones approaching 30 g. We also saw some clean orangy red rubies up to 3 g and were told about fine rubies weighing 5 g. Local and foreign gem merchants were excited by the prospect of obtaining this attractive new material, and prices escalated quickly due to fierce competition among the buyers. Several samples are currently being studied by GIA and their gemological properties will be published in the near future.

Figure 19. These sapphires and rubies (up to 2.4 g) were seen in Didy village. Photo by V. Pardieu.

Vincent Pardieu (vpardieu@gia.edu)
GIA, Bangkok

Nirina Rakotosaona
Société Miniére du Cap Ltd., Antananarivo, Madagascar

Marc Noverraz
Colorline Ilakaka Ltd., Ilakaka, Madagascar

Lou Pierre Bryl
Senoble & Bryl Ltd., Gaspe, Canada

Beryllium-bearing nano-inclusions identified in untreated Madagascar sapphire. Cloud-like inclusions are the main cause of the velvety appearance of the famous Kashmir sapphires. Similar cloudy inclusions have also been found in unheated sapphires from Ilakaka (Madagascar) and other localities. The clouds in Ilakaka samples are unusual because they are associated with traces of beryllium (Be), niobium (Nb), and tantalum (Ta), as well as light rare-earth elements and thorium (see, e.g., Fall 2011 Lab Notes, pp. 232–233). The uneven distribution of these elements in unheated sapphires indicates that they have a natural origin (A. Shen et al., "From the GIA Laboratory—Beryllium in corundum: The consequences for blue sapphire," *GIA Insider*, Vol. 9, No. 2, January 26, 2007; and the Lab Note referenced above). Yet the nature of the clouds has never been clear—are they composed of particles of a single mineral phase or an assemblage of minerals?

To identify the phase that contains the trace elements of interest—Be, Nb, and Ta—we studied an unheated rough sapphire from Ilakaka with a flat polished window (figure 20). Analysis with LA-ICP-MS revealed the following composition: Be—from below detection limit (BDL) to 2 ppmw, Nb—from BDL to 3 ppmw, and Ta—from BDL to 1.5 ppmw. The higher Be-Nb-Ta contents corresponded to the cloudy parts of the sample (i.e., the top and bottom areas in figure 20). These areas were then analyzed by a focused-ion beam system and a high-resolution transmission electron microscope (HRTEM) at the GFZ German Research Centre for Geosciences in Potsdam.

TEM study of sapphire inclusions is nothing new. A series of papers was published in the mid-1980s by A. R. Moon and M. R. Philips that examined various inclusions in sapphires from Australia, Sri Lanka, and Thailand. In one of their articles ("Inclusions in sapphire and heat treatment," *Australian Gemmologist*, Vol. 16, No. 5, 1986, pp. 163–166), they identified the inclusions in milky blue Australian sapphires and Sri Lankan "geuda" stones as twinned rutile (TiO_2). Since then, almost every gemological publication has ascribed such milky clouds to rutile.

Our research revealed that the clouds in the Ilakaka sapphire consisted of a single Ti-rich phase that formed nano-inclusions 20–40 nm long and 5–10 nm wide; some of these crystals were twinned. We could not match the diffraction patterns to rutile, however. Instead, we found

Figure 20. This 0.25 g untreated sapphire from Ilakaka, Madagascar, has cloudy areas containing traces of Be, Nb, and Ta. Photo by Shane F. McClure.

an excellent match with an unnamed high-pressure mineral that has the same composition as rutile but has the crystal structure of scrutinyite (α-PbO_2). While rutile is a tetragonal mineral, this unnamed phase is orthorhombic with the Ti and O atoms arranged in the same way as the Pb and O in scrutinyite.

This unnamed mineral was first identified in laboratory studies when scientists subjected pure TiO_2 to very high pressures. It was later found in other Ti-bearing minerals (such as garnets) as nano-inclusions. Because it occurs in extremely small sizes in nature, it has not been approved as a new mineral by the International Mineralogical Association's Commission on New Minerals, Nomenclature and Classification.

Further details of this study will be documented in a future article.

Andy H. Shen (andy.shen@gia.edu)
GIA, Carlsbad

Richard Wirth
GFZ German Research Centre for Geosciences
Potsdam, Germany

Blue sapphire discovery near Kataragama, Sri Lanka. In February 2012, Shamil and Armil Sammoon of Sapphire Cutters Ltd. (Colombo, Sri Lanka) informed GIA's Bangkok laboratory about a new find of blue sapphires in the Thammannawa area located southwest of Kataragama, near the Yala National Park on the southeastern coast of Sri Lanka. The stones were reportedly discovered on February 14, on a road construction site between Kataragama and Lunugamwehera. The soil used to cover the road reportedly came from a small farm nearby that belonged to a Mr. Ranga. As news of the discovery spread, thousands rushed to the area. The Sri Lankan authorities responded swiftly and secured the site within days, transferring 1.4 hectares of land around Mr. Ranga's farm from the Forest Conservation Department to the National Gem & Jewellery Authority (NGJA). The NGJA organized a February 24 auction in Kataragama for one-year mining rights on 49 individual lots. According to the NGJA's chairman, 40% of the proceeds from that auction will be given to the landowners.

In early March, with the support of the NGJA and some local traders, these authors visited the sites to collect samples for the GIA reference collection. Upon reaching the deposit, located at 06°22′16″N, 81°17′18″E, we saw that it was being prepared to host an estimated 500 miners. Within hours the miners began arriving at their claims, and camps sprang up from the cleared land (figure 21). Miners loaded the potentially sapphire-rich soil into bags to be taken away for washing. Only hand tools were allowed at that time (figure 22), as mechanized mining with excavators was prohibited in Sri Lanka. Subsequently, in mid-2012, mechanized mining was permitted at the deposit.

At the time our expedition ended on March 9, we were unable to see any sapphires produced from the new diggings around Mr. Ranga's house. However, we studied numerous samples obtained from local people that reportedly were found at the road construction site. The sapphires occurred as fine crystal specimens or broken pieces with sharp edges and no indication of alluvial transport (e.g., figure 23). Fissures and cavities were filled with a white powdery material.

The sapphires from the new find are notable for their size. We saw several specimens up to 150 g and heard reports of fine crystals as large as 300 g. Unfortunately, the material often contained numerous fissures as well as graphite, mica, and feldspar-like inclusions. Nevertheless, highly transparent areas were visible in the pieces exam-

Figure 21. This view shows a portion of the potentially sapphire-bearing area auctioned in 52 lots by Sri Lankan authorities. Photo by V. Pardieu.

Figure 22. Sri Lankan miners work the sapphire deposit with hand tools. Photo by V. Pardieu.

ined, and we expect to see clean faceted gems weighing more than 20 ct. Many of the crystals showed distinct color banding (with strong blue-violet to blue-green dichroism) associated with layers of minute particles. Several gem merchants onsite were excited by such Kashmir or Burma-like new material, and at the time of our visit the asking prices were already remarkably high.

Overall, the external appearance of these sapphires is similar to those from Andranondambo (Madagascar), Avisawella (Sri Lanka), and Kashmir, but preliminary chemical analyses have shown that their iron content is higher. So far relatively few faceted stones from this deposit have appeared in the market (again, see figure 23), and we expect that the combination of dichroism, color banding, and limited transparent areas will present challenges to cutters. More information on this new deposit and the properties of these sapphires is available at gia.edu/research-resources/news-from-research.

[*Editor's note*: See a full article on this deposit on pp. 98–107 of this issue of *G&G*.]

Vincent Pardieu and Lou Pierre Bryl

Andrea Heather Go
Vancouver, Canada

Sapphire and ruby carvings from Vietnam. At the 2012 Tucson gem shows, Steve Ulatowski had some sapphire carvings that were notable for their detailed forms and well-executed polish. His supplier indicated that about 20 carvings per month have been produced in mid-2011 by four carvers in a small factory in Vietnam. Of the approximately 210 carvings that have been completed, most consist of opaque blue, pink, white, or dark gray sapphires (or combinations of these colors; figure 24) that were mined from various parts of Vietnam. Some of the pieces show asterism. Rubies from Thailand and Tanzania (Longido) have also been carved. The carvings feature Asian themes and deities, and range from 2 to 10 cm tall.

Although such figurines are typically carved from jade and other (softer) materials, the very good polish covering the complex curves and depressions is notable for carvings made of corundum.

Brendan M. Laurs

Figure 23. These rough and cut sapphires are reportedly from the new Kataragama deposit. The faceted stone weighs 14 ct, and the crystal fragments weigh 4.4 and 5.4 g. Photo by V. Pardieu.

Figure 24. These Vietnamese sapphire carvings range from 4.6 × 5.0 cm to 7.4 × 3.9 cm in dimension. Photo by Robert Weldon.

Figure 25. Calibrated zoisites from Merelani, Tanzania, display a variety of colors. The loose stones are 4.5 mm in diameter (gift of Steve Ulatowski; GIA Collection no. 38497) and the pendant contains 5.5 mm zoisites that are set with diamonds. Photo by Robert Weldon.

Color suites of zoisite from Tanzania. The mines at Merelani, Tanzania, are world famous for being the world's only commercial source of tanzanite, as well as supplying a variety of other gems and minerals (see, e.g., W. E. Wilson et al., "Famous mineral localities: The Merelani tanzanite mines, Lelatema Mountains, Arusha region, Tanzania," *Mineralogical Record*, Vol. 40, No. 5, pp. 346–408). Other colors of zoisite are occasionally produced and find their way to the market as cut stones that are popular with gem collectors (e.g., D. M. Dirlam et al., "Gem wealth of Tanzania," Summer 1992 *G&G*, Vol. 28, No. 2, pp. 80–102). At the 2012 Tucson gem shows, Steve Ulatowski had calibrated sets of Merelani zoisite that were prepared specifically for jewelry use. The round brilliants (figure 25) were assembled into boxed sets consisting of a variety of colors, all untreated, in singular sizes ranging from 2 to 5 mm in diameter. Each box contained from 8 to 40 stones. The material was cut from smaller-sized rough that he had gathered over the past five years, and he has cut enough to produce 100 boxes.

Mr. Ulatowski also had a few jewelry pieces that showcased the color spectrum of these zoisites (again, see figure 25).

Brendan M. Laurs

SYNTHETICS AND SIMULANTS

Partially devitrified glass imitation of hemimorphite. In mid-2010, GIA was informed about an attractive new blue-to-green gem by Brad Payne (The Gem Trader, Cave Creek, Arizona). He had obtained some samples of the material at a local gem show, where they were represented as opalized hemimorphite. Reportedly 1,000–2,000 carats of cabochons had entered the market from Chinese fossil dealers. Mr. Payne was intrigued by the white snowflake-like inclusions in this material, as well as the color zoning shown by some of the pieces, and he loaned four samples to GIA for examination.

The cabochons weighed 10.55–31.99 ct, and were greenish blue except for two samples that ranged into yellowish green (figure 26). Microscopic examination revealed radiating clusters of fine blade-like crystals that formed a fibrous texture, along with randomly distributed clusters of white dendritic inclusions. Spot RI values were 1.50–1.51, and the hydrostatic SG ranged from 2.48 to 2.52. By contrast, hemimorphite has RIs of 1.614–1.636 and an SG of 3.45 ± 0.05. When exposed to short-wave UV radiation, the samples fluoresced very weak chalky blue and greenish yellow to pale green; they were inert to long-wave UV. No absorption lines were visible with a desk-model spectroscope. These properties ruled out the possibility of hemimorphite, but were suggestive of partially devitrified glass, which was confirmed by Raman analysis. EDXRF spectroscopy showed major amounts of Cu, Ca, Si, and Fe, and traces of Sn, Zr, and Cr.

Partially devitrified glasses are more commonly seen imitating jade (e.g., "Meta Jade"; see Summer 1995 GNI, p. 137). However, as these specimens demonstrate, we are now seeing imitations manufactured to replicate even the more obscure gem materials.

Jason Darley (jdarley@gia.edu) and Erica Emerson
GIA, New York

Figure 26. These partially devitrified glass samples (10.55–31.99 ct) were sold as opalized hemimorphite. The largest sample is a gift of Brad Payne; GIA Collection no. 38519. Photo by Brad Payne.

Figure 27. This 22.99 ct purplish pink bead resembled rubellite tourmaline but was identified as coated quartz. Photo by G. Choudhary.

Coated quartz imitation of rubellite tourmaline. Coating is one of the most common treatments performed on gemstones, especially on colorless materials such as rock crystal and topaz. Iridescent coating has become particularly popular among jewelers, designers, and consumers alike. In addition to this advanced coating method, traditional forms still exist, not only to create unusual material but also to imitate well-known gems such as emerald (see Spring 2011 GNI, pp. 71–72). A similar imitation of rubellite tourmaline (figure 27) was brought to our attention by Kashish Sachdeva during the Jaipur Jewellery Show in December 2011.

The purplish pink sample, fashioned as a tumbled bead, weighed 22.99 ct and measured approximately 21.41 × 15.39 × 11.29 mm. The bead's color initially suggested rubellite tourmaline, but its relatively dull luster raised some suspicion of a coating. To the unaided eye, no features associated with coatings were visible. We then viewed it with a microscope, particularly around the drill hole, which is the best place to find chipped-off areas in a coated specimen. No chipping was seen; rather, some abrasions typical of natural stones were observed (figure 28). These features seemed to eliminate the possibility of a coating. However, the bead did display some large internal films with a brownish epigenetic appearance, and it lacked the growth tubes and liquid reflecting films typically associated with tourmaline (although some crystalline and fluid inclusions were present). These observations prompted us to conduct further testing.

Figure 28. No chipping of the coloration was seen around the drill holes of the bead, making it quite difficult to detect the coating. Photomicrograph by G. Choudhary; magnified 20×.

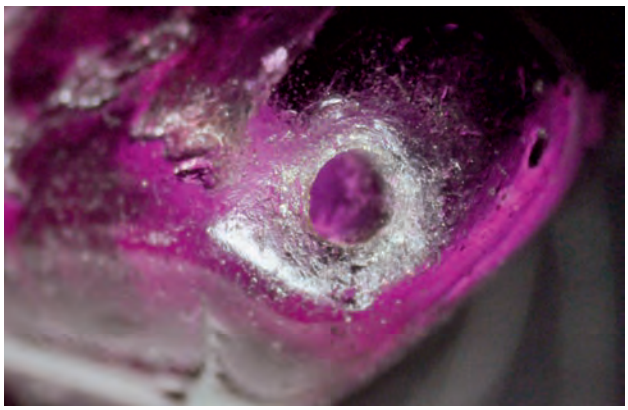

The stone displayed a vague shadow edge at ~1.54 on the refractometer and had a hydrostatic SG of 2.60. It gave a weak orange reaction to short-wave UV radiation and was inert to long-wave UV. With the desk-model spectroscope, it displayed two strong bands in the yellow and red regions at ~580 and 650 nm; a weaker band was also visible at ~540 nm in the green region. This absorption pattern is associated with red and blue dyes, and the combination of gemological properties ruled out tourmaline and suggested artificially colored quartz instead.

Further microscopic examination with transmitted light revealed color bleeding and blotchiness near some pits and cavities (figure 29, left), evidence of surface-related artificial coloration. Also seen were some tiny blue and orangy red spots from the dye (figure 29, right), indicating that a combination of these colors was used to produce the purplish pink coating substance. These colored spots appeared to be confined to the surface, another sign of coating.

The sample was confirmed as quartz by infrared spectroscopy, which also showed polymer-related bands at ~3070, 2958, 2927, 2858, 1750, and 1270 cm^{-1}. Such imitations are a concern for dealers who are equipped only with a loupe, especially when they have to make quick buying decisions.

Gagan Choudhary (gagan@gjepcindia.com)
Gem Testing Laboratory, Jaipur, India

CONFERENCE REPORTS

10th Annual Sinkankas Symposium—Topaz. Co-hosted by GIA and the San Diego Mineral and Gem Society, this annual symposium in honor of John Sinkankas took place April 21, 2012, at GIA in Carlsbad. This year's event featured topaz, and was attended by 124 people. Each attendee received an 88 pp. handout with presentation summaries as well as outside contributions; additional copies are available for $20 plus shipping from convener **Roger Merk** (Merk's Jade, San Diego, California; merksjade@cox.net).

Dr. Don Hoover (Springfield, Missouri) reviewed historical references to topaz in the literature. Many, but not all, references to topaz in the ancient texts actually refer to peridot from Zabargad Island (Egypt). The first actual topaz locality documented in the literature was probably the Saxony region of Germany, where yellow crystals were produced in conjunction with tin mining. **Robert Weldon** (GIA, Carlsbad) described how *bandeirantes* (Portuguese

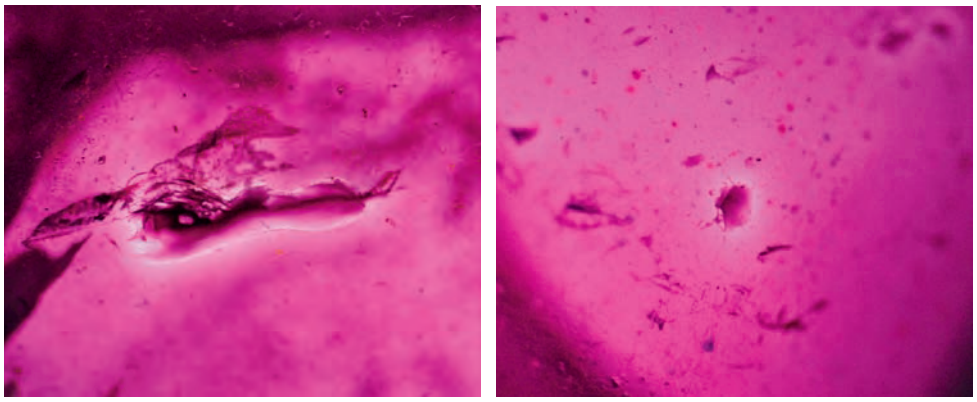

Figure 29. A few cavities on the coated quartz displayed color bleeding and blotchiness, suggesting surface-related artificial coloration (left, magnified 45×). Orangy red and blue spots from the dye showed that these colors were used in the purplish pink coating (right, 60×). Photomicrographs by G. Choudhary.

explorers) helped locate various gems in Brazil during the 1600s, which eventually led to the important discovery of the Imperial topaz deposits near Ouro Preto.

Dr. James Shigley (GIA, Carlsbad) covered the geology and localities of topaz deposits, which can be classified into magmatic, hydrothermal, and pneumatolytic types, and he offered to send a complete reference list of localities to anyone who requests it. **Dr. William "Skip" Simmons** (University of New Orleans) focused on crystal structure and mineralogy. Natural topaz shows a limited substitution of OH for F, and nearly all specimens are therefore fluorine dominant. Small amounts of Cr^{3+} and Fe^{3+} may substitute for Al^{3+} in the mineral's structure. The causes of coloration in topaz were reviewed by **Dr. George Rossman** (California Institute of Technology, Pasadena). While pink is the only easily explained color (due to Cr^{3+}), brown, yellow-to-red, and blue colors involve exposure to radiation (natural or in the laboratory), but there is no consensus on the particular mechanisms involved.

Important sources of collectable-quality topaz were described by **Bill Larson** (Palagems.com, Fallbrook, California). These include Brazil (Ouro Preto and Teófilo Otoni), California (San Diego County), Nevada (Zapot mine), Idaho (Sawtooth Mountains), Namibia (Klein Spitzkoppe), Pakistan (Gilgit-Skardu area), and Myanmar (Sakhangyi). **Meg Berry** (Mega Gem, Fallbrook, California) examined the carving topaz. In light of the mineral's perfect cleavage direction, she suggested polishing at an orientation of at least 5° from this plane, using Linde A on a tin lap. However, for an attractive frosted look, carvings can be finished with 260 grit diamond (mixed with Vaseline) on a felt wheel; this will also save a lot of polishing time.

Shane McClure (GIA, Carlsbad) covered topaz treatments, which can be classified into irradiation ± heating, coating, and possibly diffusion. The latter treatment has been used to produce blue-to-green color but is difficult to classify since the coloration is associated with Co impurities that only penetrate 50–100 nm into the stone. Microscopic features of topaz were discussed by **John Koivula** (GIA, Carlsbad), including fluid and mineral inclusions, structural irregularities, and surface (dissolution) features. He showed a specimen of topaz containing an inclusion of monazite with an associated cleavage disc that was particularly impressive for its size and beauty.

The theme of next year's Sinkankas symposium will be ruby.

Brendan M. Laurs

MISCELLANEOUS

Myanmar Gem Emporium and GEO Myanmar 2012. The 49th annual Myanma Jade, Gems & Pearl Emporium's first session for 2012 was held March 9–18 in the capital city of Naypyidaw. According to China's Xinhua News Agency, sales totaled $702.66 million, a sharp decline from the March 2011 session's earnings of $2.8 billion. The event was attended by some 6,000 gem traders, half of them from other countries throughout Asia. In all, 9,762 Burmese jade lots were sold through tender or bidding, as well as 227 gem lots and 8,367 lots of cultured pearls from Myanmar.

The emporium's mid-year session will take place in July, followed by a third sale at the end of the year. In total, the 2011 emporium took in more than $4 billion.

The GEO Myanmar 2012 conference was held on March 1–2 in Yangon. Three of the presentations pertained to gems: "The economic impact in treating Myanmar gemstones" by Ted Themelis, "Prediction of exploration target areas for gem deposits in Mogok Stone Tract by integrating remote sensing and geoscience data" by Tin Ko Oo, and "Geological characteristics of ruby from Myanmar and Thailand" by Y. Ahn et al.

U Tin Hlaing
Dept. of Geology (retired)
Panglong University, Myanmar

ERRATUM

Page 21 of the Spring 2012 article by J. E. Shigley et al. on Diamantine incorrectly reported the beam diameter of the SIMS analyses. The correct diameter is 50 µm.

The Book Reviews and Gemological Abstracts sections appear in the online version of the journal. Below are the titles of the books and articles reviewed, with the reviewer's name indicated in brackets. These sections are freely available on the *G&G* website (gia.edu/gandg) and as part of *G&G* Online (gia.metapress.com), and are paginated separately from the rest of the issue.

Book Reviews

Cartier at Prague Castle: The Power of Style. By the Prague Castle Administration, 2010 [*Delphine Leblanc*]

Lapis Lazuli: In Pursuit of a Celestial Stone. By Sarah Searight, 2010 [*Matilde Parente*]

Russian Alexandrites. By Karl Schmetzer, 2010 [*Lee A. Groat*]

Sacred and Symbolic: Ancient India and the Lure of Its Diamonds. By Hugh Durey, 2010 [*A. J .A. "Bram" Janse*]

Understanding Rough Gemstones. By Shyamala Fernandes and Gagan Choudhary, 2010 [*Edward Boehm*]

Gemological Abstracts

COLORED STONES AND ORGANIC MATERIALS

Epochs of the formation of amber and its distribution in nature. By A. V. Ivanova et al. [*Guy Lalous**]

Genesi delle agate (II parte) [The formation of agates (Part II)]. By M. C. Venuti [*Rolf Tatje**]

Molecular structure of the phosphate mineral brazilianite $NaAl_3(PO_4)_2(OH)_4$ – A semiprecious jewel. By R. L. Frost and Y. F. Xi [*James E. Shigley**]

Le point sur les perles de culture Première partie – Les perles d'eau de mer [Status quo of cultured pearls. Part 1 – Saltwater pearls]. By E. Strack [*Rolf Tatje**]

DIAMONDS

An analysis of vacancy clusters and sp^2 bonding in natural type IIa diamond using aberration corrected STEM and EELS. By I. S. Godfrey and U. Bangert [*James E. Shigley**]

Boron in natural type IIb blue diamonds: Chemical and spectroscopic measurements. By E. Gaillou et al. [*James E. Shigley**]

A comparison of modern diamond classifications. By M. A. Viktorov [*Jennifer Stone-Sundberg**]

Placer diamond potential of the Siberian craton: Possible sources and ages. By V. P. Afanasiev et al. [*James E. Shigley**]

Plastic deformation of natural diamonds by twinning: Evidence from X-ray diffraction studies. By S. V. Titkov et al. [*James E. Shigley**]

Trace element analysis of rough diamond by LA-ICP-MS: A case of source discrimination? By C. Dalpé et al. [*Guy Lalous**]

GEM LOCALITIES

Alexandrites from the Novello alexandrite-emerald deposit, Masvingo District, Zimbabwe. By K. Schmetzer et al. [*Edward R. Blomgren**]

Beryl from deposits of the Ural Emerald Belt, Russia: ICP-MS-LA and infrared spectroscopy study. By A. S. Bindy et al. [*Kyaw Soe Moe**]

Cause chimiche delle variazioni di colore degli zaffiri di Rathnapura (Sri Lanka) [Chemical causes of color variations in the sapphires from Ratnapura, Sri Lanka]. By F. M. Oltean et al. [*Rolf Tatje**]

Gem-quality Turkish purple jade: Geological and mineralogical characteristics. By M. Hatipoglu et al. [*Keith A. Mychaluk**]

The 'hill of the precious stones', Rattanak Kiri, Cambodia. By F. Payette and G. Pearson [*Edward R. Blomgren**]

Micro-Raman spectroscopy of gem-quality chrysoprase from the Biga-Çanakkale region of Turkey. By M. Hatipoğlu et al. [*Guy Lalous**]

New ruby discovery in Zimbabwe. By F. Marsh and F. Mugumbate [*James E. Shigley**]

The origin of black colouration in onyx agate from Mali. By J. Götze et al. [*James E. Shigley**]

Sequential opening and filling of cavities forming vesicles, amygdales and giant amethyst geodes in lavas from the southern Paraná volcanic province, Brazil and Uruguay. By L. A. Hartmann et al. [*Keith A. Mychaluk**]

INSTRUMENTS AND TECHNIQUES

Measurement and interpretation of growth patterns in chrysoberyl, including alexandrite. By K. Schmetzer [*James E. Shigley**]

Powder diffraction analysis of gemstone inclusions. By L. Leon-Reina et al. [*Guy Lalous**]

Una tecnica per fotografare le inclusioni nelle gemme [A method for the photography of inclusions in gemstones]. By M. Pantò [*Rolf Tatje**]

SYNTHETICS AND SIMULANTS

Diamant synthétique HPHT traité rose [Pink HPHT treated synthetic diamonds]. By J.-M. Arlabosse [*Rolf Tatje**]

Identifizierungshilfe zur Unterscheidung zwischen natürlichen und synthetischen (HPHT) gelben, gelb-braunen und rötlich-braunen Diamanten [Identification aid for distinguishing natural and synthetic (HPHT) yellow, yellow-brown and reddish-brown diamonds]. By M. Seubert [*Rolf Tatje**]

TREATMENTS

Comparative study of different types of filled rubies. By L. Jianjun et al. [*Edward R. Blomgren**]

Neue künstlich geritzte Sternsteine und ihre natürlichen Gegenstücke [New artificially scratched star stones and their natural counterparts]. By M. P. Steinbach [*Rolf Tatje**]

MISCELLANEOUS

Diamonds: A good deal for Zimbabwe? By Global Witness [*Edward Johnson**]

Poverty and livelihood diversification in rural Liberia: Exploring the linkages between artisanal diamond mining and smallholder rice production. By G. Hilson and S. van Bockstael [*Russell Shor**]

Resource curse in reverse: How civil wars influence natural resource productions. By S. McLaughlin and C. G. Thies [*Russell Shor**]

Transnational entrepreneurs, global pipelines and shifting production patterns. The example of the Palanpuris in the diamond sector. By S. Henn [*Russell Shor**]

---

* *Member of the Gemological Abstracts Review Board*

G&G Online
Book Reviews

EDITORS
Susan B. Johnson
Jana E. Miyahira-Smith

Cartier at Prague Castle: The Power of Style

By the Prague Castle Administration, 322 pp., illus., publ. by Flammarion, Paris, 2010. US$49.95.

This impressive exhibition catalogue was created for a celebration at the Prague Castle from July to October 2010. Curated by Eva Eisler, the unique exhibition of more than 400 objects included some of the most iconic pieces amassed since the early 1970s for the Cartier Collection.

The reader is taken on a fascinating journey in the style of the red box jeweler. Eisler's opening chapter notes how the exhibition was built on a relationship between the chronology and the aesthetics of the jewelry presented. Next, Pierre Rainero traces the ascendance of Cartier from its humble beginnings as a workshop of novelty dealers in the heart of 1847 Paris to a powerful luxury brand that has maintained its international status on the cutting edge of fashion and the jewelry industry. After a brief chapter by Rony Pesl on the design of the exhibit, the reader delves into the book's core chapters, starting with Pascale Lepeu's overview of the Cartier Collection of 1,400 objects assembled to celebrate the firm's history and craftsmanship. This chapter provides interesting insights into the acquisition of some of the featured pieces, with detailed archival documentation that further enhances the collection's value. The following chapters, which chronologically unveil the jewelry presented in the exhibit, are of the utmost interest for jewelry historians and Cartier aficionados.

Richly illustrated with archival photos and documents, "Jewelers to Kings: The Reign of Diamonds" depicts early Cartier jewels, from gold, silver, and diamond brooches to the first platinum and diamond pieces in the purest "garland" style at the turn of the 20th century. Two of the most memorable specimens in this chapter are a platinum, diamond, and pearl Kokoshnik tiara, designed in 1908, and a double fern-spray brooch.

"Avant-Garde and Art Deco" portrays the transition from a monochromatic classic garland style to Art Deco jewelry. Cartier achieved this transition by introducing onyx into their creations to give them more contrast and intensity. In 1915, Cartier began creating what was to become part of their signature look, a panther motif set with diamond and onyx to adorn a delicate watch-brooch. The use of transparent elements such as rock crystal also allowed the design of sizeable fashionable brooches.

Following the initiation of French Art Décos design, the reader is introduced to more exotic designs of the 1920s, when the zeitgeist demanded more color. Inspiration came from archeological discoveries—notably Egyptian (scarab brooches, including genuine antique blue faience)—as well as the accessibility of travel to Asia and the influence of royal Indian creations. In this genre, a most magnificent example was the restoration of a ceremonial necklace created for the Maharajah of Patiala. The original included sizeable diamonds provided by the Maharajah himself. The dismantled necklace, discovered in London, was patiently restored by Cartier, using cubic zirconia, rubies, and smoky quartz to replace some of the more precious stones.

In the "New Modernity" chapter, the catalog presents jewelry from the 1930s to the 1970s. The most stunning pieces include a pair of rock crystal and diamond "Gloria Swanson" bracelets designed in 1930, and an amethyst, turquoise, and diamond bib necklace designed for Wallis Simpson in 1947. During this period, Cartier's jewelry became more voluminous and colorful.

Cartier has always been known for distinctive "Flora and Fauna"–inspired designs. Although the panther is one of its most popular motifs, snakes, birds, and even crocodiles are masterfully represented. Two of the most remarkable examples in the chapter are a pair of articulated yellow diamond, emerald, and enamel tiger motif ear clips sold to Barbara Hutton, and a realistic yellow diamond, ruby, and emerald double-crocodile necklace that was custom made for the Mexican actress Maria Felix.

From the beginning, Cartier has drawn upon eclectic tastes to create noteworthy timepieces, ranging from early pocket watches to supremely elegant ladies' wristwatches from the 1930s. The most interesting pieces displayed in this section are Model A "Mystery Clocks" from 1912, so called because the platinum and diamond hands do not appear to be linked to any mechanical movement. Some objects shown in this section, such as a semispherical clock built around a Persian ceramic miniature, exemplify Cartier's flair for reviving antiquities.

One of this catalog's main assets is the detail of its photos. Their definition is so fine that the reader can almost count each diamond on a given jewelry piece, determine the type of setting, or estimate the size of a diamond's culet. The photos, which vary in scale, are consistent in their definition and carefully annotated with brief descriptions, measurements, and provenance whenever possible. Jewelry sketches have rarely been depicted with the precision displayed in this book. Like the photos, they are lighted from the upper left, the traditional format in jewelry rendering.

The superb quality of the collection displayed at the Prague Castle makes this catalog a real must-have for jewelers, appraisers, and jewelry professionals who want to fully appreciate Cartier's style from the early

Belle Époque to the most contemporary creations.

DELPHINE A. LEBLANC
Hoboken, New Jersey

Lapis Lazuli: In Pursuit of a Celestial Stone

By Sarah Searight, 228 pp., softcover, illus., publ. by East and West Publishing Ltd., London, 2010. US$42.00.

This book chronicles a love affair between author Sarah Searight and lapis lazuli, sparked in childhood by a passage in a Robert Browning poem. Searight follows her passion for lapis from Central Asia's remote mountains to global, multicultural renown.

A journalist and historian, Searight has lived much of her life in Asia and the Middle East, the latter region the subject of her previous books. To appreciate the author's obsession, the reader may need to disassociate the recent troubles of this region from the starry-sky object of the author's ardor. She terms it an eccentric pursuit, and that it is.

The book is divided into two major parts. Searight begins in the East, recounting her travels to isolated mines where imperiled workers extract the brilliant blue rock from its mountainous sanctuary, thus beginning its long and difficult journey to market. An accompanying map helps readers follow the convoluted journey lapis takes from Badakhshan across the ethnic tapestry of ancient Mesopotamia to modern-day Central Asian republics of Afghanistan, Tajikistan, Pakistan, Iran, and Iraq, and later to Siberia.

Lapis may technically be a rock, but its magic is all gemstone. Its golden pyrite glimmer against a sea of deep blue lazurite was often interpreted as combining the power of the sun and heavens with the depth and vital force of the sea. Searight recounts the stone's use in embroidery and adornment, believed to impart good fortune and protection towards safe passage. Later on, in chapters that explore Western journeys taken by lapis, Searight describes its use as a pigment, the magnificent ultramarine. Readers will be entertained by pages devoted to lapis-robed Madonnas in Renaissance painting and the gem's use in multicolored inlay as pietra dura.

The book's 168 mostly color plates portray relics, cave paintings, images from the author's travels, and pieces from varied collections. These are interspersed with images of the barren regions where lapis has been mined for more than 6,000 years. A photo of the author, a lone woman in a Peshawar lapis workshop, speaks volumes about Searight's passion and an era of travel that may have closed to all but the most daring. The range of images paints a picture as telling as the text of a gem worthy of obsession, and one of historic and multicultural depth.

While the author interweaves her travels and observations with serpentine backtracks through rulers and historical events with ease, the reader may find these meanderings and asides less than fluid. Despite its tangents, the book may fulfill the curiosity of those seeking to understand the historical importance of lapis, and will reward patient lapis enthusiasts who share the author's passion for this ancient and mysterious stone.

MATILDE PARENTE
Libertine
Indian Wells, California

Russian Alexandrites

By Karl Schmetzer, with contributions from George Bosshart, Marina Epelboym, Lore Kiefert, and Anna-Kathrin Malsy, 141 pp., illus., publ. by Schweizerbart Science Publishers, Stuttgart, Germany, 2010. US$49.90.

Alexandrite, a gem variety of the mineral chrysoberyl, is much sought after because of the distinct color change it exhibits between daylight and incandescent light. The rarity of gem-quality alexandrite leads many observers to consider it as important as diamond, ruby, sapphire, and emerald. It is also regarded as the national gemstone of Russia. In this fascinating and comprehensive book, Dr. Karl Schmetzer and contributors present an overview of alexandrite mining in Russia's Ural Mountains, the naming and historical use of the gem, its characteristics, and its importance in the gem trade.

The author points out that alexandrite has been mined since about 1833 and was named for young Alexander Nikolaevich (later Czar Alexander III, 1855–1881). Here he reproduces the first scientific publication on the gem and traces the history of two extraordinary samples, the Leuchtenberg emerald druse and Kochubei's druse.

Chapter 5 reviews morphology and twinning. Dr. Schmetzer notes that most alexandrites occur as repeatedly twinned crystals with pseudohexagonal dipyramidal habits. As is typical of the book, this chapter features beautiful diagrams and photos of real-world examples.

The chapter on mineralogical and gemological properties includes lengthy sections on structural properties (twinning and growth structures) and mineral and fluid inclusions in faceted stones. The majority of the mineral inclusions have been identified by Raman spectroscopy as phlogopite, while fluorite and apatite crystals were identified in a few samples. The chapter concludes with a section on mineral assemblages, growth conditions, and growth sequences. As the author notes, various studies have shown that the main occurrences of alexandrite are within emerald-bearing ore bodies, also known as *glimmerites*, in which it is possible to deduce two stages of alexandrite crystallization. In the first stage, emerald and alexandrite formed within mica schist or a phlogopite-rich host rock. In the second stage, additional emerald and alexandrite crystallized, along with plagioclase.

Subsequent chapters present chatoyant alexandrite, growth patterns, colorimetric data, and trace-element chemical composition (as determined by LA-ICP-MS), and locality determination. Chemical analyses show that alexandrite from Russia's Tokovaya mines can be distinguished on the basis of its chromophores (V, Cr, Fe) and its B, Ga, Ge, Sn, and Ta contents.

The appendix contains eight tables of information on such topics as morphological properties of Russian alexandrites, characteristic angles observed in Sri Lankan material from faces of the [001] zone, properties of Czochralski-grown synthetic alexandrite, colorimetric parameters of alexandrite and chrysoberyl from the Urals, and trace-element and ultra–trace element contents of alexandrite and "green chrysoberyls" obtained by LA-ICP-MS.

In general, the book is comprehensive and the writing and illustrations are clear and understandable. My complaints are few. The quality of some photos is less than ideal, and the tables would probably be better placed in the body text rather than in an appendix. Overall, though, this is a superb publication that belongs on the desk of anyone interested in alexandrite, emerald, chrysoberyl, and the history of Russian gem mining.

LEE A. GROAT
University of British Columbia
Vancouver

Sacred & Symbolic: Ancient India and the Lure of Its Diamonds

By Hugh Durey, 190 pp., illus., publ. by the author, www.hughdurey.com, 2010. US$79.00.

This is not your usual glib coffee-table book, but an interesting account of Indian history as displayed in monuments, friezes, ornaments, and jewelry. The author is a diamond exploration geologist who became fascinated by the cultural images he saw while working in India. He traveled throughout the land to relate these images to what he had read about India's history and merge them into a comprehensive account.

The main text is a straightforward account of India's cultural history, accompanied by a personal travelogue in the margin. The author portrays the complexities of ancient and medieval India by discussing how religion and life were intricately linked with gemstones, which were considered a medium between man and his gods. They were used to invoke deities and render harmony and well-being to the individual. In India, Hinduism, Buddhism, Jainism, Judaism, and Islam have all contributed to the story of diamonds.

The narrative is very well illustrated by pertinent photographs. The earliest description of a crystal known to be diamond dates from the beginning of the 4th century BCE, but the gem's use as an ornamental or sacred object may reach as far back as 1,000 BCE. There is also evidence of much earlier use as an abrasive or drilling tool. The last two chapters take us into more recent times, with descriptions of the only active diamond pipe mine (near Panna) and the Krishna River alluvial deposits, from which the famous "Golconda" diamonds were recovered. These include the Darya-i-Nur, Koh-i-Noor, Hope, Regent, Orlov, and Sancy diamonds.

Modern India is the world's most prolific nation in diamond cutting and polishing, employing up to one million people, as the link with diamonds endures. This stimulating book is well worth the attention of gemologists, art lovers, and those interested in Indian cultural history.

A. J. A. (BRAM) JANSE
Archon Exploration
Carine, Western Australia

Understanding Rough Gemstones

By Shyamala Fernandes and Gagan Choudhary, 213 pp., illus., publ. by the Indian Institute of Jewellery, Mumbai, 2010. US$25.00.

Understanding Rough Gemstones deftly combines concepts from mineralogy with gemology to show the reader how to employ gemological skills, keen observation, and logical deduction to identify rough. Authors Shyamala Fernandes and Gagan Choudhary have filled a critical void by publishing the first book to address the identification of rough gem materials.

Their passion for the subject of rough and cut gemstones is conveyed throughout the entire work. Eight chapters cover the geographic location of gems, the various species, simulants, crystallography, physical and optical properties, synthetics, enhancements, and gemological properties. The volume ends with a delightfully accurate insight into the rough gemstone trade, using actual examples. Numerous photos, diagrams, and charts reinforce these concepts. Unfortunately, most of the photos are thumbnail size, making it difficult to distinguish the crystal habits and details in the inclusion shots. This reviewer would also like to have seen more photos of typical inclusions for specific gem materials, since these features are often the only identifying characteristic when examining rough. The chapter titled "Ready Reference Tabulations" is full of useful and detailed data, ranging from chemical formulas and crystal systems to gemological properties and typical inclusions. It even includes a useful list of Hindi terms to consult when conversing with Indian rough traders or miners.

Whether buying at the mine, in a dealer's office, or at a trade show, understanding how to apply field knowledge is critical to any purchase of rough or cut gems. This work shows that many gemological concepts can be applied to the identification of rough material as well. To properly identify rough, however, it is essential to be able to combine gemological properties with mineralogical knowledge. Therefore, a basic knowledge of gemology and mineralogy is highly recommended to get the most benefit from this book. Fernandes and Choudhary wonderfully combine the principles of both disciplines to help the reader navigate the challenging world of gem rough.

EDWARD BOEHM
RareSource
Chattanooga, Tennessee

EDITOR

Brendan M. Laurs
GIA, Carlsbad

REVIEW BOARD

Edward R. Blomgren
Asheville, North Carolina

Annette Buckley
Irvine, California

Jo Ellen Cole
Vista, California

Edward Johnson
GIA, London

Michele Kelley
Monmouth Beach, New Jersey

Guy Lalous
Academy for Mineralogy, Antwerp, Belgium

Kyaw Soe Moe
GIA, New York

Keith A. Mychaluk
Calgary, Alberta, Canada

James E. Shigley
GIA, Carlsbad

Russell Shor
GIA, Carlsbad

Jennifer Stone-Sundberg
Portland, Oregon

Rolf Tatje
Duisburg, Germany

Dennis A. Zwigart
State College, Pennsylvania

COLORED STONES AND ORGANIC MATERIALS

Epochs of the formation of amber and its distribution in nature. A. V. Ivanova, S. A. Machulina, and L. B. Zaitseva [shekhun@igs-nas.org.ua], *Lithology and Mineral Resources*, Vol. 4, No. 1, 2012, pp. 18–22, http://dx.doi.org/10.1134/S0024490212010051.

In this study, the distribution of amber-type resins of various age (Paleozoic, Mesozoic, Paleogene-Neogene, and Quaternary) is mapped and their genesis is discussed. Comparing the composition of amber from different epochs provides important genetic information. A kerogen evolution diagram shows atomic ratios of three key elements: carbon, hydrogen, and oxygen. Such diagrams are used to compare fossil resins from different ages and refine their genesis and the postdiagenetic effects on them. Paleozoic and Meso-Cenozoic fossil resins occupy different areas in this diagram, suggesting a greater transformation of the older resins and different types of resin-producing vegetation in the Paleozoic and Meso-Cenozoic. The distribution of data points in the plot may provide insight into the postdiagenetic processes (magmatism and weathering) responsible for transforming some fossil resins. Epochs of intense succinosis and large-scale amber appearance are likely related to global events that fatally changed the stable environment of the resin-generating forest vegetation. Geological rearrangements and biospheric reconstructions affected climatic changes and atmospheric composition. *GL*

Genesi delle agate (II parte) [The formation of agates (Part II)]. M. C. Venuti, *Rivista Gemmologica Italiana*, Vol. 6, No. 1, 2011, pp. 51–63 [in Italian].

In this lavishly illustrated article, the author describes the "plume" and "moss" structures of agates and the factors lead-

This section is designed to provide as complete a record as practical of the recent literature on gems and gemology. Articles are selected for abstracting solely at the discretion of the section editors and their abstractors, and space limitations may require that we include only those articles that we feel will be of greatest interest to our readership.

Requests for reprints of articles abstracted must be addressed to the author or publisher of the original material.

The abstractor of each article is identified by his or her initials at the end of each abstract. Guest abstractors are identified by their full names. Opinions expressed in an abstract belong to the abstractor and in no way reflect the position of Gems & Gemology *or GIA.*

© 2012 Gemological Institute of America

ing to their formation, including Earth's gravity. Both plumes and moss are polymerized hydroxides of various metals (iron, manganese, and aluminum) and silica-forming stalactitic and dendritic structures. The metal contents derive from the surrounding rocks, which explains why plumes and moss do not occur in agates from rocks with very low metal content (e.g., sedimentary rocks).

RT

Molecular structure of the phosphate mineral brazilianite $NaAl_3(PO_4)_2(OH)_4$ – A semiprecious jewel. R. L. Frost [rfrost@qut.edu.au] and Y. F. Xi, *Journal of Molecular Structure*, Vol. 1010, 2012, pp. 179–183, http://dx.doi.org/10.1016/j.molstruc.2011.12.003.

Phosphate minerals are not often used for gem purposes—the two main exceptions being apatite and brazilianite. Infrared and Raman spectroscopy were used to investigate a brazilianite sample from the Doce Valley in Minas Gerais, Brazil. The authors correlated the features seen in both types of spectra with PO_4^{3-}, $HOPO_3^{3-}$, and OH^- stretching vibrations. The article includes a detailed interpretation of brazilianite's spectra. *JES*

Le point sur les perles de culture Première partie – Les perles d'eau de mer [Status quo of cultured pearls. Part 1 – Saltwater pearls]. E. Strack, *Revue de Gemmologie a.f.g.*, No. 176, June 2011, pp. 5–9 [in French].

China produces about 1,500 tonnes of freshwater cultured pearls per year, totaling some $150 million. By comparison, no more than 40 tonnes of saltwater products are cultivated annually, yet they have an annual value of $325 million.

Since the 1996 crisis when hundreds of millions of Japanese akoya mollusks died, saltwater cultured pearl production has been slow to recover. (Compared to >60 tonnes in 1995, 12 tonnes were produced in 2009.) Larger, high-quality cultured pearls have replaced small and low-quality production. New are larger gray cultured pearls (resembling baroque Tahitian material) and color treatments (pink, blue, lavender, and green) produced by color injection into the mollusks. Today akoya cultured pearls are also farmed in China (since 1992, about 20–25 tonnes) and marketed mainly in Japan. In Vietnam, akoya culture was introduced by Japanese farmers. In 2010, some 20 farms harvested about 1.5 tonnes. In 2009 "blue" (bluish gray) cultured pearls from Vietnam appeared in the market. Also fairly new are "Galatea Pearls" that use gem materials such as amethyst, citrine, and turquoise as nuclei and then are engraved or carved to partially expose the bead.

The author also describes the farming of Tahitian cultured pearls in French Polynesia, including a brief historical summary. In 2000, color-treated Tahitian "chocolate pearls" entered the market. Finally, the author describes the pearling industries of the Cook Islands and Fiji. Both are still on a relatively small scale but take care to produce relatively large cultured pearls of good quality. The article does not detail other important producers, such as Australia, the Philippines, or Myanmar. *RT*

DIAMONDS

An analysis of vacancy clusters and sp^2 bonding in natural type IIa diamond using aberration corrected STEM and EELS. I. S. Godfrey [iain.godfrey@postgrad.manchester.ac.uk] and U. Bangert, *Journal of Physics: Conference Series*, Vol. 281, 2011, article 012024, http://dx.doi.org/10.1088/1742-6596/281/1/012024.

The link between brown color and vacancy structures in type IIa diamond was investigated by scanning transmission electron microscopy (STEM) and electron energy loss spectroscopy (EELS). Two STEM imaging modes revealed discrete patches of stronger phase contrast, on the order of 1 nm in size, that resemble simulated images of vacancy clusters. Core-loss EELS showed a double pre-edge peak at 286 eV for brown diamond, which is absent from the spectra of colorless and treated diamonds that are annealed at 2500ºC. The authors (and others) attribute this feature to sp^2 states associated with the π-bonded lining of the vacancy clusters. They further suggest that during heat treatment, the spherical vacancy cluster grows by the uptake of mobile vacancies, until reaching a critical size where the structure collapses and forms a dislocation loop that is optically inactive and does not produce brown coloration. A second pre-edge peak at 284 eV is thought to originate from electronic states at dislocations in both brown and colorless diamonds. In the latter, it is assumed that these optically active dislocations do not occur in sufficient concentrations to cause brown color. *JES*

Boron in natural type IIb blue diamonds: Chemical and spectroscopic measurements. E. Gaillou [asteriee@yahoo.fr], J. E. Post, D. Rost, and J. E. Butler, *American Mineralogist*, Vol. 97, No. 1, 2012, pp. 1–18.

Boron is a rare trace element in natural diamond, and even when present it occurs in very low concentrations. It gives rise to a blue or blue-gray color, and the rarity of such boron-bearing diamonds suggests that they may provide unique insights into processes occurring in the mantle where diamonds form.

This study was undertaken to better understand the concentration and distribution of boron in a large group of 78 natural type IIb gem diamonds (including several famous specimens such as the Hope, the Blue Heart, and the Cullinan Blue). One sample had been HPHT-treated to remove its gray color component. Infrared spectroscopy revealed uncompensated B contents ranging up to 1.72 ppm. Results of spot analyses of eight diamonds by secondary-ion mass spectrometry (SIMS) revealed inhomoge-

neous total boron concentrations. In the Hope diamond, for example, the concentrations ranged from 0.19 to 8.4 ppm (the latter is a much higher value than previously reported). Boron caused the samples to exhibit phosphorescence—mostly a blue-green color that lasted for a few seconds, and in rare cases a strong and persistent red. These phosphorescence colors result from emission peaks at about 500 and 660 nm. Surprisingly, the intensity of the blue color only loosely correlated with the uncompensated boron content. The exact nature of the phosphorescence process is still not fully understood. *JES*

A comparison of modern diamond classifications. M. A. Viktorov [viktorov@geol.msu.ru], *Moscow University Geology Bulletin*, Vol. 66, No. 5, 2011, pp. 373–376, http://dx.doi.org/10.3103/S0145875211050103.

The author assesses current diamond classification systems and considers some potential improvements. He argues that much has been learned about diamonds since those classifications were implemented, and users of a new or updated classification system would benefit from enhanced productivity and more complete information.

The author reviews both scientific and technological classification methods, including those developed by R. D. Robertson et al., Yu. L. Orlov, and Z. V. Bartoshinsky, as well as techniques established by mining companies based on size, form, distortion, surface features, defects, and color. The study identifies key diamond classification aspects of these methods, including genetic origin, geological structural significance, and utility for mining.

The underlying commonalities of the existing diamond classification systems are characterized as unable to uniquely classify items, assign a new item into an existing group, or meet the underlying goal of classification. Potential improvements would resolve the evaluation items by: modifying classification borders; adding, subtracting, or changing groups; modifying levels of classification to accommodate new types; incorporating new measurement methods; and revising classification objectives and goals.

The deficiencies and adequacies of each reviewed method are presented, along with the author's suggestions for modifications. Ultimately, the author argues, a classification system needs to readily classify all potential samples in a meaningful way to the user. *JS-S*

Placer diamond potential of the Siberian craton: Possible sources and ages. V. P. Afanasiev [avp-dismond@mail.ru], N. P. Pokhilenko, and S. S. Lobanov, *Geology of Ore Deposits*, Vol. 53, No. 6, 2011, pp. 474–477, http://dx.doi.org/10.1134/S1075701511060031.

Placer diamond occurrences are widespread throughout Russia's Siberian craton, but only those in the northeastern portion are commercially viable. No primary sources for these alluvial deposits have been discovered so far. Diamond placers found at several levels in the stratigraphic record correspond to the Paleozoic, Mesozoic, and Cenozoic eras. Among the more than 1,000 known kimberlite pipes in this region, only those of Middle Paleozoic age have economic diamond potential. These pipes cannot account for all of the alluvial diamonds, which have varying crystal habits suggestive of different source rocks and geologic ages. The authors propose that the alluvial diamonds fall into two categories. The first, which occurs in sediments of Famennian age (374.5 ± 2.6 million years ago), resulted from erosion of the Middle Paleozoic kimberlite pipes. The second group consists of placers that host a more heterogeneous mixture of diamonds. They are found in sediments of Carnian age (228 ± 2 million years ago) and are of uncertain origin, but they appear to result from erosion of much earlier (Precambrian) unknown primary deposits and the repeated weathering and redeposition of the diamonds into younger sediments. *JES*

Plastic deformation of natural diamonds by twinning: Evidence from X-ray diffraction studies. S. V. Titkov [titkov@igem.ru], S. V. Krivovichev, and N. I. Organova, *Mineralogical Magazine*, Vol. 76, No. 1, 2012, pp. 143–149, http://dx.doi.org/10.1180/minmag.2012.076.1.143.

Indexing of a single-crystal X-ray diffraction pattern obtained for a pink-purple diamond crystal from the Internationalaya kimberlite pipe in Siberia revealed a primitive hexagonal unit cell. This hexagonal diffraction pattern was found to result from the superposition of two cubic diffraction patterns due to spinel-law twinning along (111). This result supports previous work that suggests that the rare pink-purple coloration in natural diamonds (which occurs along thin, parallel lamellae) is caused by microtwinning formed by plastic deformation.

Most natural diamonds that undergo plastic deformation do so by dislocation slipping. The authors suggest that the formation of mechanical microtwins in diamond would only take place under very specific deformation conditions such as relatively low temperatures and high strain rates. Deformation in diamond occurs during the destruction of deep-seated host rocks and during the rapid upward transport by kimberlite or lamproite magmas. Most plastic deformation in diamond is thought to occur at temperatures above 1300°C by dislocation slipping. Some undergo deformation at much lower temperatures, which the authors suggest would be more consistent with the late stages of diamond transportation in magmas. The formation of microtwins may also have been promoted by the shock impact some diamonds experienced in the earth. *JES*

Trace element analysis of rough diamond by LA-ICP-MS: A case of source discrimination? C. Dalpé [claude.dalpe@rcmp-grc.gc.ca], P. Hudon, D. J. Ballantyne, D. Williams, and D. Marcotte, *Journal of Forensic Sciences*, 2010, Vol. 55, No. 6, pp. 1443–1456, http://dx.doi.org/10.1111/j.1556-4029.2010.01509.x.

Physical and optical characteristics such as morphology, geometric defects, absorption/color, luminescence, etc., have been used in the past to describe diamond populations from different sources. These assessments relied on years of experience and studies of diamonds from many sources. The expertise remained subjective, and was not easy to transfer or validate by others, and difficult to assess in a court of law.

Laser ablation–inductively coupled plasma–mass spectrometry (LA-ICP-MS) has recently been applied to fingerprinting diamond source based on trace-element impurities. These impurities occur as either inclusions or as foreign atoms substituted into the crystal lattice. This study presents an LA-ICP-MS methodology for analyzing ultratrace element impurities in rough diamonds. Samples from two sources (Canada and South Africa) were analyzed by LA-ICP-MS, and two different statistical methodologies were applied to the data to evaluate the technique's potential to discriminate between the localities. Overall, binomial logistic regression produced a more accurate classification than linear discriminant analysis. The results suggest that using a matrix-match reference material would improve the robustness of the methodology for forensic applications. *GL*

GEM LOCALITIES

Alexandrites from the Novello alexandrite-emerald deposit, Masvingo District, Zimbabwe. K. Schmetzer, S. Stocklmayer, V. Stocklmayer, and A.-K. Malsy, *Australian Gemmologist*, Vol. 24, No. 6, 2011, pp. 133–147.

The authors describe the mineralogical and gemological properties of alexandrite from the only known alexandrite-emerald deposit in Zimbabwe: the Novello claims, located in the southern part of the country. Alexandrite is hosted by phlogopite lenses within massive serpentinite some distance from small pegmatitic intrusions (whereas the emerald is found closer to the pegmatites). Regional and countrywide geologic maps are presented to place the Novello deposit in a larger context. Although Novello yields little facetable material because of abundant inclusions and fracturing, it produces excellent collectors' specimens. It has also generated considerable interest in part because of the gems' rarity and certain similarities to those of the famous deposits in Russia's Ural Mountains.

The morphology of Novello alexandrite (single crystals and contact/cyclic twins) is compared to Russian samples with the aid of abundant photos and drawings. Cyclic twins (trillings) are most common, with single crystals and contact twins being rare. In addition to a detailed discussion of the genesis of alexandrite and emerald, the authors explore how specific chemical properties, phlogopite inclusions, and internal growth structures associated with intense color zoning characterize both rough material and the few small faceted alexandrites from Novello. Such strong color zoning is rare in Uralian material.

The color change in the Novello samples is comparable to that of Russian samples, showing a "good" change from green or bluish green to purple or purplish red. Gemological properties, particularly RI and SG, show some variations (birefringence = 0.008–0.011 and SG = 3.65–3.77). Differences in optical properties are explained by trace-element chemistry, especially the relatively high Fe and Cr values. By contrast, few Russian alexandrites show Fe values in the upper range of those from Novello. Most of the Novello rough examined, especially larger nontransparent specimens, were extremely dark green to almost black in daylight; this was due to their high Fe and Cr contents.

Russian alexandrite, collected over a considerably larger area and from numerous deposits from both surface and underground mining, shows a wider range of gemological and mineralogical features. Novello samples come from a restricted area and show less variation. *ERB*

Beryl from deposits of the Ural emerald belt, Russia: ICP-MS-LA and infrared spectroscopy study. A. S. Bidny [alexei.bidny@gmail.com], I. A. Baksheev, M. P. Popov, and M. O. Anosova, *Moscow University Geology Bulletin*, Vol. 66, No. 2, 2011, pp. 108–115.

The highest-quality Russian emeralds are located in the Ural Emerald Belt (UEB). Beryl of various colors is hosted in mafic and ultramafic "glimmerite" (mica schist), which formed along the contact zone of the Murzinka, Adui, and Kamenka granite plutons of the Late Paleozoic. Nineteen beryl crystals (green, light blue, and white) from seven deposits in the UEB were examined in this study.

Trace-element contents of the beryls obtained by LA-ICP-MS showed weak correlation among deposits—especially those from Glinka, which contained approximately 1000 ppm Cs, 100 ppm Na, and 10 ppm Mg. Beryls from the Mariinsky (Malysheva) deposit showed a nearly constant Na/Li value with variable Li/Cs, while samples from other localities gave the opposite relationship. In the Sretenjensky deposit, beryls that formed in plagioclase veins were relatively Na-rich and Li-poor. At Mariinsky, the Cs content was high in samples obtained from plagioclase veins, while Mg/Fe was low in beryls from quartz veins.

The intensity of IR bands related to type I and type II water (at 3698 and 3596 cm^{-1}, respectively) varied among samples from different mines. These differences were also observed among various generations of beryl within individual mines (e.g., in the Mariinsky, Sretenjensky, and Kvartal'nyi deposits).

One white prismatic sample from Mariinsky underwent thermal and FTIR analysis to better understand the nature of the water molecules. At 700°C, water molecules started to move out of structural channels, showing that

type I molecules were released faster than type II. All water molecules were depleted at 1000°C. This helped lower the energy of vibrations in the Si-framework, resulting in a band shift from 1151 to 1136 cm^{-1}. *KSM*

Cause chimiche delle variazioni di colore degli zaffiri di Rathnapura (Sri Lanka) [Chemical causes of color variations in the sapphires from Ratnapura, Sri Lanka]. F. M. Oltean, A. Gorghinioan, A. Marcelli, A. Exposito, and A. Mottana, *Rivista Gemmologica Italiana*, Vol. 6, No. 1, 2011, pp. 31–42 [in Italian].

The authors present a detailed investigation into the color causes of 13 violetish blue to blue to greenish blue sapphires from Ratnapura. After a visual classification into different groups, micro–X-ray fluorescence analysis was used to determine the color-causing trace element contents and their distribution. These data were then processed by multivariate and cluster analysis. As a result, correlations between the trace-element ratios and the different color groups were established. There remained, however, "a notable degree of indetermination," so further research is required. *RT*

Gem-quality Turkish purple jade: Geological and mineralogical characteristics. M. Hatipoğlu [murat.hatipoglu@deu.edu.tr], Y. Basevirgen, and S. C. Chamberlain, *Journal of African Earth Sciences*, Vol. 63, 2012, pp. 48–61.

The authors propose that a light purple gem material (consisting of 40% jadeite) is unique to the Harmancik-Bursa region of western Turkey and provide analytical parameters to aid in its identification. The material, referred to as *Turkish* or *Anatolian purple jade* by the gem trade, originates near Akpinar village from a contact metamorphic mineral assemblage between granodiorite and blueschist-facies metaclastics. The resource may be immense, though current (illegal) production is estimated at only 10 tonnes per year. X-ray diffraction of the material identified quartz, orthoclase, epidote, "chloritoid," and phlogopite in addition to jadeite. Micro-Raman spectroscopy showed the most intense peaks, in descending order, at 697, 372, 201, 1038, and 984 cm^{-1}, for which the authors provide additional detailed commentary. Mn^{3+} ions were suggested as the cause of color, though relatively high concentrations of other transition metals (notably Fe, Zn, and Ni from EDXRF data) were also noted. Further, the specific gravity measured significantly lower (3.04) than the normal range for jadeite (3.24–3.43). *KAM*

The 'hill of the precious stones', Rattanak Kiri, Cambodia. F. Payette [francinepayette@netscape.net] and G. Pearson, *Australian Gemmologist*, Vol. 24, No. 6, 2011, pp. 148–153.

Cambodia's northeastern province of Rattanak Kiri (also Ratanakiri or Rattanakiri, translated as "hill of the precious stones") is well known for its blue, brown, and colorless zircon. But it also produces amethyst, chalcedony, and tektites ("Indochinites"). However, the peridot offered in the markets of Rattanak Kiri's capital reportedly comes from nearby Mondul Kiri, to the south. This article describes the region's geology and geography, the local gem trade, and the results of an examination of locally purchased zircon, amethyst, and peridot specimens, both rough and faceted.

Samples of rough zircon were subjected to heat treatment experiments. Brown to brownish red zircon treated under oxidizing conditions, followed by heating under reducing conditions, produced an intense blue color as well as interesting absorption features, such as an emergent 654 nm absorption line. It remains uncertain whether this heat-instigated absorption was necessarily associated with the reducing conditions of heat treatment that resulted in the blue coloration.

The Cambodian amethyst is associated with granitic massifs, and can attain large size with good purple color. For the most part, the faceted amethyst offered in local markets is loupe clean or very slightly included.

The article contains photos of local gem mining and trading, as well as rough and faceted samples. *ERB*

Micro-Raman spectroscopy of gem-quality chrysoprase from the Biga-Çanakkale region of Turkey. M. Hatipoğlu [murat.hatipoglu@deu.edu.tr], U. Ören, and Y. Kibici, *Journal of African Earth Sciences*, Vol. 61, 2011, pp. 273–285, http://dx.doi.org/10.1016/j.jafrearsci.2011.08.002.

The authors characterize chrysoprase from the Biga-Çanakkale deposit in Turkey using several destructive and nondestructive analytical techniques. Raman spectroscopy allowed the separation of a chalcedonic-quartz silica phase from a crystalline-quartz silica phase in the chrysoprase matrix and in associated green-stained quartz inclusions. A total of 14 Raman bands were recorded. Five of these bands, at ~498, 460, 206, 139, and 126 cm^{-1}, were distinctive and could be related to the silica-building phases and trace elements present. Opaline silica-building phases (opal-CT and opal-C) were not detected in the chrysoprase; the dominant chalcedonic-quartz silica interval phase (moganite) indicates a higher formation temperature. This structural feature also distinguishes Biga-Çanakkale chrysoprase from the material found in Poland, Kazakhstan, Australia, Brazil, and Tanzania. The green color of chrysoprase is due to Ni ions; Fe and Cr ions modify the Turkish material's color by adding a brownish hue.

GL

New ruby discovery in Zimbabwe. F. Marsh and F. Mugumbate, *InColor*, No. 18, 2011, pp. 60–67.

Several new ruby occurrences have been found by artisanal miners in a region near Nyamapanda in northeastern Zimbabwe, near the border with Mozambique. At these locations, cabochon-quality ruby occurs as crystals and

fragments in alluvial gravels. The geology of this area, which is part of the Pan-African orogenic belt, is complex and not fully elucidated, but both igneous and metamorphic rocks are exposed in the region. The ruby material has not yet been studied to document its gemological properties, but its coloration varies from pinkish/purplish red to dark red. Recovery of the material by local miners has been done on a sporadic and limited scale. *JES*

The origin of black colouration in onyx agate from Mali. J. Götze [goetze@mineral.tu-freiberg.de], L. Nasdala, U. Kempe, E. Libowitzky, A. Rericha, and T. Vennemann, *Mineralogical Magazine*, Vol. 76, No. 1, 2012, pp. 115–127, http://dx.doi.org/10.1180/minmag.2012.076.1.115.

Onyx agate with superb black and white color contrast is found in the Gao region of eastern Mali. The continuous black color banding of these specimens demonstrates that it is not the result of staining. Analysis by several techniques revealed that the black coloration is produced by disseminated carbonaceous material in the form of nanometer-sized disordered graphite crystallites concentrated along bands in the silica matrix. These crystallites strongly absorb the incident light to produce the blackening effect; differences in crystallite concentration produce variations in color intensity.

The graphite contains some hydrogen, which suggests the possibility of a hydrocarbon precursor. The agate appears to have formed in an environment rich in organic matter. Graphite formation could be the result of hydrothermal or metamorphic alteration of methane or kerogen under various pressure-temperature conditions. *JES*

Sequential opening and filling of cavities forming vesicles, amygdales and giant amethyst geodes in lavas from the southern Paraná volcanic province, Brazil and Uruguay. L. A. Hartmann [leo.hartmann@ufrgs.br], L. da Cunha Duarte, H.-J. Massonne, C. Michelin, L. M. Rosenstengel, M. Bergmann, T. Theye, J. Pertille, K. R. Arena, S. K. Duarte, V. M. Pinto, E. G. Barboza, M. L. C. C. Rosa, and W. Wildner, *International Geology Review*, Vol. 54, No. 1, 2012, pp. 1–14, http://dx.doi.org/10.1080/00206814.2010.496253.

The impressive amethyst geode deposits hosted by the Serra Group volcanics in the Paraná Basin of Brazil and Uruguay have a complex path of formation. This six-year, multi-disciplinary study focused on geologic field observations combined with XRD, SEM, and electron microprobe analysis of hydrothermal minerals within the volcanics (basalts and rhyodacites), leading to a proposed genesis of the deposits.

Within the Paraná Basin, aeolian sands of the Botucatu Formation were buried by multiple lava flows 133 million years ago. On the edges of the basin, meteoric waters percolated into the Botucatu Formation, creating a sizeable aquifer that was heated by waning magmatic activity (producing hydrothermal fluids). Pressure from the overlying column of volcanic rock helped force this silica-rich fluid upward during three key hydrothermal events (H1–H3). High-temperature (1150°C) degassing of the lavas created initial vesicles (small cavities) within the upper and lower crusts of the basaltic flows. During the H1 event, low-temperature (30–150ºC) hydrothermal deposition of mainly clays and zeolites then began to fill many of these vesicles, effectively "sealing" the porosity within the volcanics. Then, in the H2 event, an overpressured stockwork of fluidized sand (from the Botucatu Formation) was injected into the volcanics, creating more cavities but sealing most of them; these sediments would become a major silica source for the final hydrothermal event. Finally, another overpressured pore fluid event (H3) caused intense clay alteration of the volcanics. The ascending water vapor exploded as it depressurized, lifting the upper levels of the volcanics. This process included a new phase of cavity creation, some of them very large (up to 4 m). Precipitation of remobilized silica (as amethyst) as well as calcite, gypsum, and native copper partially filled many of these cavities as geodes. Subsequent weathering produced iron-rich soil anomalies above the geode deposits (supergene alteration of the volcanics), which aid in prospecting. *KAM*

INSTRUMENTS AND TECHNIQUES

Measurement and interpretation of growth patterns in chrysoberyl, including alexandrite. K. Schmetzer [schmetzerkarl@hotmail.com], *Journal of Gemmology*, Vol. 32, No. 5/8, 2011, pp. 129–144.

Information about the external morphology of a gem-quality crystal can sometimes be revealed by the pattern of growth planes, growth zones, and twin planes observed inside a gemstone cut from that crystal. In this article, the author presents a detailed analysis of these internal growth features, which involves the accurate measurement of interfacial angles between growth planes. The necessary tools for this technique include an immersion microscope equipped with a special holder allowing the gem sample to be rotated around several axes, and an eyepiece with crosshairs and an attached 360º dial used for interfacial angle measurements. An example of applying the procedure to optically biaxial crystals is demonstrated by an analysis of alexandrites (including twinned crystals) from Russia, Sri Lanka, and Brazil. Alexandrite's strong pleochroism is a useful indicator for finding the positions of the crystallographic axes. The optic axes can be located using interference figures seen with crossed polarizing filters. Untwinned and twinned crystals of alexandrite from each of the three geographic sources displayed characteristic growth morphologies. This article demonstrates how the observation of internal growth patterns and the measure-

ment of interfacial angles between pairs of growth planes can, when used in conjunction with the sample's other gemological properties, provide valuable information on alexandrite's country of origin. *JES*

Powder diffraction analysis of gemstone inclusions. L. Leon-Reina, J. M. Compana, Á. G. de la Torre, R. Moreno, L. E. Ochando, M. A. G. Aranda [g_aranda@uma.es], *Powder Diffraction*, Vol. 26, No. 1, 2011, pp. 48–52, http://dx.doi.org/10.1154/1.3552672.

The microscope is the most important tool for characterizing inclusions, but proper identification of these features sometimes requires other methods. Powder X-ray diffraction using Cu-Kα radiation is widely used to characterize polycrystalline gem materials. Cu radiation is also effective in characterizing surface-exposed inclusions. In this study, powder X-ray diffraction using Mo radiation is reported to deeply penetrate within bulk gem materials, without damaging them. Possible improvements for inclusion analysis are discussed. *GL*

Una tecnica per fotografare le inclusioni nelle gemme [A method for the photography of inclusions in gemstones]. M. Pantò, *Rivista Gemmologica Italiana*, Vol. 6, No. 1, 2011, pp. 43–49 [in Italian].

The author discusses the combination of a webcam with a gemological microscope (in this case a model AMSCOPE T490-5MT) for photomicrography. He demonstrates the usefulness of this technique with photomicrographs in transmitted light of various samples of quartz containing inclusions of marcasite, blue fluorite, clinochlore, cacoxenite, diopside, and amphibole. *RT*

SYNTHETICS AND SIMULANTS

Diamant synthétique HPHT traité rose [Pink HPHT-treated synthetic diamonds]. J.-M. Arlabosse, *Revue de Gemmologie a.f.g.*, No. 176, 2011, pp. 13–17 [in French].

Natural type Ib diamonds can be colored pink by laboratory irradiation and annealing. As these diamonds are rare in nature, more and more HPHT-grown type Ib synthetic diamonds are being subjected to color treatment. The author uses a 0.10 ct pink brilliant by Chatham Created Gems to describe in detail how characteristics such as metallic inclusions, color zoning, and luminescence can be applied to the identification of such treated synthetics by standard gemological tests.

Abstracter's note: For the luminescence test, the author also uses the laser pointer technique described in the following abstract. *RT*

Identifizierungshilfe zur Unterscheidung zwischen natürlichen und synthetischen (HPHT) gelben, gelbbraunen und rötlich-braunen Diamanten [Identification aid for distinguishing natural and synthetic (HPHT) yellow, yellow-brown and reddish-brown diamonds]. M. Seubert, *Gemmologie: Zeitschrift der Deutschen Gemmologischen Gesellschaft*, Vol. 60, No. 1–2, 2011, pp. 53–55 [in German].

The author describes how a blue-violet laser pointer (405 nm wavelength, 1 mW) can be used to identify yellow to yellow-brown and reddish brown HPHT-grown synthetic diamonds. The laser beam causes green luminescence which reveals diagnostic growth patterns (cross-like or square, illustrated by several photos) that do not occur in natural diamonds.

The laser pointer is a practical but preliminary field testing instrument; its results should be verified by further laboratory testing. The author cautions that the user's eyes must always be protected from the direct laser beam. *RT*

TREATMENTS

Comparative study of different types of filled rubies. L. Jianjun [geoli@vip.sina.com], H. Wangjiao, S. Yuan, L. Han, C. Youfa, L. Huafeng, L. Ying, F. Chengxing, and Y. Hong, *Australian Gemmologist*, Vol. 24, No. 5, 2011, pp. 106–115.

Natural, untreated rubies are compared to three types of filled rubies: samples with glassy residues produced by heat treatment, those treated at high temperature with glass fillers, and rubies treated at low temperature with high-RI lead glass. The latter two methods are used to fill large surface-reaching fractures and cavities.

Color, UV fluorescence, and microscopic characteristics of both surface and internal features for all four groups are described. The results show that it is impossible to differentiate among them based on their color or reaction to UV radiation. However, diagnostic features include: internal flow structures in filled fractures and healed "fingerprint" inclusions; the external appearance (in luster and arrangement) observed with reflected light of surface-reaching fingerprints and fractures in both filled and unfilled stones; the presence of a blue flash effect, indicating a filler; and the intactness of needle inclusions following low-temperature heat treatment using high-RI lead glass. Useful color photomicrographs illustrate the subtleties of surface and internal features (in reflected and transmitted light, respectively) for the three types of filled rubies. The authors conclude that these microscopic observations, complemented by micro-infrared spectroscopy and qualitative EDXRF chemical analysis, allow an experienced gemologist to identify these treatments. The authors offer a protocol for the ethical and professional disclosure of such treatments based on their intent (i.e., color-enhancing vs. intentional filling of surface-reaching fractures).

ERB

Neue künstlich geritzte Sternsteine und ihre natürlichen Gegenstücke [New artificially scratched star stones and their natural counterparts]. M. P. Steinbach, *Gemmologie: Zeitschrift der Deutschen Gemmologischen Gesellschaft*, Vol. 60, No. 1–2, 2011, pp. 25–36 [in German].

About 10 years ago, some gems—namely garnet, chrysoberyl, rutile, sinhalite, cassiterite, scheelite/samarskite, tourmaline (schorl), and sphalerite—appeared on the market with stars caused by surface scratching. The parallel scratches are produced with a relatively coarse-grained grinding wheel. This article describes some new examples of stones with this type of artificial asterism: pyrite, iolite, green garnet, Cr-diopside, green tourmaline, and sapphire. The article also lists some easily verifiable characteristics to identify these products. All phenomena are illustrated by photographs. *RT*

MISCELLANEOUS

Diamonds: A good deal for Zimbabwe? Global Witness, February 2012, 22 pp., www.globalwitness.org/library/diamonds-good-deal-zimbabwe.

Released on Valentine's Day 2012 by Global Witness, a London-based NGO, this report investigates two of the main mining companies active in Zimbabwe's controversial Marange diamond field. Unraveling the complex, opaque corporate structures of both Anjin Investments and Mbada Diamonds, the findings suggest that profits from Marange are benefiting only Zimbabwe's political and military elite. There is additional concern that the proceeds are being used to fund violence and political intimidation.

The report calls upon the Zimbabwean government to: (1) pass legislation that bans the state security sector from exerting any control over mining companies or their subsidiaries, and (2) immediately audit every concession granted so far in Marange and disclose the beneficial owners of Anjin and Mbada. *EJ*

Poverty and livelihood diversification in rural Liberia: Exploring the linkages between artisanal diamond mining and smallholder rice production. G. Hilson [g.m.hilson@reading.ac.uk] and S. van Bockstael, *Journal of Development Studies*, Vol. 48, No. 3, 2012, pp. 413–428, http://dx.doi.org/10.1080/00220388.2011.604414.

This paper explores the role of alluvial diamond digging in supporting indigenous rice production in rural Liberia. As a decade of civil war and unrest caused a 75% decline in local rice production, imports of rice and macaroni, largely from the U.S., became the primary source of these staple foods. Eventually, a network of importers stifled government attempts to revive large-scale agricultural production. As a result, many small farmers are growing rice for their own subsistence and earning an economic living by mining alluvial diamonds on parts of their land plots, often hiring workers to dig in exchange for food. *RS*

Resource curse in reverse: How civil wars influence natural resource productions. S. McLaughlin [saramitchell@uiowa.edu] and C. G. Thies, *International Interactions*, Vol. 38, 2012, pp. 218–242.

According to the widely discussed "resource curse" theory, natural resources such as diamonds are often the cause of civil wars and conflict. This paper, focusing on diamonds, oil, and fisheries, maintains that the reality is far more complex, especially when considering that civil conflict often has a detrimental effect on the infrastructure and population, causing drastic declines in production of oil and diamonds. The paper concludes that a broader look at the relationship between conflict and resources is needed in view of other factors such as state strength, economic opportunities, and the nature of the diamond deposits (alluvial vs. primary). *RS*

Transnational entrepreneurs, global pipelines and shifting production patterns. The example of the Palanpuris in the diamond sector. S. Henn [sebastian.henn@utoronto.ca], *Geoforum*, Vol. 43, No. 3, 2012, pp. 497–506, http://dx.doi.org/10.1016/j.geoforum.2011.10.009.

This article examines how a closely knit community of families from Palanpur, India, created a global diamond manufacturing and trading network. The Palanpuri families, all followers of the Jain religion, entered the trade in the early 20th century. Within 30 years they had established a presence in Antwerp, facilitating the import and export of polished diamonds. Trust between the Palanpuri families helped them prevail in far-flung locations. Family members were dispatched to open offices worldwide; by 1968 they were established in New York's diamond community, and during the 1980s and 1990s they ventured into Hong Kong.

The paper also traces how the Palanpuris built their businesses cutting and trading small, lower-quality diamonds rejected by Belgian manufacturers, then expanded into larger diamonds to compete with the Antwerp establishment. *RS*

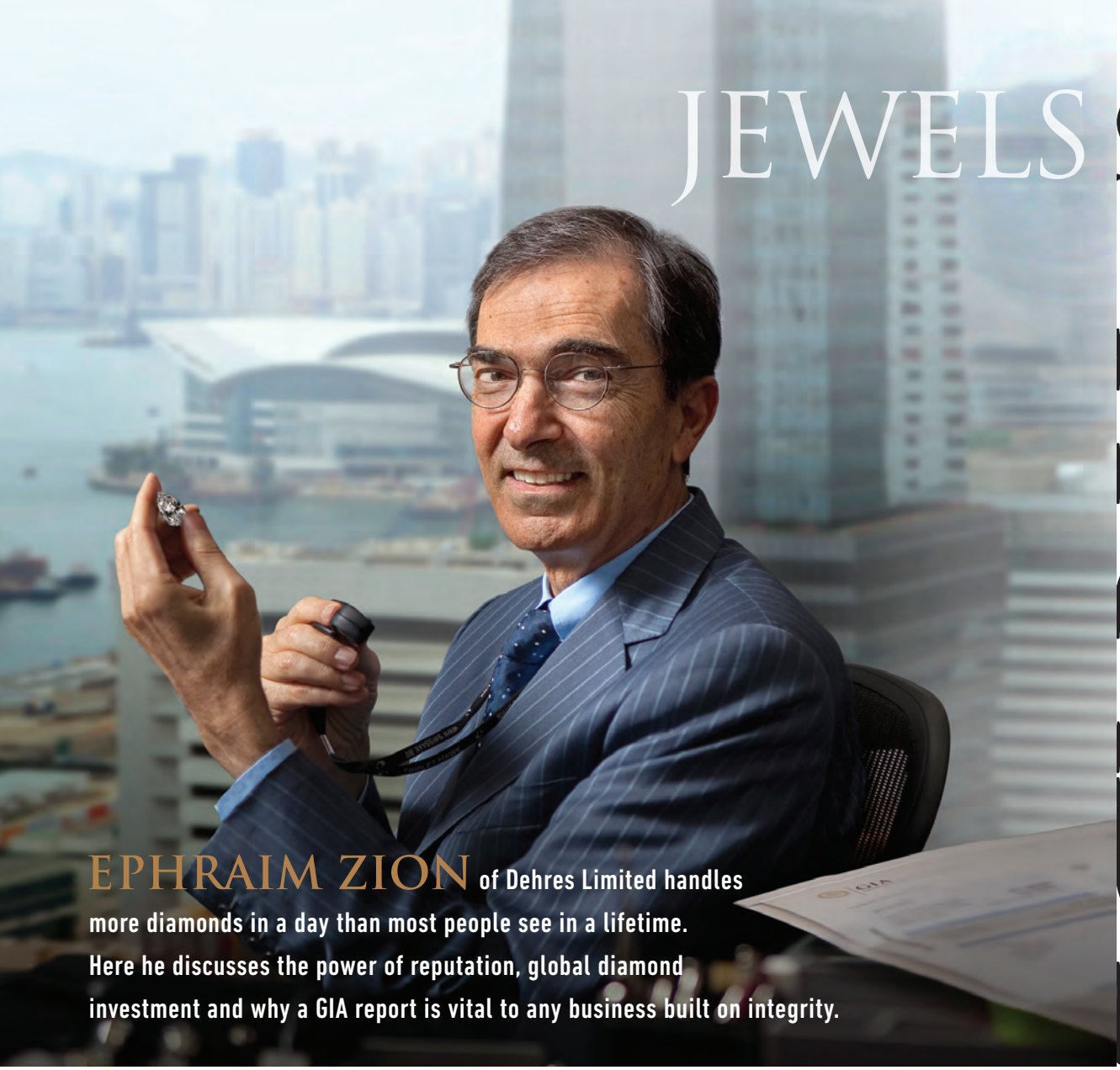

JEWELS OF THE TRADE

EPHRAIM ZION of Dehres Limited handles more diamonds in a day than most people see in a lifetime. Here he discusses the power of reputation, global diamond investment and why a GIA report is vital to any business built on integrity.

What's something most people don't know about your job? It's the only business in the world conducted on trust. You sell 1 to 5 million dollars just on the telephone, without even a signature.

A diamond dealer's most valuable asset? Reputation. Yes, you need a sense of artistic value and a knack for design, but the most essential part is integrity. You can't survive without it.

What has doing business in Hong Kong taught you about the Asian market? It's one of the strongest in the world. Every day, there are new millionaires and new businesses. Asians are very investment-conscious. Diamonds are safer and more profitable than money in a bank.

All-time favorite purchase? Most recently, a 100+ ct. D FL. Incredible brilliance and scintillation. Such a beauty. People fell down when they saw it.

Did it arrive with a grading report? Ha, ha. GIA, of course. What responsible businessman, with a good reputation and name, would sell a diamond without a GIA report?

Why is a GIA evaluation so important to one's reputation? It's the most reliable, authentic, dependable gem institute in the world. People know that, especially in the Far East. Remember what I said about reputation? A GIA report is crucial.

Business words to the wise? Selling is an idea game. The more knowledge you have, the more confidence you feel.

GIA gratefully acknowledges those who, for 80 years, have used our resources to further world expertise in gems. Invest in your success at WWW.GIA.EDU

GIA®